# Optical Control of Lipid Interaction in Photolipid Membranes

Patrick Urban


München 2021

# Optical Control of Lipid Interaction in Photolipid Membranes

Patrick Urban

Dissertation
an der Fakultät für Physik
der Ludwig–Maximilians–Universität
München

vorgelegt von
Patrick Urban
aus Starnberg

München, den 23. Februar 2021

| | |
|---|---|
| Erstgutachter: | PD Dr. Theobald Lohmüller |
| Zweitgutachter: | PD Dr. Bert Nickel |
| Tag der mündlichen Prüfung: | 12. Oktober 2021 |

# Abstract

The physics of biological membranes is governed to a great extent by the interaction between the lipid molecules. Even slight changes of the interaction exerts a drastic effect on the properties of a membrane. Photoswitchable phospholipids, also called "photolipids", provide an ideal opportunity to control the intermolecular interaction with light. Photolipids can be switched contactless and on fast timescales, allowing for reversible membrane manipulation with a high degree of spatiotemporal control.

In this thesis, the physical properties of bilayer membranes consisting of an azobenzene-containing phosphatidylcholine, *azo*-**PC**, have been investigated. The photolipid incorporates an azobenzene group in its *sn2* acyl chain that undergoes reversible photoisomerization on illumination with ultraviolet and blue light, respectively. Additionally, the main absorption peak of *azo*-**PC** in the *trans* state experiences a blue-shift when aggregated in a lipid membrane. The magnitude of the shift is sensitive to the local concentration of lipids and the phase state of the membrane.

These optical properties are used to monitor phase separation in multicomponent membranes. Macroscopic domain formation results in anisotropic photolipid distribution, affecting both the optical and the mechanical properties of the membrane. Because of the blue-shift, the assembly and disassembly of photolipids in the *trans* state into lipid domains can be monitored by UV–vis spectroscopy. On top of that, isomerization of *azo*-**PC** is used to reversibly control domain formation and membrane stiffness with light. The presence of nanoscopic domains governs the behavior of the bending rigidity of binary *azo*-**PC** containing membranes.

The photoisomerization of *azo*-**PC** allows furthermore to tune the lateral diffusion coefficient of a supported photolipid membrane by a factor of two. Similar to the effect of heat, conformational changes of the lipid tails lead to a modification of the area per lipid and hence a different diffusion coefficient. By using structured illumination, it is possible to generate compartments with specific diffusion coefficients on demand.

Finally, the permeability of photolipid membranes is explored. Isomerization of *azo*-**PC** vesicles leads to a change of the surface to volume ratio. The resulting tension is released either by vesicle splitting or by exchange of liquid through transient pores. By measuring the ionic current through the membrane, the pore dynamics are observed as step like current spikes.

The results presented in this thesis are valuable for understanding the effect of intermolecular interaction on the physical lipid bilayer properties. Using light as an immediate and precise stimulus for lipid membranes provides an ideal platform to study the dynamic response of lipid membranes themselves or the dynamics of receptors embedded in the membrane.

# Kurzfassung

Physikalische Eigenschaften von biologischen Membranen sind weitgehend durch die Interaktion zwischen den Lipidmolekülen bestimmt. Bereits kleine Änderungen der Wechselwirkung können sich drastisch auf die Eigenschaften einer Membrane auswirken. Photoschaltbare Phospholipide, auch „Photolipide“ genannt, eignen sich hervorragend, um die Wechselwirkung zwischen den Molekülen mit Licht zu steuern. Photolipide können berührungslos und schnell geschaltet werden, wodurch eine Membran reversibel und mit einer hohen räumlichen und zeitlichen Auflösung manipuliert werden kann.

In dieser Arbeit wurden die physikalischen Eigenschaften von Lipidmembranen untersucht, die aus einem photoschaltbaren Molekül aus der Gruppe der Lecithine, genannt *azo*-**PC**, bestehen. Dieses Photolipid enthält eine Azobenzol Gruppe in der Acylkette an der *sn2* Position, welche mit UV und mit blauem Licht reversibel isomerisiert werden kann. Zusätzlich wird die Absorptionswellenlänge des *trans* Zustandes von *azo*-**PC** blauverschoben, wenn das Molekül in einer Lipidmembrane aggregiert ist. Die Größenordnung der Verschiebung ist von der lokalen Konzentration und dem Phasenzustand der Membran abhängig.

Mit diesen optischen Eigenschaften kann man die Phasenseparation in mehrkomponentigen Membranen beobachten. Makroskopischer Domänen führen zu einer anisotropen Verteilung der Photolipide, die sowohl die optischen als auch die mechanischen Eigenschaften der Membran beeinflusst. Durch die Blauverschiebung kann die Bildung von Domänen mit Photolipiden im *trans* Zustand mit optischer Spektroskopie überwacht werden. Darüber hinaus können die Bildung von Domänen und die Membransteifigkeit mit Hilfe von Licht reversibel gesteuert werden. Nanoskopische Domänen beeinflussen das Verhalten der Biegesteifigkeit von zweikomponentigen Membranen, die *azo*-**PC** enthalten.

Außerdem kann durch die Isomerisierung von *azo*-**PC** der laterale Diffusionskoeffizient von Photolipidmembranen verdoppelt werden. Konformationsänderungen der Lipidschwänze führen, ähnlich wie bei Wärmeeinwirkung, zu einer Veränderung der Lipidfläche und damit auch einer Veränderung des Diffusionskoeffizienten. Mit strukturierter Beleuchtung ist es möglich, nach Bedarf Bereiche mit definierten Diffusionskoeffizienten zu erzeugen.

Abschließend wird die Permeabilität von Photolipidmembranen untersucht. Photoschalten von Vesikeln bestehend aus *azo*-**PC** Lipiden führt zu einer Veränderung des Verhältnisses von der Vesikeloberfläche und dessen Volumen. Die resultierende Spannung wird entweder durch Spaltung von Vesikeln oder durch Flüssigkeitsaustausch durch transiente Poren reduziert. Bei Messungen des Stroms durch die Membrane wird die Entstehung einer Pore durch einen diskreten Anstieg der Stromstärke beobachtet.

Die Ergebnisse, die in dieser Arbeit vorgestellt werden, heben den Einfluss von intermolekularen Wechselwirkungen auf die physikalischen Eigenschaften von Lipidmembranen hervor. Licht als unmittelbarer und präziser Stimulus für Lipidmembranen erlaubt es, die dynamischen Eigenschaften von Lipidmembranen oder von Rezeptoren, die in eine Membran eingebettet sind, zu untersuchen.

# List of Publications

## Scientific publications of results presented in this work

P. Urban, S. D. Pritzl, D. B. Konrad, J. A. Frank, C. Pernpeintner, C. R. Roeske, D. Trauner, and T. Lohmüller. Light-Controlled Lipid Interaction and Membrane Organization in Photolipid Bilayer Vesicles. *Langmuir* **34**, 13368 (2018); DOI: 10.1021/acs.langmuir.8b03241

P. Urban, S. D. Pritzl, M. F. Ober, C. F. Dirscherl, C. Pernpeintner, D. B. Konrad, J. A. Frank, D. Trauner, B. Nickel, and T. Lohmüller. A Lipid Photoswitch Controls Fluidity in Supported Bilayer Membranes. *Langmuir* 2020; DOI: 10.1021/acs.langmuir.9b02942

## Additional publications

C. Pernpeintner, J. A. Frank, P. Urban, C. R. Roeske, S. D. Pritzl, D. Trauner, and T. Lohmüller. Light-Controlled Membrane Mechanics and Shape Transitions of Photoswitchable Lipid Vesicles. *Langmuir* **33**, 4083 (2017); DOI: 10.1021/acs.langmuir.7b01020

P. Urban, S. R. Kirchner, C. Mühlbauer, T. Lohmüller, and J. Feldmann. Reversible control of current across lipid membranes by local heating. *Scientific Reports* **6**, 22686 (2016); DOI: 10.1038/srep22686

S. Simoncelli, E. M. Roller, P. Urban, R. Schreiber, A. J. Turberfield; T. Liedl,and T. Lohmüller. Quantitative Single-Molecule Surface-Enhanced Raman Scattering by Optothermal Tuning of DNA Origami-Assembled Plasmonic Nanoantennas. *ACS Nano* **10**, 9809 (2016); DOI: 10.1021/acsnano.6b05276

S. Bhattacharyya, F. Ehrat, P. Urban, R. Teves, R. Wyrwich, M. Döblinger, J. Feldmann, A. S. Urban, and J. K. Stolarczyk. Effect of nitrogen atom positioning on the trade-off between emissive and photocatalytic properties of carbon dots. *Nature Communications* **8**, 1401 (2017); DOI: 10.1038/s41467-017-01463-x

## Contributions to conferences and workshops

Control of ion transport across lipid membranes by plasmonic heating of gold nanoparticles; *7th International Symposium on Nanobiotechnology* in Bristol, UK, November 2013, **Poster** (Award, 2nd prize).

Plasmonic manipulation of lipid membranes; *SFB1032 Retreat* in Frauenchiemsee, February 2014, **Talk**.

Nanopartikel für biomedizinische Diagnostik; *NIM Nanoday* in Munich, 2014, **Poster**.

Optical manipulation of lipid membranes; *Workshop on Photonics and Optoelectronics* in Hirschegg-Kleinwalsertal, Austria, September 2014, **Talk**.

Switching Membrane Permeability by Plasmonic Heating of Gold Nanoparticles; *8th International Symposium on Nanobiotechnology* in Beijing, China, October 2014, **Poster**.

Plasmonic sensing and manipulation of lipid membranes; *SFB1032 and ESco-DNA Workshop* in Altötting, February 2015, **Poster**.

Optical properties of azobenzene phospholipids in bilayer assemblies; *Workshop on Photonics and Optoelectronics with New Materials* in Lenggries, July 2016, **Talk**.

Membrane switching with azobenzene containing phospholipids; *Workshop on Optical Spectroscopy of New Materials* in Syracuse, Italy, March 2017, **Talk**.

Membrane switching with azobenzene containing phospholipids; *SFB1032 (MGK) Summer School* in Herrsching, July 2017, **Talk**.

Controlling Membrane Properties and Domain Formation in Photolipid Bilayer Membranes; *CeNS/SFB1032 Workshop 2017 "Design and Control of Nanosystems"* in Venice, Italy, September 2017, **Poster**.

# Contents

**Abstract** i

**Kurzfassung** iii

**List of Publications** v

**1 Introduction: Rendering lipid membranes photosensitive** 1

**2 Interaction in photolipid membranes** 5

2.1 Physical parameters defining lipid membrane behavior . . . . . 5

2.1.1 Forces governing bilayer stability . . . . . 7

2.1.2 Lateral diffusion in lipid bilayers . . . . . 10

2.1.3 Phase states of phospholipid membranes . . . . . 12

2.1.4 Phase separation in multicomponent lipid membranes . . . . . 15

2.1.5 Mechanical properties of membranes . . . . . 17

2.2 Rendering phospholipids photosensitive . . . . . 20

2.2.1 Photoisomerization of the azo bond . . . . . 21

2.2.2 The photoswitchable phospholipid *azo*-**PC** . . . . . 23

2.3 Dipole coupling in dye aggregates . . . . . 26

**3 Preparation and characterization of photolipid membranes** 29

3.1 Preparing model bilayer systems . . . . . 29

3.2 Imaging photolipid membranes . . . . . 34

3.3 Characterization of azobenzene containing samples . . . . . 38

**4 Reversible domain formation in photolipid membranes** 47

4.1 Absorbance spectra of *azo*-**PC** in membranes . . . . . 47

4.2 Domain formation in ternary photolipid membranes . . . . . 55
4.3 Mechanical properties of photolipid membranes and membrane mixtures 66

**5 Illumination dependent diffusion in photolipid bilayers 73**
5.1 Lateral mobility in pure *azo*-**PC** membranes . . . . . 74
5.2 Tuning lateral diffusion with light . . . . . 77
5.3 Temperature dependent diffusion in photolipid membranes . . . . . 79
5.4 Toward optical membrane structuring . . . . . 83

**6 Light-induced permeability of *azo*-PC membranes 89**
6.1 Leaking of fluorescent dyes from GUVs upon isomerization . . . . . 90
6.2 Light-induced current steps in photolipid membranes . . . . . 94

**7 Conclusion: Controlling lipid interaction with light 97**

**A Appendix 101**
A.1 Determination of the *trans*/*cis* ratio . . . . . 101
A.2 Synthesis of *azo*-**PC** . . . . . 104
A.3 Chemical structure of lipids . . . . . 105

**Bibliography 107**

**Acknowledgments 121**

# Chapter 1

# Introduction: Rendering lipid membranes photosensitive

The cell membrane is a crucial component governing cell behavior. While only a few nanometers thin, it regulates many processes required for the function of the cell. Its selective permeability allows to maintain an electrochemical gradient across the membrane,[1,2] its mechanical properties play an important role in endo- and exocytosis and cell division,[3] and the lateral diffusion of membrane components is required for various biological functions.[4,5] The cell membrane is thus a biological system, whose function is directly connected to fundamental physical principles.

Many principles of membrane physics can be reproduced in simple model lipid systems, consisting only of one or a few different types of molecules. The reduction of components removes the complexity of cell membranes and allows a physicist to focus on the underlying physical laws. Common model systems are supported lipid bilayers (SLBs) and giant unilamellar vesicles (GUVs). SLBs consist of a single lipid bilayer attached to a solid planar support and are widely used for diffusion studies.[6,7] GUVs are spheres of a single sheet of a bilayer, enclosing an aqueous solution. Due to their size, usually a few micrometers, they provide an excellent model for cells.[8]

As we understand it today, the cell membrane is highly heterogeneous and compartmentalized into functional domains.[9] These domains facilitate the segregation of active membrane components, like proteins or other signaling molecules and are therefore crucial for proper cell function. GUVs are nowadays routinely used to study phase separation in lipid membranes. The coexistence of two liquid phases, $l_d$ and $l_o$,

in three component mixtures containing cholesterol lead to the introduction of the so-called "raft mixture", owing to the liquid phase state of cell membranes.[10] While the nature of membrane rafts is still under debate, a popular definition, as defined on a Keystone symposium on lipid rafts reads:[11] "Membrane rafts are small (10–200 nm), heterogeneous, highly dynamic, sterol- and sphingolipid-enriched domains that compartmentalize cellular processes. Small rafts can sometimes be stabilized to form larger platforms through protein-protein and protein-lipid interactions."

The first reported raft mixtures usually contained a sphingolipid, a low melting lipid such as POPC or DOPC and cholesterol at equal molar concentration.[10,12,13] The phase diagrams of these mixtures are nowadays well understood. At room temperature, membranes with these compositions exhibit macroscopic phase separation between the $l_d$ and $l_o$ phase. Later on, it was shown that the sphingolipid can in general be replaced by other lipids with a high main phase transition temperature, while retaining the ability to phase separate into two fluid phases.[14–16] Adding a fourth component to the mixture allows to tune the size of the domains.[17,18]

All these approaches are very useful to understand the thermodynamic properties of cell membranes at equilibrium, but fail to capture the *dynamic* properties. Probing these requires to change temperature, pressure or the lipid composition. The temperature can be controlled accurately, but heating of the sample chamber is slow compared to the membrane reorganization. The timescales can be decreased by using plasmonic nanoparticles[19,20] or strong laser pulses,[21,22] but these approaches require additional particles which might change the bilayer properties by themselves or high laser intensities. Changing the lipid composition is feasible by fusion of vesicles, but this process is also slow and in general not reversible.[23,24]

Light-responsive lipids, termed photolipids, provide an exciting alternative to probe the dynamic processes in bilayer membranes. An example of such a photolipid is *azo*-**PC**, a saturated phospholipid which contains an azobenzene group in one of the acyl chains. Upon isomerization, the structural conformation of *azo*-**PC**, and thus the interaction in the bilayer plane, changes substantially. The phase state of a membrane is very sensitive to such changes of the lipid conformation. It is therefore not surprising, that photolipids have been used in the past to control membrane properties with light.[25–27] Previous reports on domain formation with photoswitchable molecules have focused on perturbing systems which are known to phase separate. The photoswitchable surfactant KAON12 has been added to vesicles composed of DOPC, DPPC and cholesterol,[28] and

azobenzene containing ceramides were used in supported lipid bilayers consisting of DOPC, sphingomyelin and cholesterol.[29] The ability of *azo*-**PC** lipids to sustain macroscopic membranes by themselves permits now to explore arbitrary mixtures without depending on a host bilayer.

In this thesis, various properties of *azo*-**PC** membranes are characterized. Furthermore, the response of the membrane to optical stimuli is investigated. After introducing the physical membrane concepts in chapter 2, the methods for sample preparation and measurement setups are described in chapter 3. The results of the membrane studies are presented in chapters 4 throughout 6.

In chapter 4, phase separation of mixtures containing *azo*-**PC** are expounded. Phase behavior is governed by the interaction between the lipids, which also leads to a change of the optical absorbance spectra of *azo*-**PC** membranes. Furthermore, the ability to switch phase separation and the implications for the mechanical properties of the membranes are discussed.

Chapter 5 treats the lateral diffusion of *azo*-**PC** lipids in SLBs. The diffusion of lipids is mainly determined by their lateral footprint, which is temperature dependent and distinct for each lipid. Using photolipids, the footprint can be switched with light. The illumination conditions thus determine the local diffusion coefficient, which allows to generate patterns with varying diffusion properties.

In chapter 6, the permeability of photolipid membranes is investigated. At first, the leaking of dye molecules out of GUVs upon isomerization is observed. The mechanism is further characterized by patch-clamp measurements of lipid membranes.

# Chapter 2

# Interaction in photolipid membranes

In this chapter, the theoretical concepts that are used throughout this thesis are introduced. First, physical aspects about the cell membrane are discussed. The underlying lipid bilayer can be described as a two dimensional fluid, allowing to develop relatively simple models for this system. In the following section, the switching mechanism of azobenzene is presented. Finally, the link between the biophysical and the optical topics is given by the optical properties of aggregated dyes. Arranging optical dipoles in a crystalline order gives rise to J- and H-bands, which can be used as a probe for membrane phase states.

## 2.1 Physical parameters defining lipid membrane behavior

All cells, eukaryotic or prokaryotic, are surrounded by a thin cell membrane. The membranes mainly consist of lipids and proteins, but the exact composition varies among different types of membranes.[30] The purpose of the membrane is twofold. Primarily, it acts as a barrier between the sensitive interior of the cell and its environment. On the other hand, the cell, as a metabolic system, needs a constant stream of molecules and ions to maintain its function. The nutrients are transported into the cell, often against the concentration gradient across the membrane. The active transport is facilitated by transmembrane proteins, while the barrier function is provided by the special nature of its main constituents, phospholipids.

Lipid, stemming from the Greek word *λίπος* ("fat"), is an umbrella term for partially hydrophobic biomolecules. In a biophysical context, it describes primarily the main building blocks of the cell membrane. A substantial portion of the cell membrane is composed of phospholipids.[31] Phospholipids are characterized by their hydrophilic head group, containing a phosphate group and the two hydrocarbon chains (Figure 2.1 B).

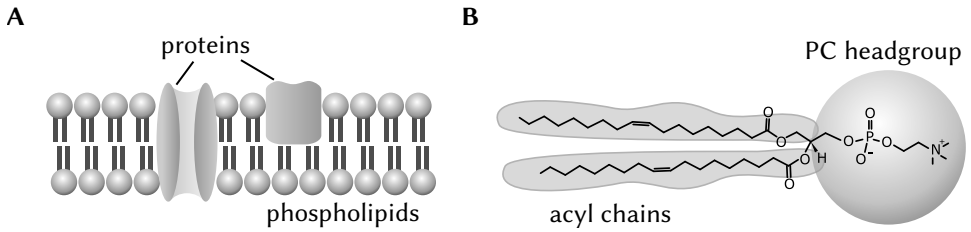


**Figure 2.1: Membrane model according to the Fluid Mosaic Model. (A)** Proteins diffuse in the two dimensional lipid bilayer phase. **(B)** An example of a lipid (DOPC), consisting of hydrophobic acyl chains and a hydrophilic headgroup.

The most popular model for the structure of cell membranes is the *Fluid Mosaic Model*.[32] The model depicts the membrane as a two dimensional sea of lipids, wherein proteins can diffuse (Figure 2.1 A). Both lipids and proteins are amphiphilic, that is, they are partly hydrophilic and partly hydrophobic. Lipids, with their hydrophilic headgroup and the hydrophobic tails, thus self-assemble into a two dimensional structure in water. Proteins are more complicated, inserting into the bilayer depending on their folded geometry.

Later on, the model was extended to include new experimental findings, especially the discovery of functional domains, induced by lipid-lipid, protein-lipid and protein-protein interaction.[33] The role and function of so called lipid "rafts"[34] is still a topic of debate.[35] Nowadays, many examples are known where proper protein function relies on the interaction with specific types of lipids.[36,37]

In order to elucidate the role of the lipid bilayer, simple model systems, consisting of only one or a few different types of molecules have long been used to study specific aspects of membrane physics. In the following, the physical aspects governing lipid bilayer self-assembly and behavior are discussed.

### 2.1.1 Forces governing bilayer stability

The main driving force of lipid self-assembly is constituted by their amphiphilic nature. The hydrophobic effect of the hydrocarbon chains tends to minimize the surface area that is in contact with water. On the other hand, the interaction between the polar headgroup and water is attractive. Those two *opposing forces*[38] give rise to the stability of the lipid assemblies. The area which is in contact with water at the minimum of the total interaction energy is then defined as the *optimal surface area per headgroup.*[39]

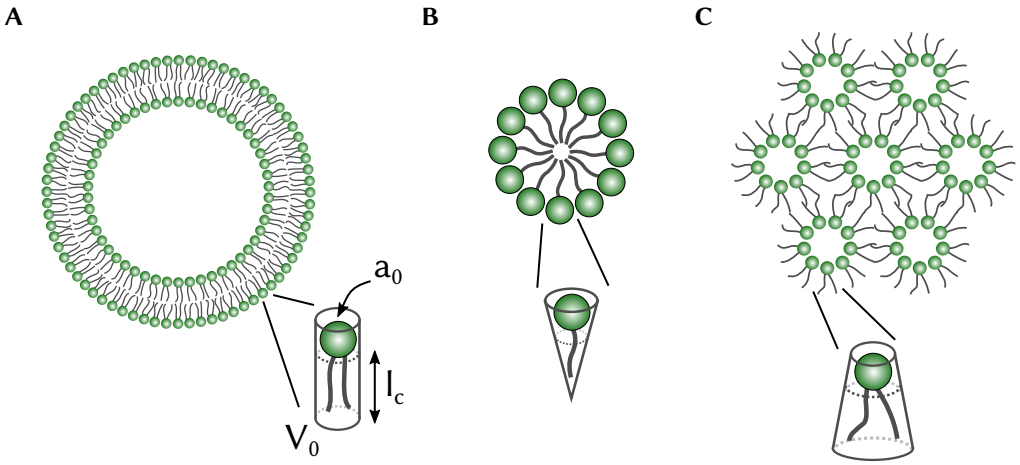


**Figure 2.2: Lipid packing of different lipid assemblies.** **(A)** For lipid bilayers or GUVs, the curvature is small, the packing parameter is ≤ 1. **(B)** Micelles are the smallest aggregates, containing no aqueous core. The packing parameter is ≤ 1/3. **(C)** For molecular packing > 1, other aggregate structures can exist, e.g. the inverted hexagonal phase.

The first unifying theory of self-assembly of amphiphilic molecules was introduced by Israelachvili *et al.*[39,40] In the following, some aspects of the theory are presented and discussed in the context of the results this thesis.

The free energy of a lipid aggregate consisting of $N$ molecules is given by $N\mu_N^0$, with $\mu_N^0$ being the mean free energy of a molecule in such an aggregate. In systems with different aggregate sizes, the chemical potential in equilibrium can be expressed as

$$\mu_N^0 + \frac{k_B T}{N} \ln\left(\frac{X_N}{N}\right) = const. \tag{2.1}$$

where $X_N$ is the fraction of molecules in aggregates of size $N$. This can be rewritten as

$$X_N = N\left[(X_M/M)\exp\left(M\left(\mu_M^0 - \mu_N^0\right)/k_BT\right)\right]^{N/M} \tag{2.2}$$

with $M$ being an arbitrary reference state. For simplicity, the monomer state $M = 1$ can be taken as reference:

$$X_N = N\left(X_1 \exp\left(\mu_1^0 - \mu_N^0/k_BT\right)\right)^N . \tag{2.3}$$

Since $X_N$ is a value between 0 and 1, a larger fraction of aggregates of size $N$ is only possible if $\mu_N^0$ is smaller than the monomer chemical potential.

For amphiphilic molecules, the free energy in an aggregate can be described by taking into account the interaction forces, the *opposing forces* as described above. The contribution due to the hydrophobic interaction arises from the surface tension $\gamma$ between water and the lipids. The energy contribution from one molecule is then $\gamma a$, where $a$ is the area at the water-lipid interface. The repulsive contributions are usually given as the first term of the energy expansion.[41] For phospholipids, the repulsive contribution can be given by $C/a$. The parameter $C$ takes up all the repulsive interactions and depends mainly on the type of headgroup.

In this work, only phospholipids with the same head-group, but different chains are used. Differences in the physical properties of lipid aggregates thus have to be attributed to effects of the chains, which mainly contribute to the repulsive interaction through steric effects. The geometric reorganization upon isomerization of *azo*-**PC** thus changes interaction between the molecules constituting the lipid aggregate and has an immediate effect on several physical properties of the bilayer, as will be expounded throughout this thesis. Since *azo*-**PC** is a purely synthetic lipid not occurring in nature, it is at this stage not possible to give quantitative information about the strength of the interaction.

By combining attractive and repulsive contributions, the free energy per molecule can be given in first approximation by

$$\mu_N^0 = \gamma a + C/a . \tag{2.4}$$

The optimal surface area per molecule $a_0$ can then be defined as the area, where the interaction free energy is at a minimum:

$$\frac{\partial \mu_N^0}{\partial a} = \gamma - C/a^2 = 0 \Longrightarrow a_0 = \sqrt{C/\gamma}. \tag{2.5}$$

Inserting into Equation 2.4 yields

$$\mu_N^0 = \gamma\left(a + a_0^2/a\right) = 2a_0\gamma + \frac{\gamma}{a}\left(a - a_0\right)^2 . \tag{2.6}$$

For different structures in which the surface area is close to the optimal area, entropy favors the aggregates consisting of the fewest molecules (Equation 2.2).

The reduction to a simple geometric surface area was extended to classify amphiphilic molecules by geometric objects, indicative of the type of assembly in water. Figure 2.2 depicts common structures of amphiphile self-assemblies. An obvious constraint is the length of the hydrocarbon chains, which cannot extend arbitrarily long. This allows to define a molecular packing parameters as $V_0/(a_0 l_c)$, with $V_0$ and $l_c$ being the volume and length of the hydrocarbon chains, respectively.

As an illustrative example, a micelle with a radius which equals the length $l_c$ of the acyl chains is considered (Figure 2.2 B). The volume and the surface area of the micelle are then given by

$$V = NV_0 = \frac{4}{3}\pi l_c^3 \tag{2.7}$$

$$A = Na_0 = 4\pi l_c^2 . \tag{2.8}$$

The optimal area per molecule $a_0$ can expressed as

$$\frac{Na_0}{NV_0} = \frac{4\pi l_c^2}{4/3\pi l_c^3} \Longrightarrow a_0 = \frac{3V_0}{l_c} . \tag{2.9}$$

The packing parameter is then $V_0/(a_0 l_c) = 1/3$. In practice, the radius might be slightly larger than $l_c$, therefore the packing parameters for spherical micelles is usually given by $V_0/(a_0 l_c) \leq 1/3$. For a bilayer with small or no curvature, $a_0 l_c$ gives the occupied volume $V_0$, hence $V_0/(a_0 l_c) \leq 1$ (Figure 2.2 A). For larger packing parameters, inverted structures, like the hexagonal phase, are possible.

In the context of this work, the most important type of lipid assembly is the vesicle. Vesicles are spherical structures enclosing a distinct volume of aqueous solution. Often,

the enclosing layer is a single lipid bilayer, the structures are then termed unilamellar vesicles. Vesicles in several size ranges can be produced for bilayer studies. Unilamellar vesicles with a diameter below 100 nm are denoted as SUVs (small unilamellar vesicles), between 100 nm and 1 µm LUVs (large unilamellar vesicles) and above 1 µm GUVs (giant unilamellar vesicles). GUVs are often used as a model system for cells, owing to their size which is similar to real cells. Vesicles consisting of one kind of lipid are usually spherical without any influence of external forces because energetically, this is the most favorable state.

### 2.1.2 Lateral diffusion in lipid bilayers

One important parameter that characterizes lipid bilayers and links macroscopic properties to the microscopic composition of the membrane is its diffusion coefficient. Diffusion is an universal physical concept that finds application in many different fields and the diffusion coefficient is a measure for the mobility of the diffusing particle. In a biophysical context, the life of a cell is driven by the interplay of diffusion and active transport of various substances. In membranes of cells, lateral diffusion of membrane proteins is often required to ensure their proper biological function.[42] The fluidity of the membrane is thus one of the key requirements of the *Fluid Mosaic Model*,[32] enabling the distribution of membrane constituents across the membrane.

For a homogeneous membrane, the diffusion is described by the *diffusion equation*, as first derived by Einstein:[43]

$$\frac{\partial c(x,t)}{\partial t} = D\nabla^2 c(x,t)\,, \tag{2.10}$$

where $D$ is the diffusion coefficient and $c(x,t)$ is the density at location $x$ and time $t$. In general, the diffusion coefficient depends on the dimensionality of the system. In two dimensions, the solution for a Dirac delta function $\delta(x)$ at $t = 0$ is the fundamental solution

$$c(x,t) = \frac{1}{4\pi Dt}\exp\left(-\frac{x^2}{4Dt}\right). \tag{2.11}$$

The diffusion coefficient is then linked to the particle movement by the mean square displacement

$$\left\langle x^2(t)\right\rangle = \iint_A x^2 c(x,t)\,\mathrm{d}A = \int_0^\infty r^2 c(x,t) 2\pi r\,\mathrm{d}r = 4Dt\,. \tag{2.12}$$

This solution holds, as long as $c(x,t)$ is a Gaussian distribution at long times. In a real cell membrane, this is often not the case. High protein content, domains or interaction with the cytoskeleton can all hinder the diffusion, leading to deviation from normal diffusion.[44] For simple model bilayer systems, the lipid diffusion can be described by a constant diffusion coefficient $D$.

### Free area theory

The lipid diffusion coefficient can be derived by an extension of the free volume theory.[45] The free volume theory was originally used to describe the diffusion in fluid glass forming materials.[46] In this theory, the liquid consists of hard spheres and unoccupied space, the "free volume", and the diffusion coefficient is determined by the distribution of free volume in the ensemble of molecules. The theory was later on extended to account for the temperature dependence of the viscosity of liquids.[47]

At finite temperatures, a molecule fluctuates around its equilibrium position due to thermal vibrations. The average occupied space is thus larger than the space that a single rigid representation of the molecule would occupy. The notion of free volume comes from this difference in volume, which is in principle available to be occupied by a neighboring molecule. In this picture, a particle can only be displaced, when the free volume in its vicinity is large enough and, additionally, enough energy is available to overcome the attractive forces with its neighbors. The model was adapted for lipid bilayers as the free area model.[48,49]

According to this theory, the diffusion coefficient is given as

$$D = D' p(a) p(E) \tag{2.13}$$

where $D'$ is a pre-exponential factor which can be interpreted as the unhindered diffusion coefficient.[45] The activation energy $E_a$ which is required to overcome the repulsive interactions with the neighboring molecules, both lipids and the surrounding

water, is accounted for by the probability $p(E)$:

$$p(E) = \exp\left(-\frac{E_a}{k_B T}\right). \tag{2.14}$$

$p(a)$ is the probability to find an area next to the diffusing particle, which is big enough to be occupied.

$$p(a) = \exp\left(-\frac{a_0}{\langle a_f \rangle}\right), \tag{2.15}$$

where $\langle a_f \rangle = a(T) - a_0$ is the temperature dependent average free area per molecule. The critical area $a_0$ is the molecular area of the lipid in a closed packed structure.

$D'$ can be derived by considering a random walk in two dimensions on a square lattice with lattice constant $\delta = \sqrt{a(T)}$.[50] At thermal equilibrium, the particle moves with an average velocity $v = \delta/\tau = \sqrt{2k_B T/m}$ in a random direction. $D'$ can then be expressed as a two dimensional diffusion coefficient:

$$D' = \frac{\delta^2}{4\tau} = \frac{\sqrt{a(T)}}{2\sqrt{2}}\sqrt{\frac{k_B T}{m}} \tag{2.16}$$

Inserting back into Equation 2.13 yields

$$D = \frac{1}{2\sqrt{2}}\sqrt{\frac{k_B T a(T)}{m}} \exp\left(\frac{-a_0}{a(T) - a_0} - \frac{E_a}{k_B T}\right) \tag{2.17}$$

The parameters $a(T)$ and $a_0$ are experimentally accessible by techniques such as NMR or X-ray scattering. The only unknown parameter is hence the activation energy $E_a$. This energy is in general assumed to be temperature independent and can be obtained by fitting to experimental data. The theory has been successfully applied to explain the effect of cholesterol on the diffusion of a lipid bilayer.[49]

### 2.1.3 Phase states of phospholipid membranes

Lipid bilayers can exist in different states of matter, or lamellar phases, which are mainly distinguished by their fluidity. For bilayers consisting of a single lipid species, the two main phases are the gel or solid phase ($L_\beta$ or $s_o$) and the fluid, or liquid disordered, phase

($L_\alpha$ or $l_d$). The lipids are nearly immobile in the gel phase, while they can diffuse freely in the fluid phase. Typically, the diffusion coefficient of fluid membranes is D≥1 μm$^2$ s$^{-1}$.

At low temperatures in the $L_\beta$ phase, the tails of the lipids are mostly elongated in the all-*trans* configuration. The lipids themselves are arranged in triangular lattice with long range order. Membranes composed of lipids with a phosphatidylcholine head group are in this phase tilted with respect to the membrane normal, denoted as $L_{\beta'}$.[51] At high temperatures, lateral order is lost and the membranes behave like a two dimensional liquid. The aliphatic chains loose their all-*trans* configuration and show many *gauche* isomerizations in their C – C bonds. The melting process from the gel to the fluid phase takes place over a narrow temperature range (<1 °C). The lipids thus do not melt independently, but rather simultaneously in clusters.

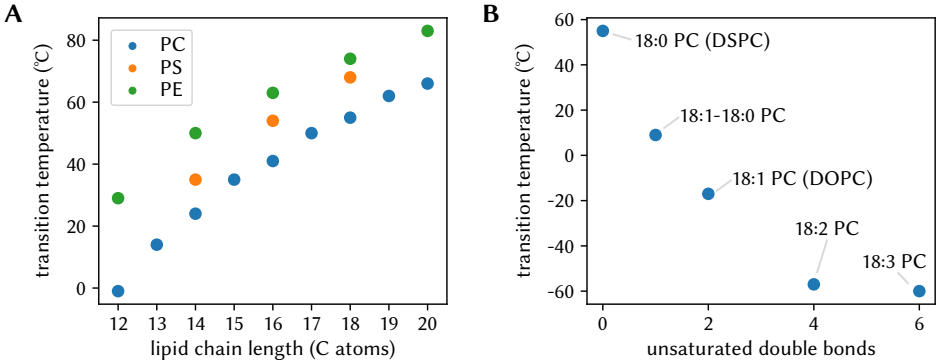


**Figure 2.3: Melting temperature of different phospholipids.** (**A**) The main transition temperature is dependent on both the length of the hydrocarbon chain and the headgroup type. (**B**) For lipids with the same chain length, the number of unsaturated C = C bonds has a huge effect of the transition temperature. The phase transition temperatures are obtained from Avanti Polar Lipids.[52]

Several parameters affect the melting temperature of the lipid bilayer (Figure 2.3). The melting temperature $T_m$ can be derived as $T_m = \Delta H_t / \Delta S_t$, where the index $t$ indicates the changes in both entropy and enthalpy at the transition temperature.[53] Both transition entropy and enthalpy are linear in the chain length, but contributions from the chain ends lead to a higher transition temperature for longer chains. The curve is flattening for high number of carbon atoms, because end effects become less important.

While the overall trend is insensitive to the headgroup type, the absolute temperature values are heavily influenced by the headgroup. This effect comes from the different electrostatic interaction between the head groups and the hydrogen bonding

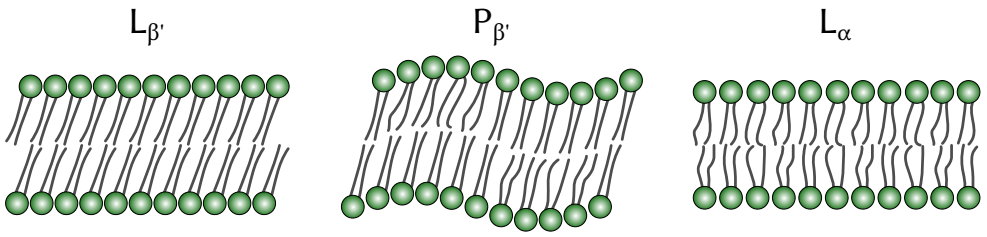


**Figure 2.4: Membrane phases in single component lipid bilayers.** At low temperatures, lipid bilayers of long chain phospholipids with a PC headgroup are in the $L_{\beta'}$ phase. At temperatures higher than the pre-transition temperature, the rippled $P_{\beta'}$ phase can exist. Increasing the temperature past the main phase transition puts the bilayer in the fluid $L_{\alpha}$ phase.

to the surrounding water molecules.[54] Bilayers with phosphatidylserine head groups have a higher phase transition temperature than bilayers with phosphatidylcholine head groups. The smallest head groups, phosphatidylethanolamine, lead to the highest melting temperatures.

The amount of unsaturated double bonds induces the largest effect on the transition temperature. For a PC lipid with two hydrocarbon chains consisting of 18 carbon atoms each, the degree of saturation can account for a difference of almost 120 K (Figure 2.3 B). The unsaturated double bonds do not undergo *trans-gauche* isomerization and effectively decouple the individual saturated chain segments. An increasing number of such bonds has thus the same effect as shortening the chains, leading to a lower phase transition temperature. The conformation of the double bond influences also the transition temperature, albeit not dramatically. Just as the azo group in azobenzene, the C = C bond has two stable isomers, *trans* and *cis*. For 18:1 (Δ9-Trans) PC, the melting temperature is 12 °C, 29 °C higher than 18:1 (Δ9-Cis) PC (DOPC).[52] In cells, almost all C = C double bonds exist in the *cis* form, which allows the membrane to maintain higher fluidity.

In addition to the two main phases, as discussed above, lamellar lipid bilayers can exist in several other phases. Just below the main phase transition, a bilayer can be in the so-called ripple phase ($P_{\beta'}$). The lipids are still in the all-*trans* configuration, but the bilayer is no longer planar but consists of periodic, quasi-lamellar segments. The most important phases of single component lipid bilayers are depicted in Figure 2.4.

The presence of cholesterol induces an additional phase, which is also highly relevant for biological membranes. Cholesterol is especially abundant in membranes of

mammalian cells.[31] In two component lipid bilayers containing saturated PC phospholipid and cholesterol, the phase transition temperature range of the gel to liquid phase is broadened for increasing cholesterol content and disappears almost completely near 50 mol%.[55] Cholesterol is, just as a phospholipid, an amphipathic molecule and inserts into a bilayer in a certain orientation. In gel state bilayers, the fused ring system of cholesterol is located in the highly ordered region of the phospholipid hydrocarbon chains. The geometry of the molecule disturbs the order of the phospholipids and increases their mobility. Similarly, the rigid ring system hinders the appearance of kinks due to *trans-gauche* isomerization and exerts an ordering effect on bilayers in the $l_d$ phase. The fluidization of gel phase membranes and the ordering of fluid membranes lead to the naming of this intermediate state, the "liquid ordered" ($l_o$) phase.

### 2.1.4 Phase separation in multicomponent lipid membranes

In contrast to the single component model systems as discussed so far, the cell membrane is a highly heterogeneous system with a high amount of different lipids and proteins.[30] Primarily the discovery of membrane rafts[34] lead to our current understanding of the role of functional domains in cell membranes. Nowadays, many examples of nano- or microdomains have been demonstrated, including in prokaryotic or plant cells.[56,57] The underlying principle of this compartmentalization is presumed to originate in the complex interplay between lipids and proteins.

Studying lipid domains *in vivo* is difficult, because they are usually smaller than the diffraction limit of light and have often a relatively short lifetime.[9] To study the influence of different lipids on domain formation, simple model systems containing a limited number of different lipids are often used. Commonly used model systems also highlight the prominent role of cholesterol in this process. Binary systems consisting of two phospholipids only show phase separation and hence domain formation between the $s_o$ and $l_d$ phase.[58] Cell membranes are however completely fluid, precluding the usefulness of such systems. Cholesterol is abundant in mammalian cells[31] and induces the liquid ordered phase in lipid membranes. Mixtures containing at least three components, one of them cholesterol, exhibit phase coexistence between two liquid phases, $l_d$ and $l_o$.[12,13,59] These ternary mixtures have since been used extensively as model systems for lipid rafts.

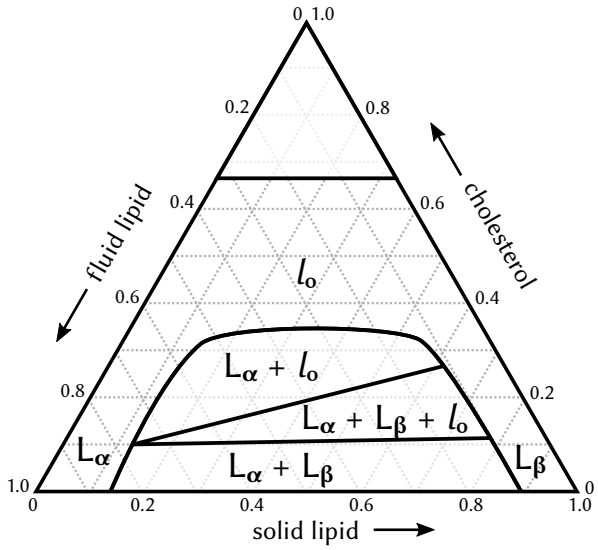


**Figure 2.5: Generic phase diagram for ternary lipid mixtures.** The Gibbs phase triangle is often used to depict the phase behavior of three component lipid mixture. Every composition can be represented as a point on the triangle. The displayed phase diagram is based on the phase diagram of DOPC, DSPC and cholesterol,[60] but the general phase behavior for mixture containing a lipid below the main transition temperature $T_m$, a lipid above $T_m$ and cholesterol is surprisingly independent of the exact lipid type.[61] Solid lines represent phase transitions, above 70 % cholesterol, solid crystals of cholesterol can be found in solution.

Nowadays, many different compositions containing cholesterol are known to exhibit liquid-liquid coexistence. The requirements for a composition to show phase separation can be loosely summarized as follows: The mixture needs to contain a lipid with a high melting temperature, a lipid with a low melting temperature and cholesterol. At a temperature between the two melting temperatures of the phospholipids, mixtures with low cholesterol concentrations can exhibit $s_o/l_d$ phase separation. At higher cholesterol concentration, the $l_o$ phase appears and any combination of the three phases can coexist (Figure 2.5).[16]

From a thermodynamic point of view, phase separation in a lipid membrane is governed by the interaction between the different types of lipids. One parameter, characterizing the interaction energies between two types of lipids can be used to describe the tendency of a mixture to phase separate.[62] For two different lipid species A and B, three different interactions are possible, A-A, B-B and the interaction between unlike lipids A-B. In this model, the parameter quantifying the difference between the

interaction of *like* and of *unlike* molecules is given by

$$\omega_{AB} = g_{AB} - \frac{1}{2}\left(g_{AA} + g_{AB}\right) , \tag{2.18}$$

where $g_{AB}$ is the Gibbs free energy of interaction between lipid A and lipid B, and $g_{AA}$ and $g_{BB}$ are the Gibbs free energies of interaction between two A or two B molecules, respectively. The change in the Gibbs free energy upon exchange of two molecules $\Delta G$ can be expressed in terms of $\omega_{AB}$.[62] While entropy will favor complete mixing of the molecules, the phase separated situation can become energetically favored if $\omega_{AB} > 0$. For $\omega_{AB} < 0$, the interaction between unlike molecules is favored over the interaction between the same lipids and the membrane is mixed completely.

While this model is very simple, it captures the basic properties of phase separated membranes. For ternary mixture containing cholesterol and two different phospholipids, three different interaction parameters $\omega_{AB}$ have to be considered. Phase separation can occur in these mixtures, if $\omega_{AB} < 0$ for the interaction between cholesterol and the lipids constituting the ordered phase and $\omega_{AB} > 0$ for the interaction between the disordered lipids and both cholesterol and the ordered lipid.[63] This corresponds to the situation found experimentally in model membrane systems, where the liquid ordered phase is rich in cholesterol.[64]

### 2.1.5 Mechanical properties of membranes

Lipid assemblies with a packing parameter sustaining bilayers fold up to vesicles, or liposomes, in aqueous solution. For cells, lipid membranes provide mechanical stability, alluding to the strong forces holding the bilayer together. On the other hand, there are many biological processes, where the cell membrane undergoes morphological changes. In cell division, for example, forces constrict part of the cell until the membrane separates at some point.[65] Endo- and exocytosis are also processes, in which membrane curvature has to be generated locally.[3]

The cell membrane as the barrier between the cell and its surrounding has to adapt to any shape change of the cell itself. While these processes are driven by the complex cell machinery, shape transformations resembling biologically relevant processes can also be observed in pure lipid vesicles.[66,67] Mechanically, lipid membranes are almost incompressible, but can easily deform due to their low bending rigidity. Due to the huge

difference between the bilayer thickness (≈5 nm) and the lateral expansion in cell sized vesicles (>10 µm), models derived from continuum mechanics can be used to describe many mechanical and morphological properties.

One can think of a lipid bilayer as a two-dimensional elastic surface, embedded into a three-dimensional space. This elastic surface can undergo two mechanical deformations, bending and stretching. The energy required to stretch a membrane patch or area $A_0$ can be described in the linear elasticity regime as[68]

$$E_{\text{stretch}} = \frac{1}{2} K_A \frac{(A - A_0)^2}{A_0} \tag{2.19}$$

with the *area expansion modulus* $K_A$. For phospholipid membranes, typical values $K_A$ are around 250 mN/m.[69] The resulting lateral stress $\Sigma$ one the membrane upon an area expansion is given by

$$\Sigma = \frac{\partial E_{\text{stretch}}}{\partial A} = K_A \frac{A - A_0}{A_0} \tag{2.20}$$

and is thus linear in the expansion of the membrane. When the stress exceeds a certain threshold, the membrane ruptures. For phospholipid membranes, the breakdown happens already at low values, usually at a few mN/m.[70] The membrane thus is not very flexible in this sense, allowing only for an expansion of less than 10 %. When a lipid bilayer ruptures, at first small transient pores are formed. If the pore size exceeds a critical size, the membrane is not able to heal itself anymore and ruptures.

For the bending rigidity, the situation is a bit more complicated, because one needs two parameters to describe the curvature on a flexible sheet, called *principal curvatures*, $c_1$ and $c_2$ (Figure 2.6 A). For discussing the bending energy of membranes, one typically sees different parameters, the *total curvature* $K$ and the *Gaussian curvature* $K_G$.

$$K \coloneqq c_1 + c_2 \tag{2.21}$$

$$K_G \coloneqq c_1 c_2 \,. \tag{2.22}$$

In 1973, Helfrich introduced a geometric Hamiltonian describing lipid membranes using the variational principle. For small curvatures compared to the inverse membrane thickness, the Hamiltonian can be written as[68,71]

$$H = \int \mathrm{d}A \left\{ \frac{1}{2} \kappa (K - c_0)^2 + \bar{\kappa} K_G \right\} \tag{2.23}$$

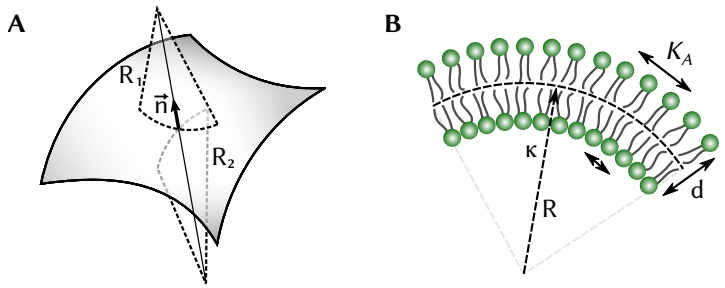


**Figure 2.6: Membrane mechanics. (A)** On a two dimensional surface, the curvature can depend on the direction it is evaluated. The curvature at each point is fully defined by the two principal curvatures $c_1 = 1/R_1$ and $c_2 = 1/R_2$. **(B)** The bending moduli and expansion modulus are related, if a finite thickness $d$ of the lipid bilayer is considered. Without lipids hopping from one surface to the other, bending of a bilayer will lead to an expansion and hence stretching of the outer layer and a compression of the inner layer. Within the layer, a neutral surface exists which is not strained at all.

with $c_0$ being the *spontaneous curvature*, $\kappa$ the *bending modulus* and $\bar{\kappa}$ the *Gaussian curvature modulus*. In the context of a lipid bilayer, the spontaneous curvature only occurs, when the bilayer leaflets are asymmetric, which would lead to a curved structure at equilibrium. The Gaussian curvature modulus can be neglected for closed vesicles due to the Gauss-Bonnet theorem, but has to be considered when the topology changes, e.g. by fusion or fission of vesicles.[72] The bending modulus is then the parameter, that is usually used to describe membrane mechanics. Several techniques exist to measure the bending modulus, including fluctuation spectroscopy or micropipette aspiration.[73]

The bending modulus and the area expansion modulus can be correlated by taking the microscopic structure of the bilayer into account. The Helfrich Hamiltonian is derived by considering a thin, homogeneous layer. The bilayer consists however of two weakly coupled layers of lipids. Bending this layer only leads to a stress free situation at a specific plane in the middle of the bilayer. Without exchange of lipids, the outer membrane needs to stretch, to accommodate the increased surface area, while the inner layer is compressed accordingly. By using a polymer brush model, the mechanical moduli are related by[69]

$$\kappa = \frac{K_A d^2}{24} \tag{2.24}$$

with $d$ being the bilayer thickness (Figure 2.6 B).

Vesicle shapes are calculated from the Helfrich Hamiltonian by taking into account the osmotic pressure $\Delta p$ and the surface tension $\sigma$

$$\Delta p - \sigma K + \kappa \left( \Delta K - \frac{1}{2}(K - c_0)\left[(K - c_0)K - 2K^2 + 4K_G\right] \right) = 0 \tag{2.25}$$

Vesicles in equilibrium will assume the shape, which leads to the lowest curvature energy under the appropriate constraints. Solutions of Equation 2.25 lead, in addition to spherical solutions, to many non-spherical solutions, which have also been confirmed experimentally.[74]

For multicomponent membranes, one has to distinguish in general between phase separated systems and the homogeneous bilayers. For phase separated membranes, a line tension arises at the boundaries between the domains due to the hydrophobic mismatch. The line tension can drive processes such as budding or invagination.[75] If no macroscopic phase separation occurs, the local inhomogeneities in the composition can lead to spontaneous curvature contributions and thus to deviations from a spherical shape.[76]

## 2.2 Rendering phospholipids photosensitive

Nature found various ways to convert its prime energy source, the sunlight, into usable energy.[77] In general, those system are highly specialized and complex, but very effective. The light harvesting complex 2, for example, absorbs light by in total 27 bacteriochlorophyll *a* molecules that are arranged in a highly ordered fashion by proteins.[78] The absorbed energy is then very efficiently transferred to the reaction center. Another intriguing example is the process that leads to human vision. A simple isomerization of a rhodopsin molecule initiates a cascade of events, which eventually end up as a stimulus in the brain.[79]

From a synthetic point of view, it is very attractive to use light as a stimulus, because it is contactless, immediate and very precise. A simple model photoswitch, that has been used in many applications is azobenzene (Figure 2.7). Azobenzene consists of two benzene rings that are linked by an azo group. It exists in two isomeric forms, defined by their configuration around the N=N bond, *trans* and *cis*. Interconversion between the two isomers is possible by illumination with light.

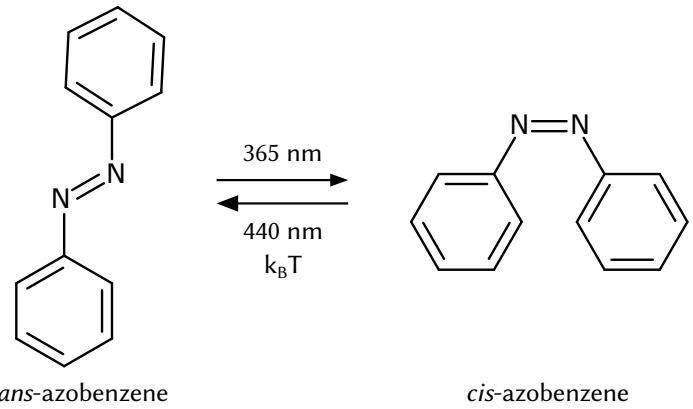


**Figure 2.7: Azobenzene.** The two azobenzene isomers, *trans* and *cis*, can be interconverted by light and heat.

Additionally, many synthesis methods for azobenzene are known, which makes it relatively easy to create new photoswitchable molecules. By carefully combining function with geometry, this can be used to switch between two different properties with light. In polymers, this has been used for a variety of macroscopic changes, including bending of a polymer sheet or optical pattering of a surface.[80,81] Further properties that are advantageous for biological systems are its size and the isomerization process itself.[82] Due to the small size of azobenzene, it is possible to incorporate it into known drugs without changing their properties dramatically. The fast isomerization, within a couple of ps, prevents the formation of singlet oxygen, which could induce cell damage.

### 2.2.1 Photoisomerization of the azo bond

The absorbance spectrum of the *trans* state of azobenzene is characterized by two peaks, the dominant peak at 320 nm and a weaker one at 440 nm.[83] In the *trans* state, the molecule assumes a planar geometry. The peak at 440 nm corresponding to the $n\pi^*$ transition ($S_0 \longrightarrow S_1$) is therefore parity forbidden due to its $C_{2h}$ symmetry. In azobenzene derivatives like *azo*-**PC**, the symmetry is lifted and hence, the transition can be observed (Figure 2.8 A). The strong peak in the UV region, at 320 nm, corresponds to the $\pi\pi^*$ transition ($S_0 \longrightarrow S_2$).

Upon illumination with UV light, the spectrum starts to change. The peak at 320 nm shifts further into the UV, to 280 nm. The $n\pi^*$ transition stays at the same spectral position, but gets more intense. This is an indication of the geometric rearrangement of

the molecule from the *trans* to the *cis* form. The benzene rings move out of the plane and hence the symmetry is lifted. The back reaction can be initiated by illuminating with blue light (440 nm). Furthermore, the *cis* state is metastable and at room temperature, azobenzene slowly converts back to the *trans* form.

The exact mechanism of the interconversion is still not fully understood. The process is completed within several ps and the quantum yields of isomerization depend on the energy level, the molecule is excited to. After excitation of a *cis* state molecule, the *trans* state is reached with a probability of ≈50 %.[84] For the isomerization from *trans* to *cis*, the quantum yield upon $\pi\pi^*$ excitation is ≈12 % and upon $n\pi^*$ excitation ≈25 %.[84] A lower quantum yield after excitation into the the $S_2$ state compared to excitation into the $S_1$ state is a violation with the Kasha-Vavilov rule,[85] a symptom of the complexity of isomerization mechanism. The quantum yield furthermore depends on temperature, solvent viscosity and solvent polarity,[86] but the isomerization still works under strong steric constraints.[83]

The different quantum yields suggest, that multiple decay paths exists that are selectively activated, depending on the excitation energy. Upon $n\pi^*$ excitation, a part of the excited population can undergo isomerization to the *cis* state via concerted motion that includes changes in both the C – N = N – C dihedral angle and the N = N – C angles simultaneously.[87] Recent experiments suggest, that $\pi\pi^*$ excitation opens up an additional decay channel to the *trans* ground state that is inaccessible upon $n\pi^*$ excitation.[88] The population is then split up into a part that takes this channel, while the other part decays to the $n\pi^*$ state and then via the same pathway as mentioned above to the ground state. A simplified diagram of this process is shown in Figure 2.8 B.

The important aspect to note is, that there is a finite probability of ending in *trans* or *cis* state after excitation to any state. The difference in wavelength of the $\pi\pi^*$ transition allows to generate >90 % of *cis* isomers in a population of azobenzene molecules. The largest fraction is achieved, when illuminating close to the minimum of the *cis* state absorbance at ≈365 nm. When an excited state takes one of the multiple pathways to the *cis* state, the molecule is essentially trapped in this state, because it has only negligible absorbance at this wavelength (Figure 2.8 A). The back reaction is on the other hand efficiently enabled by exciting to the $n\pi^*$ state, with substantially higher absorbance in the *cis* state compared to the *trans* state. The behavior of the ensemble is thus always depending on the wavelength, the light intensity and the length of the illumination. Switching between the two photostationary states (PSSs) with the maximum content

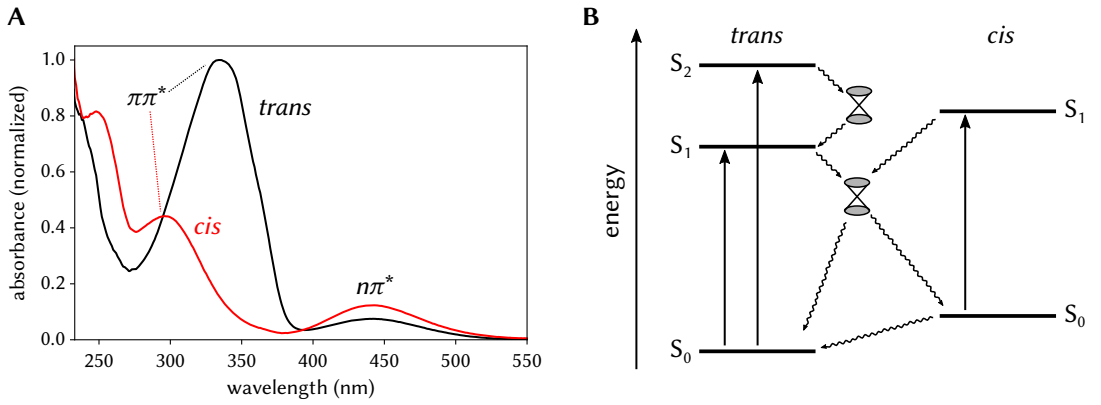


**Figure 2.8: Absorption spectra and energy levels of *azo*-PC. (A)** Absorption spectrum of an azobenzene derivative, *azo*-**PC**. The *cis* spectrum is obtained after extended illumination with UV light. **(B)** Simplified illustration of the energy levels. The *cis* state is metastable and will relax slowly to the *trans* state. The transitions between the energy levels are mostly non-radiative via conical intersections.

of either of the two isomers is usually achieved by exciting "long enough" (i.e. until the absorbance spectrum doesn't change any more) with an illumination source with the "best" wavelength. Using multiple wavelength ranges with controlled intensity ratios, on the other hand, allows to control every desired PSS in between.

### 2.2.2 The photoswitchable phospholipid *azo*-PC

Photoswitchable molecules have been used in the past to control membrane properties. The principle is in most cases the similar: Several different amphiphilic molecules have been synthesized, that either assemble as a membrane itself, or intercalate into a membrane. Changes of the basic membrane properties, as discussed above, are then reported upon illumination with light, attributed to the isomerization of the photosensitive molecule. The first experiments with photoswitchable lipids reported on the reversible size change and the photoinduced permeability of vesicles containing these lipids.[25,89] Later on, aspects like morphological changes or domain formation in a membrane have also been investigated.[28,29,90,91]

In most cases, the photoswitchable molecule was used just as an additive to a known bilayer system, because synthesized lipids do not sustain a membrane by themselves. In addition, the yields for lipid synthesis have been presumably low, preventing a thorough study of a photoswitchable membrane system. Recently, we started to use a

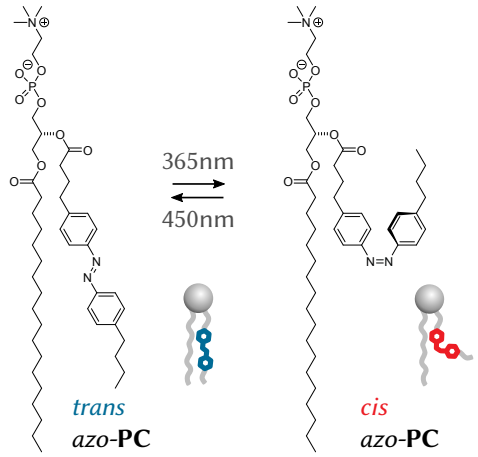


**Figure 2.9: Molecular structure of *azo*-PC.** The phosphocholine lipid contains a saturated fatty acid at the *sn*1 position and an azobenzene group at the *sn*2 position. The switching properties of the photolipid are very similar to azobenzene. Isomerization to the *cis* state is facilitated by UV light, while the back-reaction is efficiently initiated by illumination with visible light. The azobenzene group mimics a unsaturated double bond, that can also exist in the *trans* or the *cis* state.

photoswitchable phosphocholine lipid, termed *azo*-**PC**, to explore dynamical membrane processes. A new strategy was developed for the synthesis of *azo*-**PC**, which contains an azobenzene group in the acyl chain at the *sn2* position (the synthesis is outlined in section A.2).[92]

The photoswitchable lipid ("photolipid") retains most of the properties of azobenzene, with slight shifts in the absorption peaks (Figure 2.8). The $S_0 \longrightarrow S_2$ transitions are located at 340 nm for the *trans* state and at 295 nm for the *cis* state, respectively. The $S_0 \longrightarrow S_1$ transitions remain both at 440 nm, but the *trans* state carries , unlike azobenzene, some oscillator strength, due to the lifted symmetry of the molecule. Isomerization is most efficiently facilitated by illumination at 365 nm and 440 nm respectively.

Most importantly, *azo*-**PC** sustains bilayers at 100 % photolipid concentration, in contrast to lipids containing an azobenzene group in both acyl chains, for example. Being independent of a host lipid renders it possible to carry out a thorough investigation of the full range of bilayer properties as has been done extensively for standard model lipids like DOPC or DPPC. Furthermore, steric hindrance, which can prevent the isomerization of azobenzene in self assembled monolayers,[93] does not inhibit the isomerization in lipid bilayers. These unique properties allow to study the *response* of a photosensitive membrane to controlled and precise external stimuli, exerted by light.

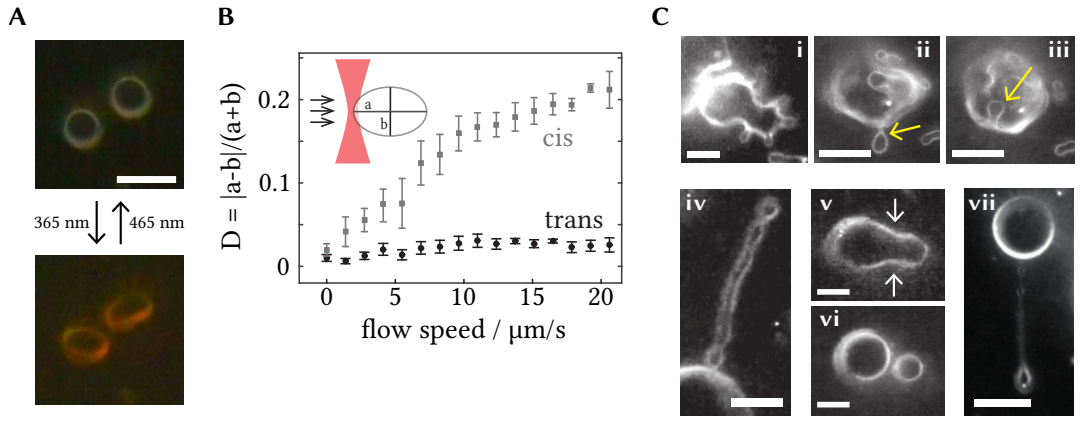


**Figure 2.10: Mechanical properties of *azo*-PC GUVs.** **(A)** GUVs consisting of 100 % *azo*-**PC** fluctuate and deform upon illumination with UV light. The process is reversible after illumination with blue light when the deformations are small. (scale bar = 5 µm) **(B)** The elongation of a vesicle held by an optical tweezer in an external flow is sensitive to the phase state of the membrane. The increased aspect ration in the *cis* state hints towards a lower bending rigidity. **(C)** By varying the experimental conditions, several different types of mechanical deformations are possible. Several different budding transitions (**i-iii**), pearling transitions (**iv**), neck formation (**v**) and vesicle splitting (**vi**) have been observed. Additionally, vesicle tubes can be pulled from *cis* state vesicles (**vii**). These results have been reported in Pernpeintner *et al.*[94]

In first experiments, we probed the mechanical properties of photoswitchable GUVs.[94] Upon illumination, GUVs consisting of 100 % *azo*-**PC** start to fluctuate strongly, indicating a softening of the membrane. By using optical tweezers,[95] the bending moduli of the isomeric states were calculated, confirming the softening of the membrane. Furthermore, many morphological changes like budding and invagination could be induced with light. Pulling membrane tubes out of *cis* state vesicles act as a storage of mechanical energy, that can be retrieved by illumination with blue light.

Thorough investigation of further membrane properties of *azo*-**PC** lipid bilayers was the goal of the experiments presented in this thesis. The main focus was put on the ability to form domains and the diffusional properties of these membranes. Finally, the mechanism, which is responsible for the photoinduced permeability of GUVs is discussed.

## 2.3 Dipole coupling in dye aggregates

In 1936, E.E. Jelly discovered, that the optical properties of pseudoisocyanine chloride in aqueous solution change depending on the concentration.[96] The absorption maximum shifted to lower energies and became sharper and more intense at the same time This was independently also discovered by Scheibe *et al.*[97] and quickly identified to be due to the self-assembled structure of the dye. Nowadays, assemblies with such a behavior, a pronounced redshift of the aggregate band compared to the monomer band, are generally termed J- or Scheibe aggregate. The reverse process, shifting of the absorption maximum to lower wavelength, is termed H-aggregate (H from *hypsochromic*). In contrast to J-bands however, H-bands usually exhibit a broad vibrational structure.

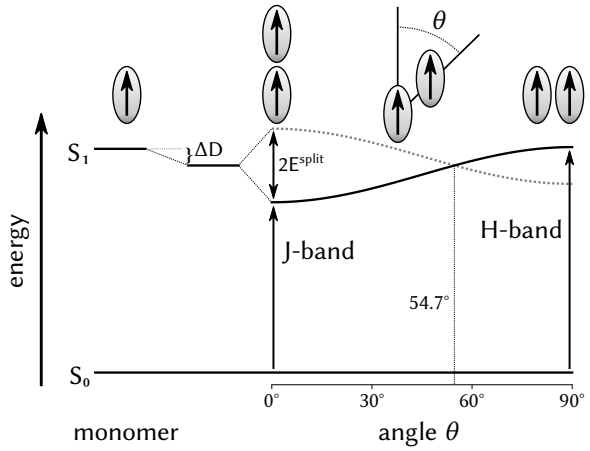


**Figure 2.11: Optical transitions of aligned molecules.**[98] The excited state energy of dimers with parallel transition dipoles shifts by $\Delta D$ to lower values compared to the monomer due to van der Waals interaction. Additionally, the excited state splits into a symmetric and an antisymmetric part. The energies associated to the two states depend on the angle $\theta$ between the displacement vector and the transition dipole vector. Optically allowed is only the transition to the antisymmetric state, giving rise to J- and H-bands of molecular aggregates.

### The dimer model

The direction of the shift can be calculated by considering coupling of two molecules in the point-dipole approximation, as described by the *molecular exciton theory*.[99] For a dimer consisting of two (identical) molecules $u$ and $v$ with ground state wave-function

$\Psi_G = \psi_u \psi_v$, the Hamiltonian is given by

$$H = H_u + H_v + V_{uv}\,. \tag{2.26}$$

$H_u$ and $H_v$ are the Hamiltonians for the isolated molecules and $V_{uv}$ is the interaction potential. In the molecular exciton theory, the latter is approximated by the point-dipole point-dipole terms of the multipole expansion. The energy of the ground state is then given by

$$\begin{aligned} E_G &= \iint \psi_u \psi_v H \psi_u \psi_v \,\mathrm{d}\tau_u \,\mathrm{d}\tau_v \\ &= E_u + E_v + \iint \psi_u \psi_v V_{uv} \psi_u \psi_v \,\mathrm{d}\tau_u \,\mathrm{d}\tau_v\,, \end{aligned} \tag{2.27}$$

with $E_u$ and $E_v$ being the ground state energies of the isolated molecules, respectively. The last terms describes the decrease in interaction energy due to van der Waals interaction. For the excited state, the wave-function splits into a symmetric and an anti-symmetric state.

$$\begin{aligned} \Psi_E^s &= \frac{1}{\sqrt{2}} \left( \psi_u^\dagger \psi_v + \psi_u \psi_v^\dagger \right) \\ \Psi_E^a &= \frac{1}{\sqrt{2}} \left( \psi_u^\dagger \psi_v - \psi_u \psi_v^\dagger \right) \end{aligned} \tag{2.28}$$

where $\psi_u^\dagger$, $\psi_v^\dagger$ are the monomer excited state wavefunctions of molecules $u$ and $v$, respectively. With these wavefunctions, the energies of the Hamiltonian as given in Equation 2.26 are

$$\begin{aligned} E_E^s &= E_u^\dagger + E_v^\dagger + \iint \psi_u^\dagger \psi_v \, V_{uv} \, \psi_u^\dagger \psi_v \,\mathrm{d}\tau_u \,\mathrm{d}\tau_v + \iint \psi_u^\dagger \psi_v \, V_{uv} \, \psi_u \psi_v^\dagger \,\mathrm{d}\tau_u \,\mathrm{d}\tau_v \\ E_E^a &= E_u^\dagger + E_v^\dagger + \iint \psi_u^\dagger \psi_v \, V_{uv} \, \psi_u^\dagger \psi_v \,\mathrm{d}\tau_u \,\mathrm{d}\tau_v - \iint \psi_u^\dagger \psi_v \, V_{uv} \, \psi_u \psi_v^\dagger \,\mathrm{d}\tau_u \,\mathrm{d}\tau_v\,. \end{aligned} \tag{2.29}$$

The first integral is again the van der Waals interaction energy. The second integral leads to splitting of the excited state energies, which is the dipole-dipole interaction term[99]

$$E^{split} = \frac{\vec{\mu}_u \cdot \vec{\mu}_v}{|\vec{r}|^3} - \frac{3\left(\vec{\mu}_u \cdot \vec{r}\right)\left(\vec{\mu}_v \cdot \vec{r}\right)}{|\vec{r}|^5} \tag{2.30}$$

$\vec{\mu}_u$ and $\vec{\mu}_v$ are the transition dipoles and $\vec{r}$ is the vector separation of both monomers. The transition energies are then given by the difference between the ground and the excited state.

$$\Delta E = \Delta E^M + \Delta D \pm E^{split} \tag{2.31}$$

where $\Delta E^M$ is the energy difference of the monomers and $\Delta D$ the difference of the van der Waals interaction energy. The transition energy is therefore decreased and splits depending on the angle between the two monomers (Figure 2.11). Only the transition to the antisymmetric excited state is possible, because of the symmetric wavefunction of the ground state.

While very simple, the model captures the energy shift of J- and H-aggregates and works also for larger aggregates. The band shape of the aggregates can be estimated by taking the vibrational states into account. For the J-band, the shape of the absorbance narrows in the strong coupling regime, when the aggregate absorption is shifted to a region of low monomer absorption.[100] The absorption of H-aggregates is less well understood, but a higher transition energy of the aggregate can couple to vibrational modes of the monomer, leading to a richer vibrational structure of the aggregate absorption spectrum.

# Chapter 3

# Preparation and characterization of photolipid membranes

Working with novel types of molecules requires new protocols for the characterization or at least adaption of known procedures for the specific system. In the first part of this chapter, novel protocols to generate photoswitchable bilayer systems, based on *azo*-**PC**, are described. Characterizing a photosensitive system with light is challenging, because the interaction of the probing light with the sample can also change its properties. In the second part of this chapter it is therefore described, which optical and spectroscopic techniques have been used to characterize the samples, and how they are adapted to minimize the isomerization of the sample.

## 3.1 Preparing model bilayer systems

### Synthesis of giant unilamellar vesicles with electroformation

Giant Unilamellar Vesicles (GUVs) are often used as cell model systems, because they are relatively easy to prepare and the size is similar to real cells. "Giant" seems to be contradictory at first given the typical size of GUVs, between 1 µm and 100 µm, but can be explained by taking into account the thickness of the bilayer. A typical lipid bilayer is only 3 nm thick[101] and therefore several orders of magnitudes smaller than the diameter, but vesicles are remarkably stable over weeks in solution. In fact, GUVs can still be found in samples stored for over a year at 4 °C.

Several methods exists to prepare GUVS, most notably by hydrating a lipid film ("gentle hydration"), assisted by an electric field ("electroformation") or from water oil emulsions.[102] Here, the electroformation method has been used, due to its simplicity, the high yield of unilamellar vesicles with the preferred size and the purity of the bilayer. Shortly after recognizing that lipid bilayers start to swell in an electric field, Angelova *et al.* introduced the idea of using AC electric fields to aid the formation of GUVs.[103,104] The mechanism is depicted in Figure 3.1.

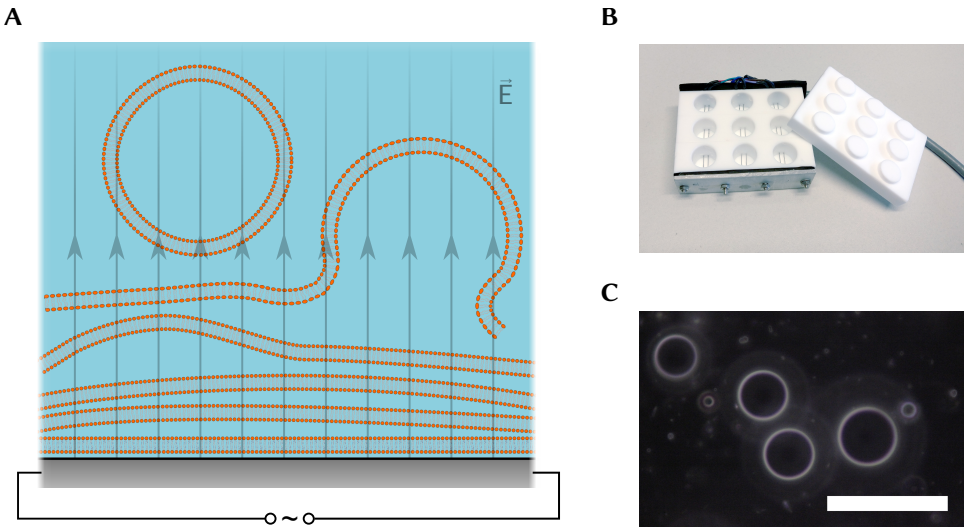


**Figure 3.1: Preparation of GUVs with electroformation.** **(A)** Lipid Bilayers, stacked on a platinum electrode, start to detach from the surface and form vesicles upon hydration. An actuated electric field assists the process, forming large and unilamellar vesicles. **(B)** Platinum wires are spanned across nine chambers, allowing for the simultaneous preparation of different samples with otherwise identical settings. **(C)** Dark-field images of GUVs consisting of DPhPC. Scale bar = 50 µm.

For this work, a home built chamber made of polytetrafluoroethylene (PTFE) was used to prepare the vesicles. In order to apply the electric field, platinum wires with a diameter of 0.5 mm are spanned with a distance of 3 mm in the PTFE chambers. Since vesicles are sensitive to osmotic pressure, the chamber can be sealed to prevent evaporation and hence an increase in osmolarity of the extra vesicular solution during electroformation.

The desired lipid composition is prepared at a concentration of 6.36 mM in chloroform and 6 µl of this solution is spread drop wise on the wires. For reference, the

chemical structure of all lipids used within this work is depicted in section A.3. After evaporation of the solvent, the lipids form stacked layers on top of the conducting surface. Thereafter, the lipids are hydrated by adding 1.5 ml of pre-heated aqueous solution to the chambers. Adding sugar to the solution increases osmolarity, which increases the stability of the GUVs. Vesicles used for imaging were prepared in 300 mM sucrose and GUVs for patch-clamp measurements in 1 M of sorbitol. The chamber was closed and put on a hot plate. Temperatures were chosen sufficiently above the main phase transition of the used lipids if applicable. In general, higher temperature increases vesicle yield but also leads to evaporation of the solution, changing the sugar concentration. As a compromise, a temperature of 60 °C was usually chosen.

The platinum wires were connected to a function generator, which could be programmed with a specific protocol. The highest vesicle yield was achieved with a voltage of 3000 mV peak to peak at 5 Hz for 120 min, with a short ramp of the voltage from 0 mV to 3000 mV in the first 6 min and a continuous decrease of the frequency from 5 Hz to 1 Hz for the last 8 min. Immediately thereafter, vesicles are fully detached from the wires by gently pipetting a couple of times and then the suspensions are transferred to Eppendorf tubes. The vesicles are stored for further use at 4 °C or at room temperature, if a high melting lipid species is present.

The choice of the organic solvent, specifically the stabilizer for the chloroform, is the most critical step of the protocol. Stabilizers are necessary to scavenge toxic free radicals resulting from the decomposition of chloroform. Typical choices are ethanol at a concentration of at least 1 % or amylenes, effective already at a concentration of 100 ppm.[105] Since ethanol evaporates slower than chloroform,[106] its concentration increases when the dissolved lipids are spread onto the platinum wires. The increased ethanol concentration hinders the formation of stacked layers of lipids on the wires. Consequently, the yield of vesicles was very low for electroformation with ethanol stabilized chloroform. Amylenes on the other hand have a lower boiling point than chloroform[106] and the yield of GUVs was usually very high.

## Breaking down vesicles with ultrasound

For further experiments, small unilamellar vesicles (SUVs) are used as membrane model systems. They can be prepared at relatively high concentrations and they have a rather narrow size distribution. Several methods exist to break down larger lipid

aggregates to form SUVs. Most commonly encountered are extrusion,[107] freeze-thawing or sonication.[108] Freeze-thawing is not suitable for saturated lipids and was therefore not tested.[109] Extrusion through a polycarbonate membrane gives in general a very narrow size distribution, but preliminary tests with *azo*-**PC** showed that this method is not suited to prepare photoswitchable SUVs. A large percentage of the lipids adhered to the filter or the filter support and therefore, the final concentration of SUVs was very low, canceling the main advantage of having a high concentration of lipids in solution. Therefore, tip sonication was used for all experiments employing SUVs. High power sonication generates acoustic waves which are strong enough to break down larger lipid aggregates. On the other hand, high amounts of energy are transferred to the solution leading to substantial heating. The two effects have to be balanced, to prevent oxidation but still to convert a large fraction to the homogeneous vesicle distribution.

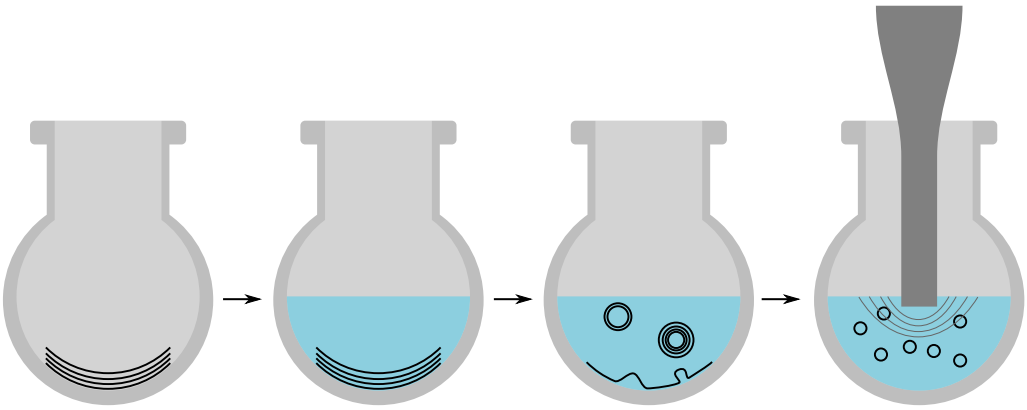

**Figure 3.2: Preparing SUVs with tip sonication.** Dried lipids form stacked bilayers on the glass surface. Upon hydration and mild sonication the lipids detach and are present as multilamellar vesicles. Intense tip sonication ruptures the vesicles, yielding a rather uniform distribution of SUVs.

As a general guideline for the development of the preparation route for photoswitchable SUVs, the protocol by Lin *et al.*[110] was used. A schematic of the process is shown in Figure 3.2. Similar to the preparation of GUVs, the lipids are first dried and then resuspended. Then, the lipids are transferred to the aqueous solution with a short sonication step. The resulting suspension is slightly opaque, indicating the existence of larger lipid aggregates.

Before sonication of the lipid suspension, the tip of the sonicator (Bandelin SONOPULS) was prepared. If the surface of the tip appears damaged, it was sanded with abrasive

paper until it is homogeneous. The tip was cleaned by two 30 s sonication step, first in a 1:1 mixture of ethanol and water, then in pure water. The efficiency of the sonication process can be optimized by changing the power while observing the cavitation. Optimal energy transfer is achieved when one can hear a high pitched sound and no big bubbles are created. The power was set usually between 25 % and 30 %.

The lipid suspension was transferred to a 15 ml centrifugation tube and sonicated twice for 30 s. Care was taken that the tip is immersed by at least 5 mm and does not touch the wall of the tube. When lipids with unsaturated double bonds were present, the sonication was done on ice. If the suspension was not clear after sonication, the procedure can be repeated after letting the sample cool down.

## Preparing supported lipid bilayers

The most common method to prepare supported lipid bilayers (SLBs) is vesicle fusion (Figure 3.3). For optical microscopy, the substrate of choice is borosilicate glass. By destabilizing the membrane of SUVs that are attached to the glass surface, the vesicles rupture, forming membrane patches on the substrate. When the density of SUVs is high enough, the patches merge until constituting a continuous bilayer. Parameters affecting the quality of the bilayer are the purity of the lipids and the homogeneity and size of the SUVs, the cleaning protocol of the substrate and the buffer solution used for the experiment.[111–114] Especially the influence of the substrate should be minimized as much as possible. Therefore, the substrates are usually rendered hydrophilic, to promote a thin water layer between the substrate and the SLB. Common methods are piranha etching, base etching, treating with plasma or UV illumination.[110] Due to the simplicity of the protocol and the sufficient quality of the resulting SLBs, plasma cleaning was the method of choice. Pre-cleaning of the substrates was still necessary for the successful bilayer formation. The glass cover slides are cleaned of any organic residues with successive sonication for 5 min in acetone, isopropanol and dd$H_2O$. After the final sonication step, the substrates are rinsed with dd$H_2O$, dried under a gentle stream of nitrogen and stored until further use.

Immediately prior to preparing a SLB, the substrate is put for 5 min in air plasma (Harrick Plasma, Basic Plasma Cleaner) at medium RF power setting. After mounting the substrate in a flow chamber, 200 µl of the vesicle suspension and 200 µl of PBS (2x) are drop casted onto the surface and mixed. The SUVs are allowed to settle for 30 min

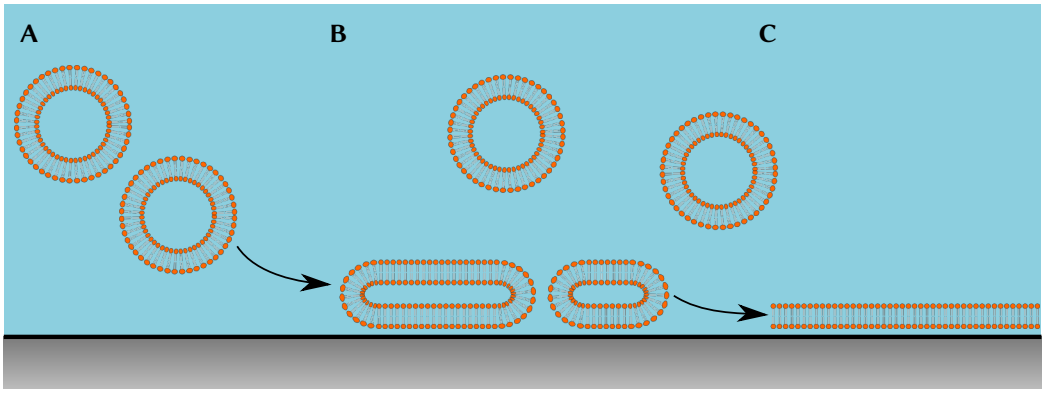


**Figure 3.3: Vesicle Fusion.** **(A)** The SUV suspension is added with PBS to a cleaned glass substrate. **(B)** The SUVs attach to the surface and rupture, forming small bilayer islands. At sufficient high concentrations, the individual bilayer patches start to merge to bigger structures. **(C)** When the surface is completely covered, the excess SUVs are rinsed away and ideally only the single bilayer remains.

at room temperature and then the remaining unbound vesicles are thoroughly rinsed with PBS (1x). The resulting supported lipid bilayers are used immediately for diffusion measurements, but are stable over several hours.

## 3.2 Imaging photolipid membranes

Most biological samples are hard to image with classical light microscopy. The refractive index of such samples is close to the refractive index of water and hence scattering of the object is weak.[115] For lipid bilayers, the situation is further complicated, because they are only 3 nm thin, much smaller than the wavelength of light.[101] Therefore, imaging techniques which use the phase information of the light have been invented. By enhancing the effect of changes in the refractive index, methods like phase contrast[116] or differential interference contrast[117] greatly improved on the imaging quality of cells. Also dark field microscopy, which only collects the scattered light of the sample, were used to enhance the contrast of biological samples.

All these methods can be used for imaging of GUVs (Figure 3.4). The circumference of the vesicles provides the longest path length where light can scatter and hence, vesicles can be observed as circles. On the other hand, the interaction path length of supported membranes, which are by design perpendicular to the propagation direction

of light, is very short and hence supported bilayers cannot be seen with standard light microscopy. Additionally, structures within bilayers, if present, do not change the refractive index by a large amount.

Nowadays, these problems are circumvented by using fluorescent labeling.[118] Fluorescence tags emit fairly isotropic in every direction and can be localized with nanometer resolution.[119] Furthermore, specific structures can be labeled by designing the molecule accordingly. There are some drawbacks, most importantly that "natural" systems have to be synthetically modified, which questions the validity of the results *in vivo*.[120] Nonetheless, the advantages in most cases far outweigh the drawbacks and tools for fluorescence observation are nowadays standard in any lab working in the context of cell biology.

## Fluorescence microscopy of dye-labeled lipid bilayers

Fluorescence imaging of lipid bilayers is conveniently facilitated by adding a small percentage of fluorescently labeled phospholipids to the lipid mix before preparing the sample. In addition to staining the bilayer itself, they can be used to highlight structure within the bilayer, as induced by e.g. phase separation, since most labeled lipids preferentially partition in specific phases of the bilayer.[121]

Due to the photosensitive nature of *azo*-**PC**, special requirements are needed for the imaging setup. For one, the excitation light should not interfere with the switching process. This is achieved by exciting in the green wavelength region, where *azo*-**PC** has almost no absorbance. A suitable dye is Texas Red 1,2-Dihexadecanoyl-*sn*-Glycero-3-Phosphoethanolamine (TR-DHPE). Lipids with a Texas Red headgroup partition preferentially into the $L_d$ phase in phosphatidylcholine based bilayer systems.[121] This dye also has a small absorbance peak in the UV and is hence additionally excited when isomerizing *azo*-**PC** from *trans* to *cis*. Furthermore, the illumination intensity has to be carefully controlled, balancing fluorescence excitation intensity and isomerization efficiency.

The main components of the microscopy setup are illustrated in Figure 3.5. The system is based on a conventional inverted microscope (Olympus IX81), equipped with a TIRF illumination unit. Fluorescence illumination can be facilitated with a mercury arc lamp (HBO 103/W) or two different diode lasers, one at 488 nm (Omicron LuxX, 100 mW) and one at 561 nm (Cobolt Jive, 100 mW). Filter cubes, equipped with suitable

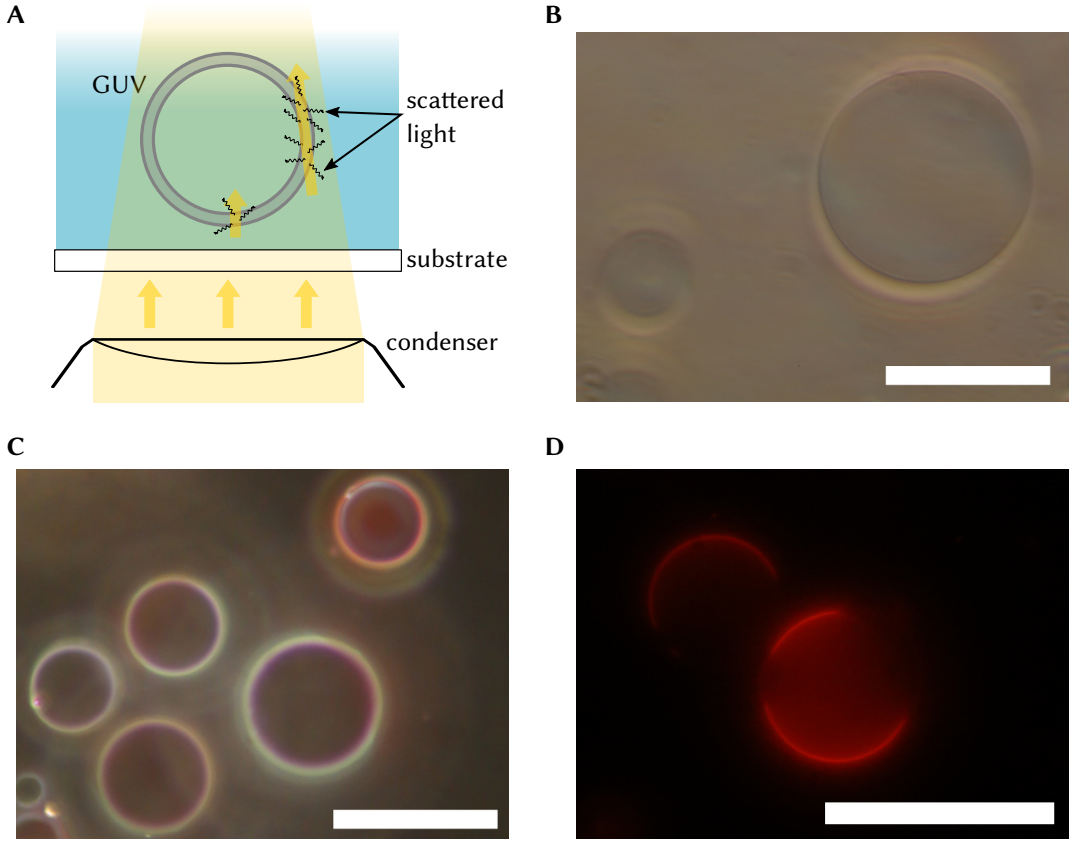


**Figure 3.4: Vesicle Imaging. (A)** Illustration of the interaction path length of light with a GUV. Only the circumference gives non-negligible scattering signal. **(B)** Phase contrast imaging of a GUV. In addition to the circumference, the inside of the vesicle is slightly darker, because the refractive index of the internal solution is larger in this case. **(C)** Dark-field image of several GUVs. The main contribution comes from scattering at the circumference. Fluorescence is visible as a faint red color. **(D)** Fluorescence imaging of phase separated vesicles. The signal comes solely from fluorescence dyes, no complete image of the vesicle can be observed. Scale bar = 30 µm.

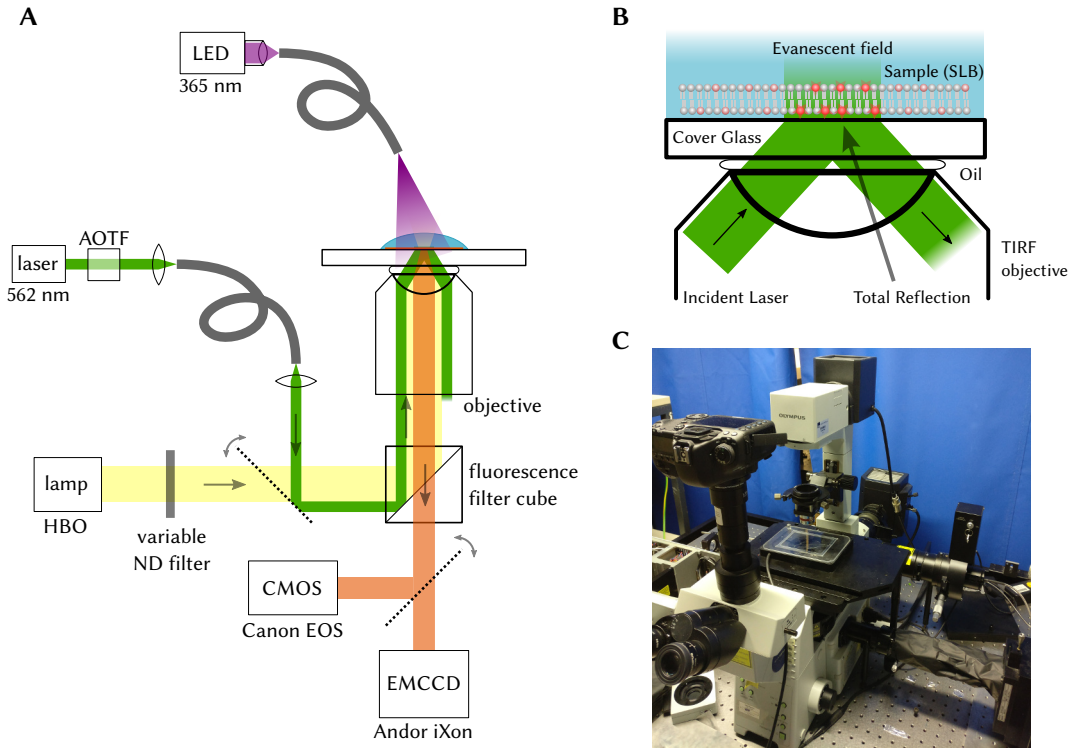


**Figure 3.5: Fluorescence Microscopy. (A)** Schematic of the main setup used for the experiments presented in this work. **(B)** Illustration of the principle of TIRF microscopy. The incident laser beam is totally reflected at the glass-water interface and only the evanescent field can excite fluorophores. **(C)** Photograph of the setup. Light sources enter from the back, while detection with the CCD is to the right.

dichroic filters, are used to direct the excitation light onto the sample and separate the excitation from the emission. For the laser, a multiband dichroic beamsplitter is used, allowing to use both lasers at the same time. Standard Olympus filter cubes are used for epifluorescence (U-MWU2, U-MNB2 and U-MWG2). Additionally, a high-power UV LED (365 nm, Prizmatix Mic-LED), coupled to an optical fiber, can be used to illuminate the sample from the top. This light source is, compared to the laser and the mercury arc lamp, not focused with an objective and hence the maximum illumination power is much lower. Additional longpass filters can be added to the emission path to block the 365 nm light.

The fluorescent light is directed to either of two cameras. For qualitative color pictures, a commercial CMOS camera (Canon EOS 550D or EOS 5D Mark IV) can

provide images at high resolutions. Under low light conditions, or to gather quantitative information, a monochrome scientific EMCCD (Andor iXon 897) is used.

In order to reduce background fluorescence, imaging of SLBs is best facilitated with total internal reflection (TIR) illumination. The excitation laser is coupled into the microscope slightly off-center and focused on the back-focal plane of the objective. In this configuration, the laser is guided onto the sample substrate at a high angle (Figure 3.5 B). Above a critical angle $\theta_c$, the light is totally reflected at the glass-water interface. Beyond the surface boundary, an evanescent field decays exponentially into the medium. This field excites fluorophores sitting close to the surface of the substrate, which is ideal for SLBs. Since the field is confined within a few tenths of nanometers, the background noise is strongly suppressed.

## 3.3 Characterization of azobenzene containing samples

In addition to the setup described above, several other techniques were used to characterize lipid samples. *Azo*-**PC**, just as azobenzene, was directly characterized by its absorbance spectrum. An UV-vis spectrophotometer (Cary 60 or Cary 5000) was employed to obtain these spectra for bulk solutions. The lipid suspensions were measured in quartz cuvettes (Hellma Analytics), for high UV transmission, with a light path length of 2 mm or 10 mm. The fluorescence of the staining dyes was measured with a fluorescence spectrophotometer (Cary Eclipse). A defined excitation wavelength was set via a monochromator, focused on the sample cuvette and the resulting the fluorescence was analyzed perpendicular to the excitation axis with another monochromator.

The size of the SUVs can be characterized by dynamic light scattering (DLS).[122] A laser is illuminating a sample solution containing the samples of interest and the scattered light is detected at a defined angle. Due to the Brownian motion of the particles, the detected signal fluctuates. By taking the autocorrelation of the time trace of the signal and fitting appropriate models, the size distribution of the particles can be obtained. DLS measurements for this work were performed on a Zetasizer Nano ZS (Malvern) in standard 10 mm cuvettes. The instrument employs a 633 nm laser and equilibrates the sample previous to the measurement to a set temperature.

## Probing membrane mechanics with micro-pipette aspiration

The mechanical properties of membranes were probed with micropipette aspiration.[123,124] A vesicle, attached to a micropipette, was exposed to a controlled pressure. From the elongation of the membrane tube in the pipette in response to the pressure, the bending rigidity and the area expansion modulus were calculated.

The experimental setup is shown in Figure 3.6 A. The micropipette (Hilgenberg GmbH) was positioned with a manual micropositioner. The pressure applied to the pipette was controlled by the height difference between two reservoir tanks and monitored with a pressure transducer (DP15, Validyne, Inc.). The system was integrated an upright microscope (Zeiss Scope.A1) in phase contrast configuration. A CMOS camera (Canon EOS 550D) was used for imaging through a 100x water immersion objective (Achroplan 100x, W 1.00 NA, Ph3, Zeiss). The setup is decoupled from the environment by a platform, which actively suppresses vibrations (Halcyonics_i4, Accuron).

An example of an aspirated vesicle is shown in Figure 3.6 C. The mechanical bilayer properties are linked to the vesicle shape according to

$$\frac{\Delta A}{A} = \frac{k_b T}{8\pi k_c} \ln\left(1 + \frac{\tau A}{\pi^2 k_c}\right) + \frac{\tau}{K_A} \tag{3.1}$$

with $A$ being the vesicle surface area and $\Delta A$ the change in surface area induced by the membrane tension $\tau$. Bilayer in water undergo thermally excited out-of-plane fluctuations, or undulations, which depend on the bending rigidity $k_c$.[125] At low tension, the fluctuations decrease the effectively observed membrane area. At high tension values, the undulations are fully smoothed out and the linear reaction to the membrane tension, characterized by the area expansion modulus, dominates. From one measurement series, the bending rigidity and the area expansion modulus can thus be derived.

From the elongation of the membrane tube in the pipette, the surface area change and the membrane tension can be extracted according to

$$\tau = \frac{D_P}{4\left(1 - \frac{D_P}{D_V}\right)} \Delta p \quad \text{and} \tag{3.2}$$

$$\Delta A \approx \pi D_P \left(1 - \frac{D_P}{D_V}\right) L_P \tag{3.3}$$

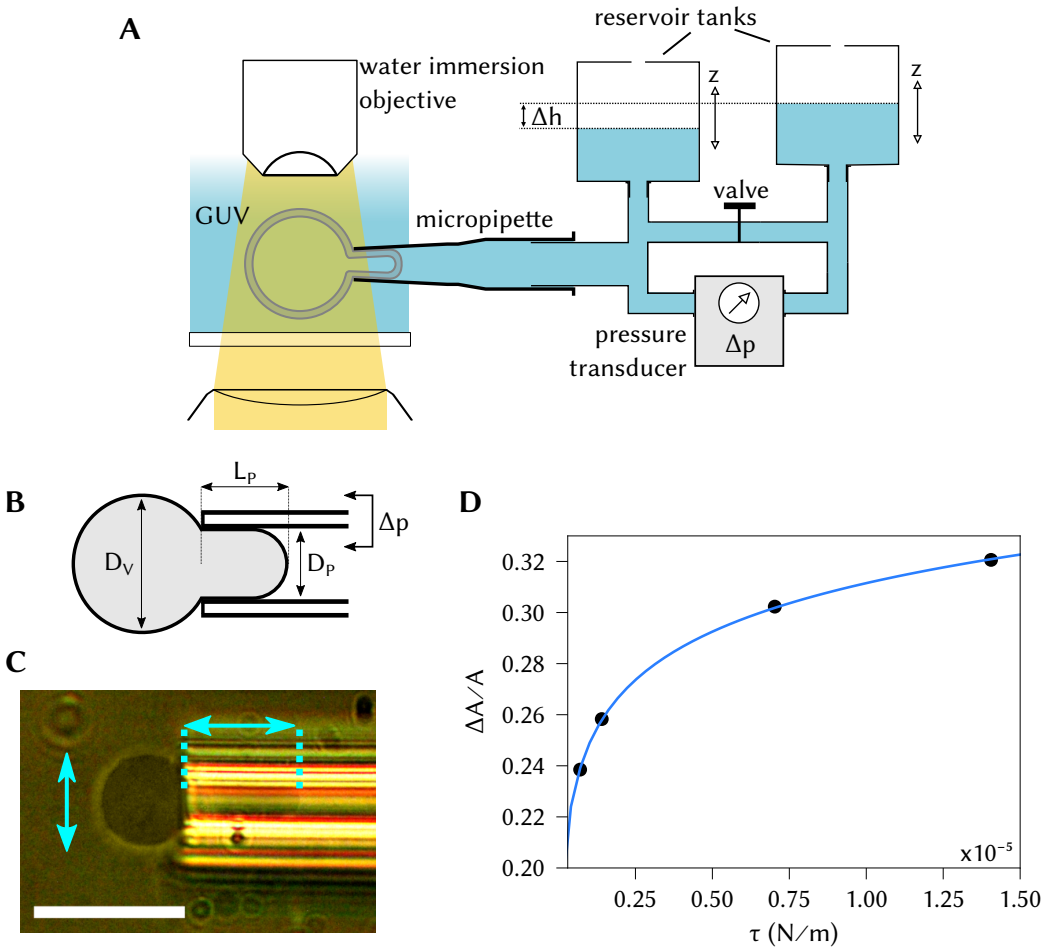


**Figure 3.6: Micropipette aspiration. (A)** A simplified schematic of the setup. Two reservoir tanks, which can be moved in $z$ direction, are connected to a micropipette. The height difference controls the applied pressure, which is monitored with a pressure transducer. The micropipette is used to aspirate GUVs. Imaging is done with a microscope in phase contrast configuration. **(B)** The relevant parameters for the calculation of the mechanical parameters are shown. **(C)** From the phase contrast images, the diameter of the GUVs and the length of the membrane tube are extracted. **(D)** The area expansion is plotted versus the applied tension $\tau$ (black circles). From the fit (blue), the mechanical moduli are extracted.

with $D_P$, $D_V$ being the diameter of the pipette and the vesicle, respectively, $L_P$ being the membrane tube in the pipette, and $\Delta p$ being the applied pressure.

## Determination of lateral diffusion in lipid membranes

Fluorescent Recovery After Photobleaching (FRAP) is a well known technique to measure the lateral diffusion of phospholipids in lipid bilayers. It was developed to measure the kinetics in cell membranes,[126] but can conceptually used for diffusion measurements of any fluorescent particle in solution.

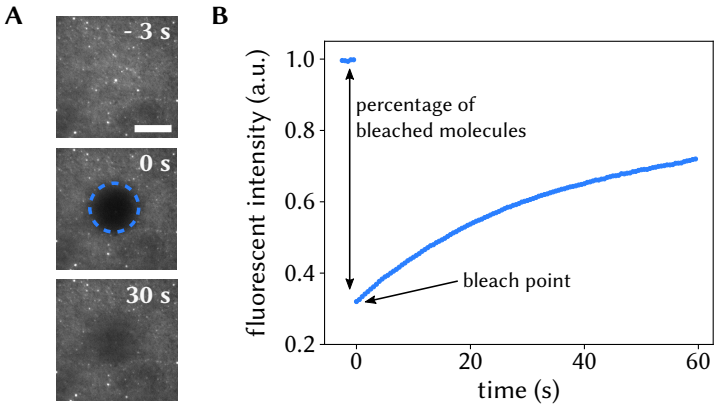


**Figure 3.7: Fluorescent recovery after photobleaching. (A)** Fluorescent images of a SLB consisting of *azo*-**PC** and TR-DHPE (1 mol%). The bleaching area is marked with a blue circle. **(B)** Normalized recovery curve of the FRAP experiment. From the recovery kinetics and the bleaching geometry, the diffusion coefficient is calculated. Scale bar = 10 µm.

In a FRAP experiment, a high intensity laser beam is used to photobleach a defined area in the fluorescent sample. Then, the fluorescence of the sample is recorded with highly attenuated excitation intensity to prevent further photobleaching. Due to the diffusion from the unbleached molecules into the bleaching area, the fluorescent intensity in this region slowly recovers. From the recovery curve, the diffusion characteristics of the fluorescent probe is determined.

While the conceptual idea and the experiment itself are quite simple, just using the recovery half-time obtained from an exponential fit is not enough to determine the true diffusion coefficient. The relation between the recovery time and the diffusion coefficient depend in general on the bleaching geometry.[127] For the uniform circular geometry as typically used throughout this work, a closed form expression was derived

by Soumpasis in 1983:[128]

$$f(t) = e^{-2\tau_D/t}\left[J_0\left(\frac{2\tau_D}{t}\right) + J_1\left(\frac{2\tau_D}{t}\right)\right] \tag{3.4}$$

with $J_0$ and $J_1$ being the first-order Bessel functions. $f(t)$ is the fractional recovery, defined as

$$f(t) = \frac{F(t) - F(0)}{F(\infty) - F(0)}\,. \tag{3.5}$$

The diffusion coefficient $D$ can then be derived from the characteristic diffusion time $\tau_D$ by $\tau_D = r_b^2/4D$ with $r_B$ being the radius of the bleaching area.

Throughout this thesis, a more sophisticated model for bleaching areas with arbitrary circular geometry is used. It is based on the Hankel transform of the diffusion equation (Equation 2.10) in polar form. The diffusion coefficient can then be calculated with the solution[129]

$$H(\kappa, t) = H(\kappa, 0)\exp\left[-4\pi^2 D\kappa^2 t\right]\,. \tag{3.6}$$

$\kappa$ is the spatial frequency and $H(\kappa, t)$ is defined as

$$H(\kappa, t) = 2\pi\int_0^\infty (1 - c(r, t))J_0(2\pi\kappa r)r\mathrm{d}r\,. \tag{3.7}$$

The fluorophore concentration $c(r, t)$ is proportional to the fluorescence intensity. The concentration is corrected for measurement artifacts like additional photobleaching or variation in the excitation light intensity. This method proved to be robust in terms of noise or intensity fluctuations and was hence chosen over the direct fit of Equation 3.4.

Here, FRAP is used to determine the diffusion coefficient of the phospholipids in a SLB (Figure 3.7). A FRAP experiment on a SLB is convenient, since the sample is homogeneous over the field of view and the geometry is simple and clearly defined. As the fluorescent probe, TR-DHPE is used, since it matches the 562 nm laser excitation wavelength and is reasonably photostable, but can still be photobleached within ms with unattenuated excitation light.

Imaging and bleaching is either performed in TIRF configuration or with epifluorescence. For epifluorescence, the excitation and bleaching intensity is controlled with suitable neutral density filters. For laser excitation, an acousto-optic tunable filter is used during bleaching and proper attenuation for the determination of the recovery curve. In either case, the bleaching geometry was defined by a pinhole in the excitation

path. A few frames are recorded previously to the bleaching pulse as reference. After bleaching, sufficient frames to resolve the recovery curve are recorded, usually until the bilayer is fully recovered. The frame rate is chosen to ensure good signal to noise. Data analysis was performed in MATLAB with a script based on the method described above.[129,130]

## Measuring ion permeability with patch-clamp

The patch-clamp technique was invented to measure the conductance of single ion channels in cell membranes.[131] In early implementation of the technique, a glass micro-pipette with a flame polished tip was used to pull a small membrane "patch" out of a cell. When using a clean and smooth glass surface and applying a moderate suction, the membrane patch attaches tightly to the glass surface, generating a so called *Gigaseal*. The patch is then electrically insulated from the environment with a resistance of several GΩ, allowing to measure the conductance state of individual protein channels.[132] In the voltage clamp configuration, the membrane potential is kept at a fixed voltage and the current through the membrane is measured with a sensitive amplifier. Patch-clamp has also been successfully used to study the conductivity of ion channels reconstituted in GUVs.[133] By carefully controlling the measurement conditions, even measurements in whole-cell (or rather whole-GUV) configuration can be performed.[134]

Here, a commercial variant of the standard method is employed. The micro-pipette is replaced with a micrometer sized hole in a planar glass chip.[135] Cells or GUVs are placed on top of the hole by suction and gravity. For cells, a combination of voltage- and pressure ramps leads to the Gigaseal configuration. GUVs usually burst upon contact with the glass and a Gigaseal is formed almost immediately upon contact. The voltage is applied and the current measured with an electrode consisting of AgCl. We used this setup previously to measure the temperature dependent permeability of standard lipid bilayers.[20]

The experiments were performed on a commercial device for planar patch-clamp (Port-a-Patch, Nanion), employing the standard NPC-1 chips as consumables. The provided protocols were used with small modifications, as presented briefly below. GUVs consisting of 100 % of *azo*-**PC**, filled with 1 M Sorbitol, are prepared by electroformation. KCl solution (100 mM, adjusted to pH 7.2 with KOH) is used as intra- and extravesicular solution. 5 µl of the vesicle suspension are pipetted into 10 µl of KCl solution on top of

the cap. Due to gravity, the vesicles sink to the glass surface and pressure of −20 mbar is used to guide a vesicle to the micrometer sized hole, leading in most cases to a Gigaseal configuration. Consequently, the external solution is carefully exchanged to achieve symmetric conditions. Measurements are performed at a voltage of 50 mV. The bilayer is illuminated with fiber coupled LEDs (365 nm and 465 nm). The illumination cycles are synchronized to data acquisition using the patch-clamp amplifier (HEKA EPC 10 USB).

## Measuring lipid monolayer properties

Lipid monolayers share many properties of their bilayer counterparts and have been successfully used to study the interfacial properties of membranes.[136,137] Monolayers are usually prepared in Langmuir-Blodgett troughs (Figure 3.8). These troughs provide a stable environment for amphiphilic molecules at the water-air interface. The area per lipid can be calculated from the area of the water-air interface and the amount of lipids added to the surface. Teflon spacers are used to compress the monolayer, while the surface pressure is measured with a tensiometer. The resulting surface pressure-area isotherm yields valuable information about the phase state of the monolayer.[138]

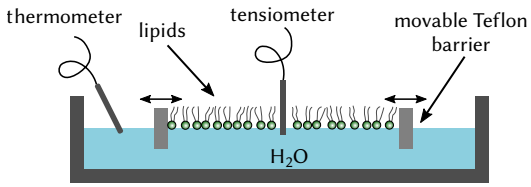


**Figure 3.8: Schematic of a Langmuir trough.** Lipids are deposited at the water-air interface. Teflon barriers are used to compress the monolayer, and the resulting surface pressure is measured with a tensiometer.

The experiments presented here have been performed in a commercial Langmuir trough (Microtrough G2, Kibron). The sample chamber is filled with $ddH_2O$ and movable Teflon spacers are used to compress the monolayer. Lipids are dissolved in chloroform at a concentration of $1\,mg\,mL^{-1}$. After adding the solution dropwise to the water surface, the chloroform evaporates and a monolayer forms. The monolayer reduces the surface tension of the water-air interface. The difference between the tension of the pure water surface and the lipid monolayer is the surface pressure and

is measured with a Wilhelmy probe. Switching between the *trans* and the *cis* state is achieved with fiber coupled LEDs (365 nm and 465 nm, as described previously), which illuminate the whole monolayer area. The surface pressure-area isotherms are constructed by compressing the monolayer and simultaneously recording the surface pressure.

# Chapter 4

# Reversible domain formation in multi-component photolipid membranes

Photolipids bear an exciting potential to elucidate how lipid bilayers react to changes of the lipid composition or intermolecular interaction. The physical properties of lipid membranes at thermal equilibrium are in general well understood.[31,51] A membrane of a living cell is however never at thermal equilibrium, driven by constant influx and efflux of phospholipids and the complex cell machinery coupled to the membrane. Changing the lipid conformation and thus their lateral interaction with light allows to manipulate a lipid membrane in a controlled environment.

Here, this concept is applied to investigate the domain formation of *azo*-**PC** in mixtures with standard lipids. At first, the effect of the bilayer structure on the optical properties of the photolipid are presented. Then, several lipid compositions and their ability to form macroscopic domains are explored and linked to the optical properties. Finally, the implications for the mechanical bilayer properties are discussed. The main findings presented throughout this chapter are published in *Langmuir*.[139]

## 4.1 Absorbance spectra of *azo*-PC in membranes

In order to characterize the effect of the lipid interaction on the optical properties of *azo*-**PC** in membranes, SUVs consisting of 100 % photolipids were prepared. The

absorbance of these suspensions was measured with a spectrophotometer. The spectra of the photolipid assemblies were compared to spectra of *azo*-**PC** monomers, dissolved in chloroform. SUVs yield higher concentrations of lipid per volume compared to GUVs and are therefore more suited for absorbance measurements. The *trans* state spectra were recorded in the dark adapted state, and the *cis* state spectra after illumination with LED light at 365 nm until no more changes of the absorbance spectra could be observed.

Notably, the main peak of the *trans* state spectrum ($S_0 \longrightarrow S_2$) was blue shifted by ≈20 nm compared to the spectrum of *azo*-**PC** in chloroform (Figure 4.1). The $S_0 \longrightarrow S_1$ transition gets weaker, but does not shift within the detection resolution of the instrument. The peak positions of the *cis* state spectra do not change. The shape of the peaks is also comparable, besides an increased absorbance in the wavelength region between 320 nm and 360 nm. Furthermore, a vibronic progression can be observed for the $S_0 \longrightarrow S_2$ transition of the *trans* state, which is more pronounced for the bilayer.

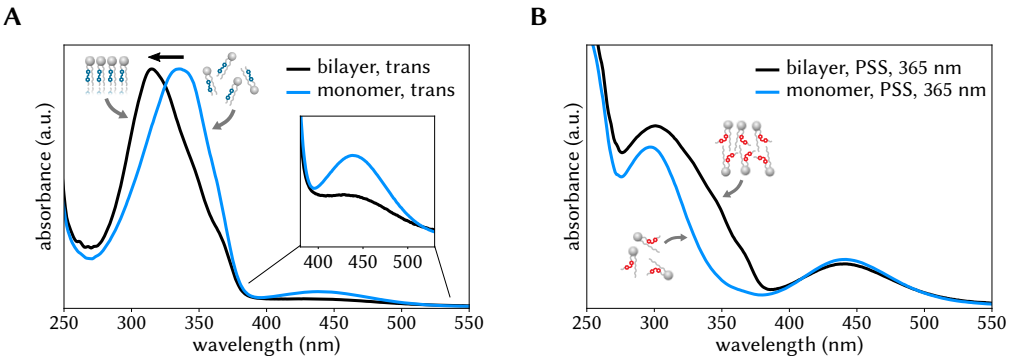


**Figure 4.1: Hypsochromal effects observed in *azo*-PC containing lipid membranes.** **(A)** The absorbance spectrum of bilayers consisting purely of *azo*-**PC** (black) is in the *trans* state blue shifted compared to the spectrum of the photolipid dissolved in chloroform. Additionally, the $S_0 \longrightarrow S_1$ transition is weaker for the bilayer. The spectra are normalized to the maximum of the $S_0 \longrightarrow S_2$ transition. This *hypsochromic* shift originates in the coupling of the transition dipole moments. **(B)** For the PSS after illumination with 365 nm, no shift can be observed.

This blue- or *hypsochromic* shift has already previously been observed for azobenzene groups in lipid membranes.[90,140] In these experiments, azobenzene was added as a surfactant to a host bilayer like DOPC. The shift of the absorbance peak has then been attributed to the formation of H-aggregates as physical aggregates of azobenzene in the membrane. In this study, the membrane consists purely of photoswitchable

lipids. The bilayer itself is a structure which exhibits a certain degree of order. The azobenzene units are therefore naturally arranged parallel to each other, which is an essential property of H-aggregates.

For the *cis* state, no shift of the $S_0 \longrightarrow S_2$ transition and no decrease of the $S_0 \longrightarrow S_1$ absorbance is observed. Hence, the *cis* state does not exhibit aggregation induced changes of the optical properties. The reason for this is likely to be found in the orientation of the transition dipole moments. For the *cis* state, the dipole moment is not aligned on the long axis of the molecule any more.[141] Additionally, the coupling strength is dependent on the magnitude of the transition dipole, which is lower for the *cis* state. Furthermore, membranes in the *cis* state are softer than membranes in the *trans* state,[94] hinting towards a lower degree of order, which also prevents the formation of H-aggregates.

An integral property for the application of photoswitchable molecules is the ability to *switch* between the isomeric states with light. The exact ratio of the isomeric conformers at the photostationary state depends on the ratio between the absorbance at the wavelength of irradiation. For azobenzene, it is possible to generate more than 95 % of *cis* state molecules by irradiation with UV light at the minimum of the *trans* state spectrum.[82] For blue light illumination, even higher concentrations of *trans* state molecules can be achieved.[82]

Since the isomer ratios after prolonged illumination are determined by the absorbance spectra, the photostationary state also depends on effects which change the optical properties of the photolipids. The shift induced by aggregation of *azo*-**PC** is quite substantial, altering the composition at the photostationary state

The difference between the positions of the $S_0 \longrightarrow S_2$ transition in the *trans* and the *cis* state decreases upon aggregation, since only the *trans* state transition is exhibits a blueshift for SUVs compared to monomers. Therefore, a higher percentage of *trans* state molecules is retained after illumination with 365 nm. At 465 nm, the $S_0 \longrightarrow S_1$ transition is relevant. For H-aggregates, the transition strength is decreased. The PSS after this excitation wavelength is therefore close to the pure *trans* state. From the relevant absorbance spectra, the isomer ratios can be calculated using the vibronic progression, which is present in the *trans*, but not in the *cis* spectra.[142] In a bilayer, 7 % of *trans* state molecules are retained after illumination with 365 nm, while in chloroform, only 3 % are in the *trans* state. The calculation of the ratio and of the pure *cis* state spectrum are presented in section A.1.

## Implications for the bilayer phase state

To further characterize the properties of H-aggregates, the optical shift was measured for mixtures with standard phospholipids. Dilute samples thus increase the average distance between the azobenzene units, thereby decreasing the coupling strength. A normal PC lipid like DPhPC is optically inert for the relevant wavelength regions of the transition dipoles of *azo*-**PC** and thus does not interfere with the dipole-dipole coupling between the azobenzene units.

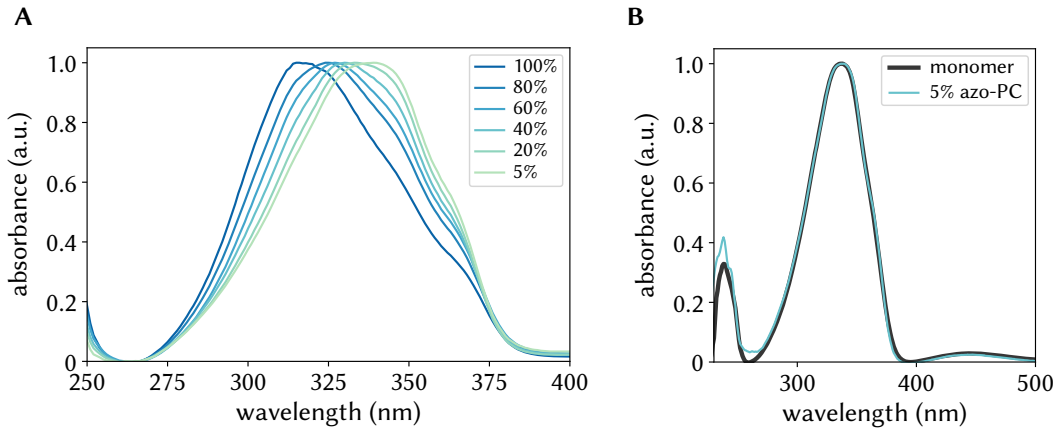


**Figure 4.2: Concentration dependent peak positions. (A)** The peak position of the absorbance of *azo*-**PC** vesicles depends on the local concentration and therefore the mean distance of the azobenzene units. Diluting a bilayer with an optical inert lipid, in this case DPhPC, leads to a shift of the $S_0 \longrightarrow S_2$ transition towards the monomer spectrum. The spectra are background subtracted and normalized to the maximum of the $S_0 \longrightarrow S_2$ peak. **(B)** For SUVs containing only 5 % *azo*-**PC**, the spectrum matches the spectrum of the photolipids in chloroform closely.

SUVs with mixtures of *azo*-**PC** and DPhPC, between 5 % and 100 % of the photolipid, were prepared and the absorbance of the samples in the *trans* state was measured (Figure 4.2 A). All spectra were obtained at room temperature. The maximum of the $S_0 \longrightarrow S_2$ transition shifts from 315 nm for the pure *azo*-**PC** sample to 340 nm at 5 % *azo*-**PC**. The spectrum matches the spectrum obtained in chloroform, where lipids are dissolved as monomers (Figure 4.2 B). The absorbance spectrum of a solution of vesicles containing *trans*-*azo*-**PC** therefore gives information about the local concentration of the photolipid in the membrane.

The local properties of a membrane are mainly determined by its phase state. A characteristic property of a phase in lipid bilayers is the order parameter of the acyl

chains.[143] A central requirement for the formation of H-aggregates is the parallel alignment of the transition dipoles and therefore of the acyl chains containing azobenzene. This was experimentally investigated by adding cholesterol. Cholesterol is known for its condensing effect, which decreases the area per lipid and thereby increases the chain ordering.[144,145]

For the absorbance measurements, SUVs consisting of *azo*-**PC** and cholesterol concentrations between 0 % and 40 % have been prepared in dd$H_2O$. Above 20 %, the SUV suspension is not stable any more and precipitates. The absorbance spectra are shown in Figure 4.3. For low cholesterol concentrations, the $S_0 \longrightarrow S_2$ transition is slightly blue shifted (≈1 nm) compared to SUVs without cholesterol. For precipitated suspensions, the transition is red shifted by 10 nm.

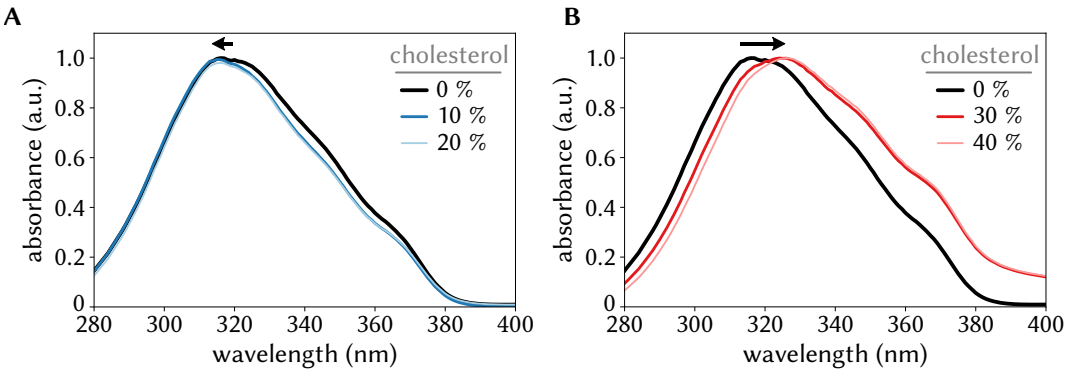


**Figure 4.3: Spectra of SUVs consisting of *azo*-PC and cholesterol.** **(A)** Up to 20 mol% cholesterol content, absorbance spectra of SUV suspensions exhibit a slight blue shift compared to the pure *azo*-**PC** SUVs. **(B)** For higher cholesterol concentrations, the peak position shifts to lower energies. The offset of the spectra is due to the scattering of the precipitated opaque lipid suspensions. The spectra are normalized to the maximum absorbance values.

These results show, that the absorbance spectra are sensitive to the phase state of the membrane. For low cholesterol concentrations, the absorbance spectra exhibit stronger H-type coupling, even though cholesterol effectively dilutes the sample. The condensing effect thus counteracts the increased spacing of the molecules due to the additional cholesterol molecules incorporated into the bilayer. For higher concentrations, the order of the molecules in the bilayer is decreased, manifested as a weaker H-type coupling of the azobenzene units.

## Isomerization kinetics in photolipid membranes

The population dynamics of any azobenzene derivative depends on the exact position and shape of the different transitions, as discussed in section 2.2. Therefore, the spectral shifts induced in photolipid membranes also affect the rate of isomerization. SUV suspensions from DPhPC and *azo*-**PC** were prepared as previously discussed, with the total lipid concentration being constant for all samples. The absorbance of these suspensions was measured continuously with a spectrophotometer. As a reference, the absorbance of *azo*-**PC** in chloroform was measured with the same lipid concentration. The dynamics were determined by illuminating with 365 nm or 465 nm, respectively, until the PSS is reached. The fiber output of the LEDs was positioned ≈2 cm above the cuvette (Figure 4.4 A). This geometry and the output power of the LED (≈80 mW) were kept constant throughout the experiment.

Upon UV illumination, the spectra changed continuously from the *trans* state to the PSS state (Figure 4.4 B). The switching dynamics were determined by measuring the time-dependent absorbance at 330 nm. For the isomerization from the *trans* to the *cis* state, clear differences between the individual samples were observed (Figure 4.4 C). The fastest switching rate is achieved for the molecules dissolved in chloroform. For the SUV suspensions, only samples with low *azo*-**PC** content exhibited monoexponential behavior, as is typical for azobenzene isomerization..[146,147] The time constant of the sample containing 5 % *azo*-**PC** was ≈9 s and increased for higher *azo*-**PC** concentration.

The switching kinetics deviated from monoexponential behavior for increasing fractions of *azo*-**PC**. The switching rate is slower in the beginning of the isomerization process. The dynamics are consistent with the spectral observations. With higher *azo*-**PC** content, the $S_0 \longrightarrow S_2$ transition of the *trans* state shifts to higher energies. The separation between the $S_0 \longrightarrow S_2$ peaks of the two isomers is therefore reduced and the absorbance ratio changes, leading to a lower switching rate from *trans* to *cis*.

For the reverse process, *cis* to *trans*, the switching rates were overall much faster and followed monoexponential behavior (Figure 4.4 D). The rates for the bilayer system were constant with a time constant of 4.4 ± 0.3 s, independent of the *azo*-**PC** content. The isomerization rate of *azo*-**PC** dissolved in chloroform is again faster compared to the rates of the photolipid aggregates. Since the $S_0 \longrightarrow S_1$ transition is not affected by the H-type coupling, the absorbance profile is essentially the same, independently of

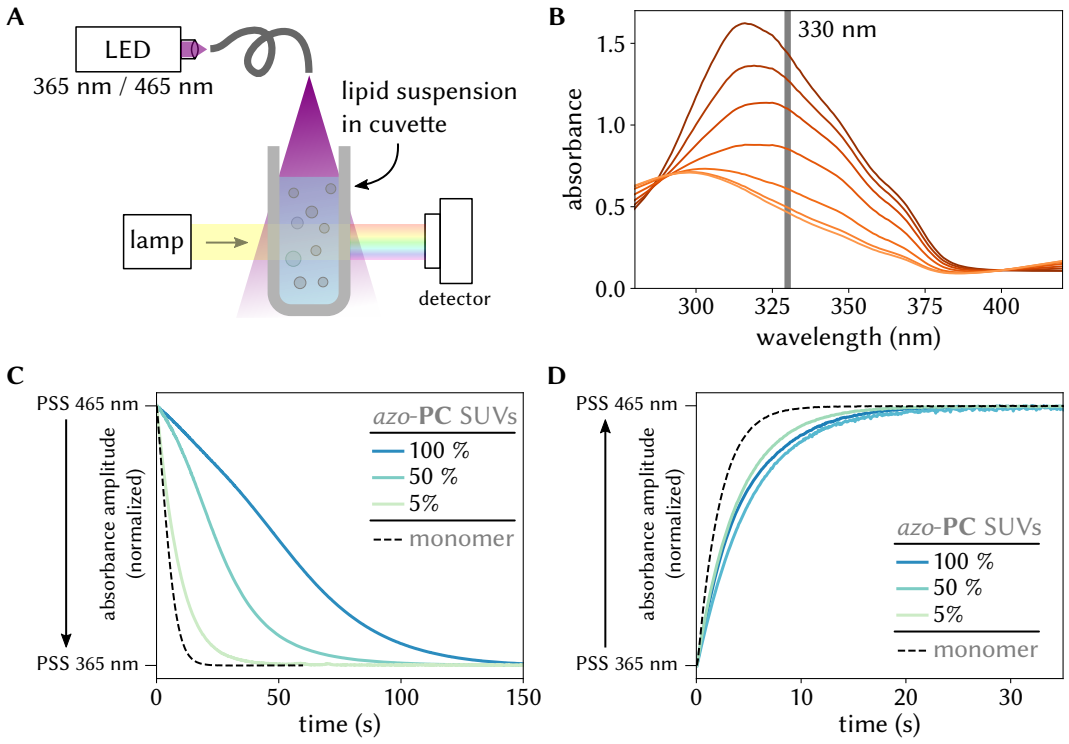


**Figure 4.4: Switching kinetics of aggregated *azo*-PC. (A)** Illustration of the setup used to examine the switching kinetics of *azo*-**PC**. The absorbance of the sample is measured with a standard spectrophotometer while illuminating with a fiber coupled LED. **(B)** Taking spectra after defined time steps shows the time evolution of the switching process. Monitoring the absorbance values at a defined wavelength, here 330 nm, allows to calculate switching rates. **(C)** The measurements show the absorbance of SUV suspension consisting of *azo*-**PC** and DPhPC while illuminating with 365 nm, the concentration of *azo*-**PC** is indicated. Absorbance values are normalized between the respective PSSs. For UV-A illumination, the rate shows a clear dependence on the aggregation state. **(D)** Switching from *cis* to *trans* by illuminating with 465 nm is only slightly different for SUVs with different *azo*-**PC** concentration, but still faster for monomers in chloroform.

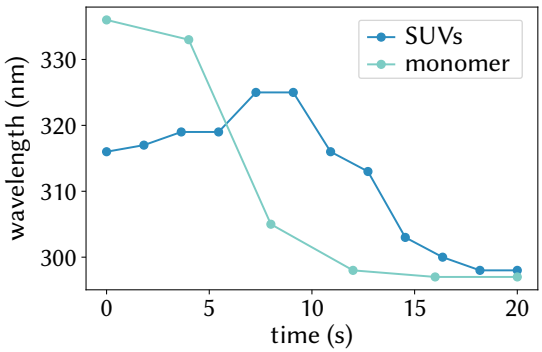


**Figure 4.5: Peak position during isomerization.** The peak position of the $S_0 \longrightarrow S_2$ is obtained from spectra after defined illumination doses, as shown in Figure 4.4. The time and therefore dose depended peak positions are shown for SUVs consisting of 100 % *azo*-**PC** and for monomers in chloroform. To compensate for the different switching rates at the same illumination condition, the time axis for the SUVs is scaled by 5.5.

the aggregation state of the system. The rate of the *cis* to *trans* isomerization is thus independent of H-aggregate formation.

The switching rates for *azo*-**PC** in chloroform is however faster than in bilayers in every case, even for low *azo*-**PC** content. For 5 % *azo*-**PC**, the spectra of the bilayer spectrum converges to the monomer spectrum (Figure 4.2). The different isomerization rates can thus not be explained by the different absorbance spectra alone.

A similar effect, which could explain this observation, is found in self-assembled monolayers containing azobenzene.[148,149] These monolayers gained a lot of attention due to the potential for applications in optical information storage[150] and molecular electronic switches.[151,152] One key aspect for the usefulness of these monolayers in real-world applications is their ability to isomerize efficiently. In several such systems, however, the isomerization is strongly hindered or even completely suppressed. In addition to the excitonic coupling of the dye molecules, this is attributed to the steric constraints within a tightly packed monolayer.[147,153] A fluid bilayer is not as rigid as a tightly packed monolayer, the switching rate is thus only reduced and switching not completely prohibited.

The deviation from the monoexponential behavior can again be explained by the formation of H-aggregates. Upon starting to isomerize the molecules, the concentration of *trans*-*azo*-**PC** decreases. Therefore, the coupling between the individual monomers weakens and the position of the $S_0 \longrightarrow S_2$ transition redshifts.

This is observed when monitoring the peak position during the illumination process (Figure 4.5). For *azo*-**PC** in chloroform, the peak shifts continuously from 336 nm to 297 nm upon UV illumination. The peak of the pure *azo*-**PC** bilayer shifts at first to higher wavelengths, from 316 nm to 325 nm. Only after this shift, almost half-way through the isomerization process, the peak blueshifts to its PSS at 298 nm.

In summary, the assembly of *azo*-**PC** into bilayer structures changes the optical properties of the molecule. Both the electronic levels and the isomerization pathways, governed by the energy landscape, are affected. In the following, it will be detailed, how these changes can be used to obtain information about the phase behavior of more complicated systems.

## 4.2 Domain formation in ternary photolipid membranes

The key for the optical effect induced in a bilayer is the intermolecular interaction between the azobenzene units. As discussed in section 2.1, the formation of domains is also governed by the interaction between the lipids. Since limited data on *azo*-**PC** is available, the phase behavior in ternary mixtures with a standard phospholipid and cholesterol was first examined. Phase separation leads to mixtures which are not isotropic and therefore to clustering of molecules. It was therefore tested, how non-isotropic mixtures affect the ability of *azo*-**PC** to form H-aggregates and lipid domains.

### Phase behavior of *azo*-PC, DPhPC and cholesterol

The domain formation in *azo*-**PC** membranes was investigated in GUVs prepared by electroformation as explained in section 3.1. Previous experiments have demonstrated, that the phase state of *azo*-**PC** membranes is fluid phase at room temperature.[94] In order to identify the lipid mixture, which lead to phase separation, GUVs containing a 4:4:2 ratio of *azo*-**PC**, a standard PC lipid and cholesterol have been prepared, labeled with 1 % TR-DHPE.

Mixtures containing DPhPC as the PC lipid show extensive domain formation. DPhPC is a saturated lipid and therefore less prone to photooxidation and hence a good candidate for fluorescence imaging. The fluorescence pictures, excited with green

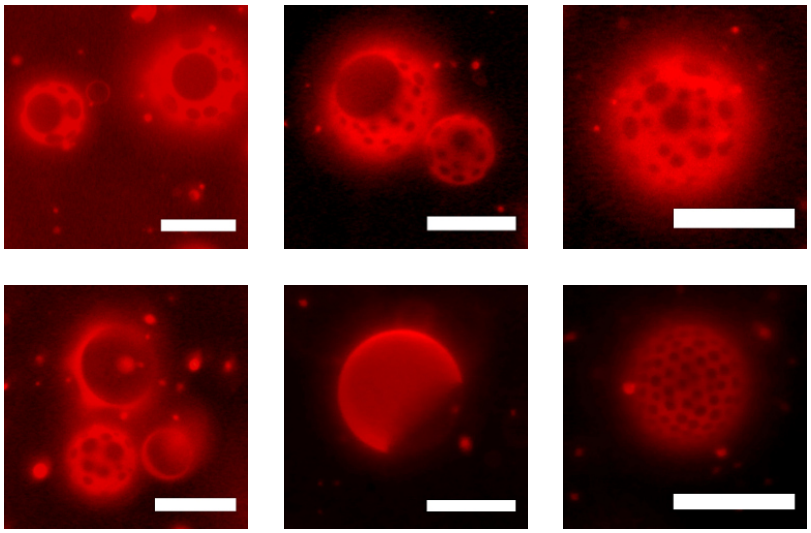

**Figure 4.6: Examples of ternary photoswitchable vesicles.** GUVs consisting of *azo*-**PC**, DPhPC and cholesterol exhibit spherical dark domains. Vesicles are phase separated completely, when left to settle at room temperature for a while. (scale bar = 20 µm)

light (510 nm - 550 nm) show dark spherical domains in otherwise bright membranes (Figure 4.6). Since TR-DHPE partitions preferentially into the $l_d$ phase[154] and DPhPC is only weakly miscible in $l_o$ domains due to its unusual acyl chain structure,[155] the dark domains are rich in *azo*-**PC** and cholesterol.

## Linking domain formation and absorbance spectra

Next, the behavior of the ternary mixture was further examined by exploring its phase diagram. As this is the first time, that this combination of lipids is investigated in detail, vesicles for large sections through the full phase diagram were prepared and characterized. The GUVs were synthesized as described in section 3.1 and individual GUVs were imaged with a fluorescent microscope. To link the phase behavior of the vesicles with their optical properties, absorbance spectra were taken from the resulting vesicle suspension.

Initially, the concentration of cholesterol was kept constant at 20 % and the concentrations of *azo*-**PC** and DPhPC were varied (Figure 4.7 B). Domains were observed between a 1:3 and a 3:1 ratio of *azo*-**PC** and DPhPC (Figure 4.7 A). The surface area

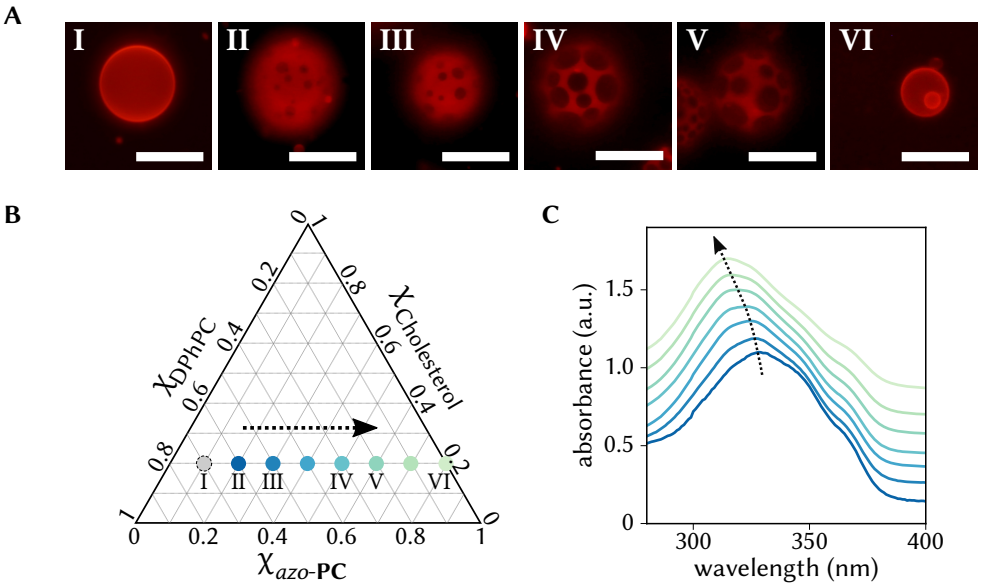


**Figure 4.7: Ternary mixtures with** 20 % **cholesterol concentration (A)** Examples pictures of ternary GUVs with different ratios of DPhPC and *azo*-**PC**. **(B)** The different lipid compositions are indicated in the phase diagram. The fluorescent images are indicated by roman numerals and the matching absorbance spectra are color coded. **(C)** Absorbance spectra of the GUV suspensions, as indicated in **(B)**. Spectra are scaled to match the peak height and offset for clarity.

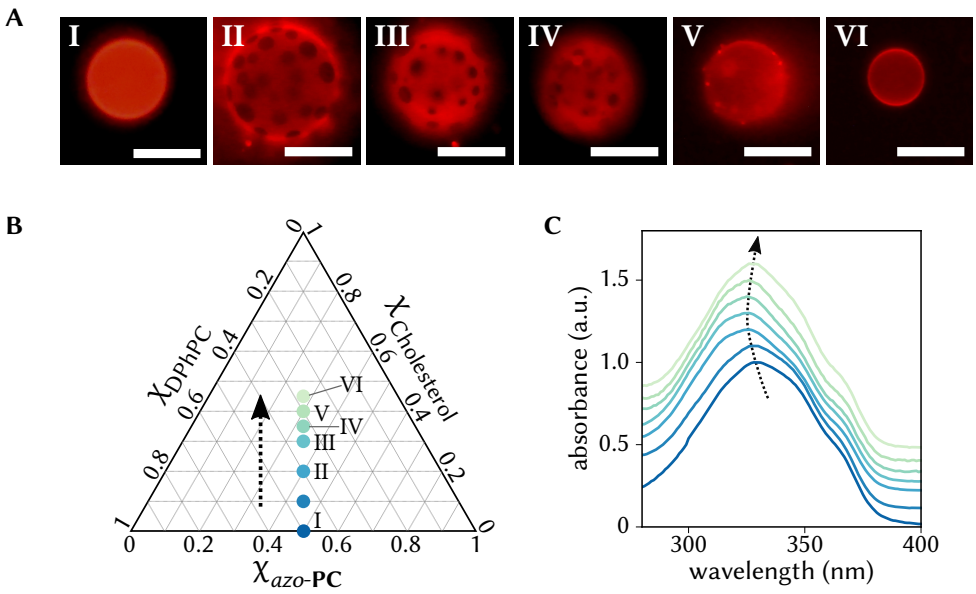


**Figure 4.8: Ternary mixtures with a 1:1 ration of *azo*-PC and DPhPC (A)** Examples pictures of ternary GUVs with increasing concentration of cholesterol. **(B)** Circles indicate the position of the employed concentrations in the phase diagram. The fluorescent images are indicated by roman numerals and the matching absorbance spectra are color coded. **(C)** Absorbance spectra of the GUV suspensions, as indicated in **B**. Spectra are scaled to match the peak height and offset for clarity.

covered with dark domains increases with the proportion of *azo*-**PC**, consistent with the assumption that the dark areas are domains with higher order and rich in *azo*-**PC**.

The absorbance spectra exhibit a hypsochromic shift of the $S_0 \longrightarrow S_2$ transition for increasing amounts of *azo*-**PC**, as is to be expected from the previous measurements of the binary lipid composition. This also demonstrates, that the phases, while distinct in their physical properties, are still mixtures of different lipids. Otherwise, the spectra would strongly blue shift upon the first indication of phase separation.

Next, the ration between DPhPC and *azo*-**PC** was kept constant at 1:1 and the concentration of cholesterol was varied. Domain formation was observed only for cholesterol concentrations between 10 and 35 mol% (Figure 4.8 A). The absorbance spectra show again differences, depending on the lipid composition (Figure 4.8 C). At low cholesterol concentrations, the $S_0 \longrightarrow S_2$ transition blue shifts with increasing cholesterol content, even though the concentration of *azo*-**PC** decreases. The shift coincides with the appearance of domains at ≈20 mol%. Further increasing the concentration of cholesterol leads to fewer domains, but the spectral signature remains the same. At

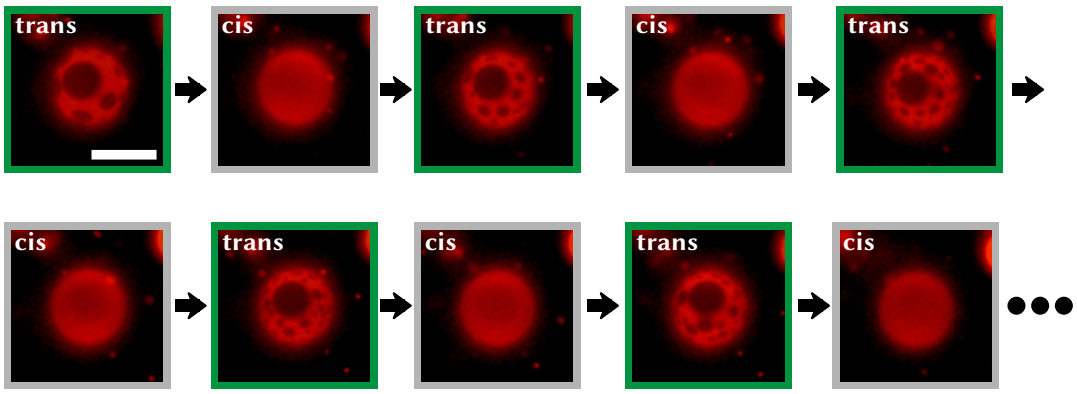


**Figure 4.9: Switching cycles in ternary photolipid vesicles.** GUVs consisting of *azo*-**PC**, DPhPC and cholesterol exhibit phase separation in the *trans*, but not in the *cis* state. The frames indicated the fluorescent filter cube used for excitation and detection. Green frames indicate green (510 nm to 550 nm) excitation and gray frames indicate illumination with UV-A light (330 nm to 385 nm). Due to the robust photo-isomerization, switching between the two states is possible over many cycles, mostly limited by the photobleaching of the dye (scale bar = 20 µm).

high cholesterol concentration, the domains disappear. At the same time, the peak shifts to lower energies, as one would expect for a decreasing concentration of *azo*-**PC** in the bilayer.

The absorbance spectra of GUV suspensions can thus be used to determine the ability of the mixture to form domains and phase separate. The bulk spectrum is thereby a superposition of all domain concentrations observed in the sample.

## Switching domain formation

Isomerization of the vesicles was facilitated by switching the excitation light from green to UV (330 nm - 385 nm). The UV light illumination initiates the isomerization from *trans* to *cis* while also exciting the Texas Red dye due to higher energy levels, which overlap the photon energy. The light intensity is chosen high enough that the isomerization itself is fast compared to the lipid dynamics (see section 5.2 for a detailed discussion about the isomer composition under different illumination conditions). Upon isomerization, the domains disappear until the vesicles appear homogeneous. After switching back with green light illumination, the domains reappear again. The process is reversible over many cycles, mostly limited by photobleaching of the dye (Figure 4.9).

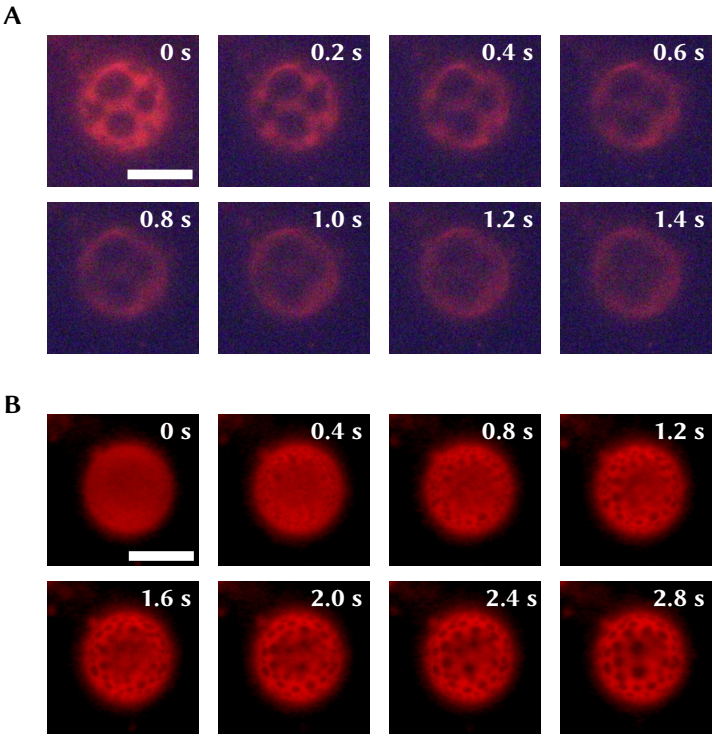


**Figure 4.10: Detailed switching cycles. (A)** Upon switching from *trans* to *cis* with UV-A light, the domains start to smear out. Driven by diffusion, the vesicles appear homogeneous within seconds. Bigger domains can be observed longer, because it takes longer of the fluorescent dyes to diffuse from the edge of the domain to the center. **(B)** For the reverse process, dark domains nucleate within milliseconds. Subsequently, the domains fuse until a steady state distribution is reached. (scale bar = 20 µm)

Since isomerization and domain formation are essentially decoupled, the behavior of the vesicle can be attributed to the behavior of the lipids. Upon UV light illumination, the boundaries of the domains start to smear out (Figure 4.10 A). While areas with small domains are homogeneous within seconds, bigger domains are visibly darker for longer times, since the fluorescent molecules diffuse slowly from the previously disordered domains to the center of the darker domains.

After isomerization back to the *trans* state, the fluorescence intensity recovers within a few frames, indicative of the lower quenching efficiency of the *trans* state compared to the *cis* state (see section 5.4 for a discussion of quenching effects for *azo*-**PC** membranes). Simultaneously, small domains appear, which can be resolved with diffraction limited microscopy after less than a second (Figure 4.10 B). The domains quickly coalesce to form bigger domains.

Since the properties of the two isomeric states are fundamentally different, a new degree of freedom is added to the phase diagram. The system consisting of *azo*-**PC**, DPhPC and cholesterol is therefore a four component system, which can be tuned with light. So far, the light intensity was chosen so high, that the isomerization is fast compared to the diffusion, which governs the formation of domains. By controlling the illumination conditions, especially the wavelength ranges and the intensity ratios, it is possible to tune the composition of the photolipid membranes continuously between the pure *trans* and *cis* state.

## Domain formation in mixtures with *azo*-PC in the *cis* state

The ternary mixture composed of DPhPC, *azo*-**PC** and cholesterol exhibits macroscopic domains, when the photolipid is predominantly in the *trans* state, but no domains could be observed in the *cis* state. A complete mixing of the lipids suggests, that *azo*-**PC** in the *cis* state is in a similar phase as DPhPC at room temperature, namely in the $l_d$ phase. The phase properties of the *cis* state photolipid membrane were investigated more thoroughly in ternary mixtures with phospholipids with different phase transition temperatures. DOPC is fluid at room temperature ($T_m = -17\,^{\circ}\mathrm{C}$), while DPPC and DSPC are solid ($T_m = 41\,^{\circ}\mathrm{C}$ and $T_m = 55\,^{\circ}\mathrm{C}$, respectively). DMPC membranes exhibit a phase transition close to room temperature ($T_m = 24\,^{\circ}\mathrm{C}$). For reference, the chemical structure of all lipids used within this work is depicted in section A.3.

GUVs containing *azo*-**PC**, cholesterol and one of these phospholipids were prepared in a ratio of 4:2:4. Fluorescent observation was facilitated by addition of 0.5 % TR-DHPE and Marina Blue™ DHPE (MB-DHPE). MB-DHPE is excited most efficiently in the UV, at 365 nm and emits blue light ($\lambda_{max}$ = 460 nm). Furthermore, MB-DHPE does not appear to have a phase preference for the $l_d$ or the $l_o$ phase. Liquid ordered phases in co-doped vesicles with both TR-DHPE and MB-DHPE thus appear blue, when both dyes are excited. The disordered phases appear red, because the emission of TR-DHPE appears stronger than the blue light emission. All experiments were performed at room temperature.

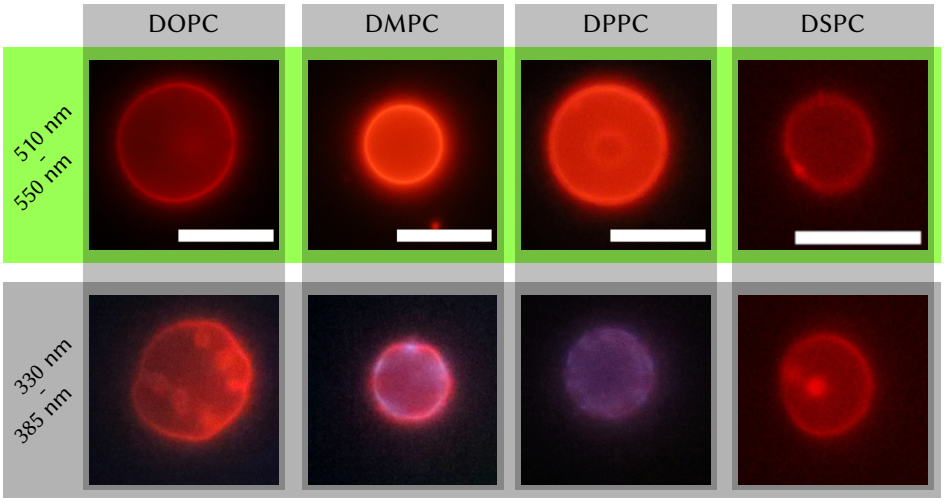


**Figure 4.11: Domain formation for more lipid compositions.** Several ternary lipid compositions were prepared and examined for phase separation in epifluorescence. The lipid ratio of each composition was 4:4:2 (*azo*-**PC**:DxPC:cholesterol, with x being O, M, P or S), stained with 0.5 % of TR-DHPE and, for DMPC and DPPC, additionally with 0.5 % of MB-DHPE. Each GUV is imaged once with green excitation light, keeping the photolipid mostly in the *trans* state and once with UV light illumination, for a PSS with high *cis* fraction. (scale bars = 10 µm)

Example pictures of these GUVs are depicted in Figure 4.11. For excitation with green light, when most photolipids are in the *trans* state, no macroscopic phase separation can be observed in any of these compositions. For UV light excitation however, macroscopic domains can be observed for compositions containing DMPC and DPPC, while DOPC and DSPC vesicles appear completely homogeneous.

DOPC, as the only fluid lipid at room temperature from this selection of lipids, should be comparable best to DPhPC. However, the vesicles appear homogeneous also

in the *trans* state of *azo*-**PC**. In the terminology of domain formation in ternary mixtures, both DPhPC and DOPC count as a "low $T_m$" lipid at room temperature, since lipid membranes are in the $l_d$ phase. Lipids forming disordered phases play an important role in stabilizing the liquid ordered domains composed mostly of the "high $T_m$" lipid and cholesterol.[155] Additionally, DPhPC induce a stronger stabilizing effect than DOPC due to the unique structure of the phytanoyl chains.[155] This difference is enough to prevent phase separation in the ternary mixture with DOPC and in *azo*-**PC** in the *trans* state. When the photolipid is in the *cis* state, no phase separation is observed for neither DPhPC nor DOPC.

The remaining three lipids are all fully saturated and can therefore be regarded as high $T_m$ lipids. For the *trans* state, none of these compositions exhibit macroscopic domains. For the *cis* state, on the other hand, domains can be observed for mixtures with DMPC and DPPC. This shows, that the *cis* isomer behaves like a low $T_m$ lipid, at room temperature. For DSPC, no domains can be observed. A possible explanation is the similarity of *azo*-**PC** and DSPC. The acyl chain of *azo*-**PC** at the *sn1* position is the same as both acyl chains of DSPC (stearoyl). Also, the azobenzene containing chain in the *trans* state has a similar length as stearoyl. The mismatch induced by the *cis* bond disturbs the bilayer therefore not enough to induce phase separation.

## Domain formation between the *cis* and *trans* state

The previous experiments have shown, that *azo*-**PC** can behave as a "low $T_m$" lipid or a "high $T_m$" lipid at room temperature, depending on the isomeric state. The question arises then, if it is possible to induce domain formation just with *azo*-**PC** and cholesterol.

To observe this, the ratio between *trans* and *cis* isomers has to be held constant for the time the lipids need to phase separate. To this end, another fluorescent dye was used, DPPE, tagged with ATTO 633 ($\lambda_{exc}$ = 630 nm, $\lambda_{em}$ = 651 nm). By exciting at a higher wavelength, between 600 nm and 640 nm, isomerization is reduced and it is possible to optically observe GUVs while changing the isomer ratio only slowly. Additionally, the excitation light intensity is reduced with suitable neutral density filters towards the detection limit of the CCD camera. Still, the excitation leads slowly, over several tens of seconds, to the PSS which consists mostly of *trans* state molecules. The experiments were thus carried out as follows: First, a GUV is illuminated with UV light until the

PSS is reached. Then, the behavior of the vesicle was recorded while illuminating with red light.

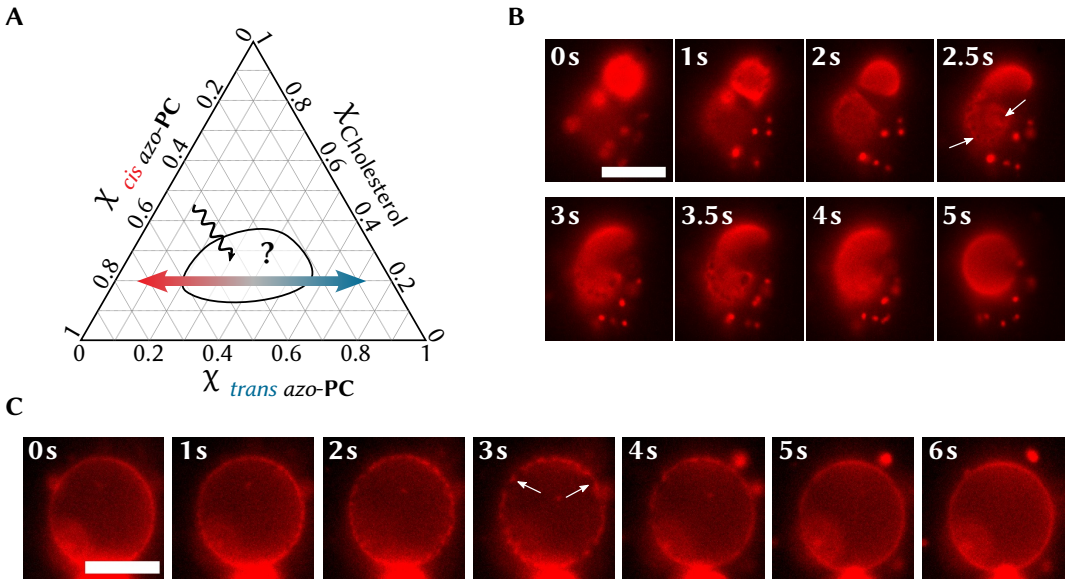


**Figure 4.12: Domain formation in *azo*-PC/cholesterol GUVs. (A)** The exact location of fluid-fluid coexistence in the phase diagram is not known, but tuning the isomer ratio of *azo*-**PC** continuously with light allows to traverse the coexistence region. **(B)** Fluorescence image of a vesicles aggregate, focused near the surface to observe a large membrane area. Upon red light excitation with weak intensity, the vesicles exhibit phase separation for ≈1.5 s and subsequently fuse to a single homogeneous vesicle. **(C)** Image of a vesicle near its equator. Only the vesicle circumference is in focus. Again, domain formation can be observed for a short time upon weak red light excitation. White arrows are used to indicate examples of domains. (scale bars = 25 µm)

The results are depicted in Figure 4.12. GUVs are prepared with a a 8:2 ratio between *azo*-**PC** and cholesterol, doped with 0.5 mol% ATTO 633 DPPE. In the beginning, the vesicles appear homogeneous. After a few seconds, domains start to appear, often accompanied with large changes of vesicle geometry. Domains do not have enough time to grow to their equilibrium shape but disappear completely after a few seconds. While it is not possible to keep the composition at a defined point in the phase diagram for a long time due to the constant illumination necessary for observation, it is clear that there is a region of liquid-liquid coexistence.

## Discussion

After characterization of these different lipid mixtures, a clearer picture of the nature of the phase behavior of *azo*-**PC** in its isomeric states emerges. First, owing to the fluid nature of *azo*-**PC**, the ternary system of the *trans* state together with DPhPC and cholesterol demixes and forms stable macroscopic domains. DPhPC is known for its ability to constitute stable domains over large composition ranges, but mostly in composition with high melting lipids. In mixtures with low melting lipids, domain formation is also possible, but only a few degrees above the melting temperature of the lipid.[156]

It is therefore likely, that the reason for domain formation is found in the unusual acyl chain structure of *azo*-**PC**. The photolipid is a saturated lipid, but mimics the structure of POPC, which has one unsaturated double bond and a melting temperature of −2 °C.[52] Both can also occur in the *cis* or *trans* isomeric conformation, but the azobenzene group is quite bulky and disturbs the bilayer packing. Additionally, the spherical shape of the GUVs and of the domains indicates a liquid phase, but the diffusion constant is lower than for the *cis* state and for typical lipids in the $l_d$ phase (as discussed in chapter 5). *Azo*-**PC** in the *trans* state therefore retains enough properties of high melting lipids to sustain macroscopic domain formation in combination with DPhPC. Similar properties can be found in the comparison of POPC and the respective counterpart with containing a *trans* double bond.[157] Chains with the *trans* unsaturated bond are more ordered in a bilayer and have a higher affinity for cholesterol compared to the respective molecule with a *cis* bond. *Trans* state lipids can thus be seen as a state in-between the saturated lipid and the unsaturated lipid with a *cis* bond. These properties seem to be retained for *azo*-**PC**, designating this lipid as an excellent model system to study the dynamics in a bilayer system.

Another aspect governing the size of the lipid domains is the line tension between the individual phases at the domain boundary.[158,159] The domain size at equilibrium arises from the competition between entropic contributions and the line tension. Merging of domains leads to a lower line tension energy due to the reduced boundary length, but on the other hand to a decrease in entropy. Only at high line tensions macroscopic domains emerge, which can be observed with light microscopy.

This helps in understanding the behavior of compositions containing saturated lipids and *cis* state photolipids. As can be seen in Figure 4.11, domains are smaller for

DPPC than for DMPC, indicating decreased line tension for longer acyl chains. For DSPC, the line tension is therefore so low, that domain sizes are below the diffraction limit.

Understanding the origin of the line tension thus helps understanding the behavior of the ternary photolipid mixtures. The line tension mainly arises due to the height difference between the two domains, and is influenced also by their mechanical properties.[160,161] In the following, these bilayer properties are investigated more thoroughly.

## 4.3 Mechanical properties of photolipid membranes and membrane mixtures

The mechanical properties of the photolipids were measured with the micropipette technique, as explained in section 3.3. Both the bending rigidity $k_c$ and the area expansion modulus $K_A$ can be extracted from the area increase when exposed to tension. The mechanical moduli were determined for GUVs, composed of *azo*-**PC**, DOPC and DPhPC, both under blue (465 nm) and UV (365 nm) illumination (Figure 4.13).

The mechanical properties of DOPC and DPhPC membranes exhibited now dependence on illumination conditions and match well with reported literature values.[69,162,163] For both the bending rigidity and the area expansion modulus, the values for the photolipid membrane were lower than for the standard phospholipids. The aromatic rings in the *azo*-**PC** chains hence destabilize the membrane, leading to an overall softer membrane. The difference between the two isomeric states matches well with our previous observations.[94] Both the bending rigidity and the area expansion modulus is lower in the *cis* state compared to the *trans* state. When both lipid tails contain an azobenzene unit, the lipids do not even form GUVs in water.[140] The stability is hence even further decreased.

From the bending rigidity and the area expansion modulus, the bilayer thickness can be calculated with the polymer brush model.[69] The model treats the lipid tails as short polymers, described as an ideal chain, which neglects any interaction between the monomers. The free energy of this polymer only depends on the chain extension and the number of segments. By minimizing the free energy of a monolayer under these assumptions, the mechanical properties of the bilayer can be related to the hydrocarbon

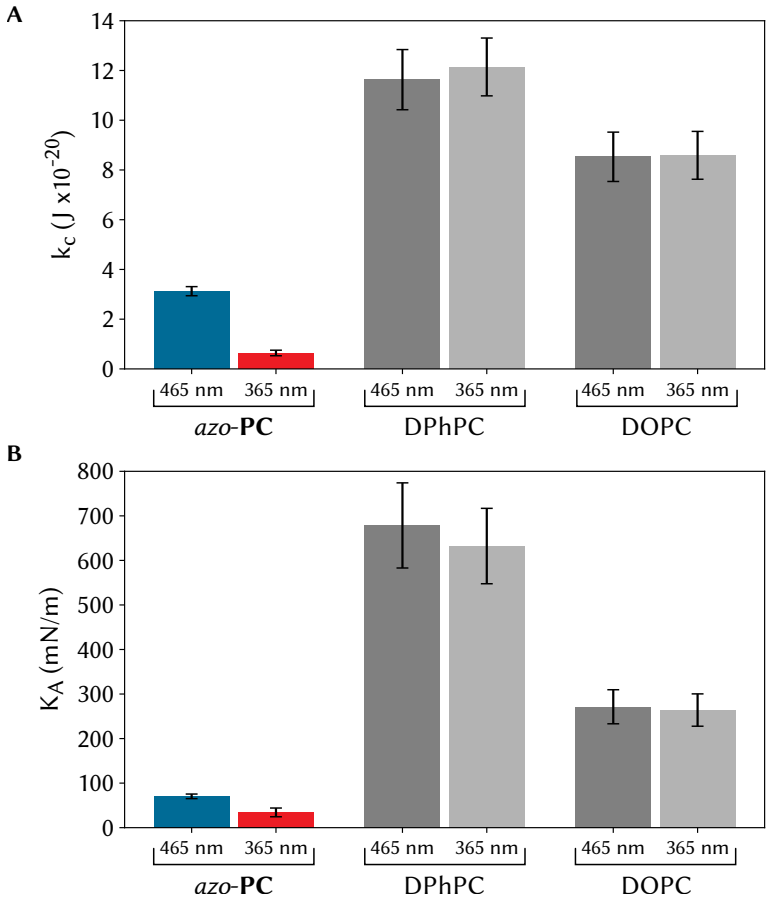


**Figure 4.13: Mechanical properties of *azo*-PC in comparison to other phospholipids.** The bending rigidity $k_c$ and the area expansion modulus $K_A$ have been extracted from micropipette aspiration measurements of GUVs. **(A)** The bending rigidity of *azo*-**PC** is lower than for DPhPC or for DOPC. Upon isomerization from *trans* to *cis*, the photolipid membranes become softer, already indicated by the higher fluctuations of GUVs one can observe under the microscope. **(B)** For the area expansion modulus, the same relation holds. The modulus is lower for *azo*-**PC** than for both DPhPC and DOPC, and higher for the *trans* state than for the *cis* state.

thickness $h$ of the bilayer by

$$h = \sqrt{\frac{24k_c}{K_A}} \tag{4.1}$$

The results of this calculation using the measured mechanical parameters for *azo*-**PC**, DOPC and DPhPC are depicted in Figure 4.14. While the thickness for the DOPC bilayer agrees well with literature values,[164] the value for DPhPC is with 31.5 ± 2.5 Å smaller than in the literature (35.4 Å).[165] The trend is however correct since DPhPC membranes are thinner than DOPC membranes. The polymer brush model was originally developed for single branched phospholipids, therefore it is not surprising that the model deviates for DPhPC, and presumably cannot be used quantitatively for *azo*-**PC** as well.

According to the model, the *azo*-**PC** bilayer in the *cis* state is thinner than in the *trans* state. Upon isomerization, a kink is introduced in the azobenzene-containing tail, effectively shortening the lipid and leading to an effectively thinner bilayer. A similar effect can be observed for unsaturated lipids with the bonds either in the *trans* or the *cis* conformation. For 18:1 (Δ9-Cis) PC (DOPC), the bilayer thickness is 37 Å and for 18:1 (Δ9-trans) PC, the bilayer is 43 Å thick.[69] The decrease of the membrane thickness of more than 25 % is however larger than what can be reasonably expected for the photolipid bilayer, especially since the PSS contains a large percentage of *trans* state molecules due to the white light illumination during the micropipette aspiration measurements.

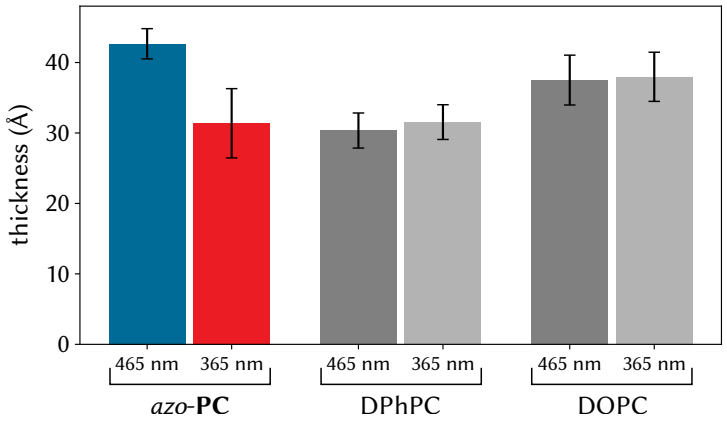


**Figure 4.14: Bilayer thickness, calculated according to the polymer brush model.** Bilayer thickness of *azo*-**PC**, DOPC and DPhPC under UV and blue light illumination, calculated from the mechanical properties according to the polymer brush model.

The thickness of DOPC membranes seems to be closer to the *trans* state photolipid membrane than the thickness of DPhPC membranes. The line tension between different domains in therefore smaller in ternary mixtures containing DOPC than in compositions containing DPhPC, explaining the formation of macroscopic domains for DPhPC but not with DOPC. Furthermore, the saturated lipids have a higher melting temperature and are more elongated at the same temperature than their counterpart with unsaturated bonds. The resulting thicker membrane fits better to the *trans* state photolipid membrane, another reason for the domain formation in the *cis* state for these mixtures.

## Mechanical properties of mixed photolipid membranes

The mechanical measurements so far were done for single component membranes. As shown previously, changes of the membrane composition go hand in hand with a modulation of the mechanical properties of the bilayer. To further quantify the effect of local inhomogeneity as present in lipid mixtures, the bending moduli of vesicles with different *azo*-**PC**/DPhPC compositions were measured with the micropipette aspiration technique (Figure 4.15 A).

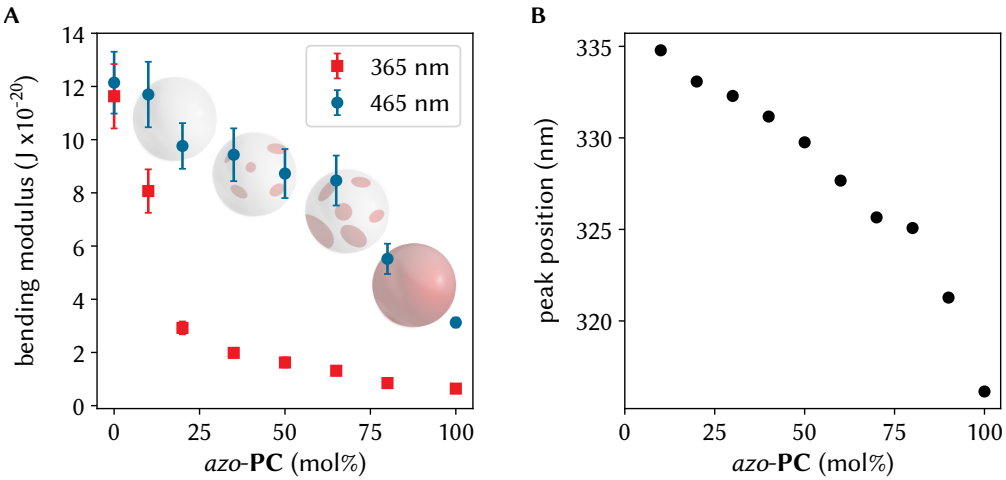


**Figure 4.15: Bilayer rigidity and $S_0 \longrightarrow S_2$ peak position of DPhPC/*azo*-PC mixtures.** **(A)** Bending rigidity of GUVs consisting of the binary lipid mixture. For each data point, three GUVs were measured with micropipette aspiration, under both UV and blue light illumination. For the *trans* state. the plateau region could be explained with the presence of nanodomains. **(B)** Peak position of the $S_0 \longrightarrow S_2$ transition in the *trans* state, in dependence of the *azo*-**PC** concentration.

For the *trans* state, the bending modulus drops slowly with increasing concentration of *azo*-**PC** until 65 %. At high *azo*-**PC** concentrations, the bending modulus quickly drops to the value of pure *azo*-**PC**. In the UV adapted state, the behavior is reversed. The bending rigidity approaches the values of pure *azo*-**PC** already at low percentages (≈25 %) and then stays almost constant until 100 %. As a result of this behavior, the maximum difference between the blue adapted and the UV adapted state is not given for a pure photo-membrane, but rather for a mixture of 65 % *azo*-**PC** and 35 % DPhPC.

The plateau region for the *trans* state, between 25 % and 65 % *azo*-**PC** corresponds well to the region where the ternary mixture exhibits phase separation (Figure 4.7). For the binary mixture however, no macroscopic domains can be observed. But it is likely that the membrane is not completely homogeneous and contains nanoscopic domains, since cholesterol stabilizes domains otherwise smaller than the diffraction limit of light. Since the $S_0 \longrightarrow S_2$ transitions carries information about the phase properties, the peak position was recorded also for the mixtures (Figure 4.15 B). Overall, the peak position follows a similar trend as the bending rigidity, with a steeper drop off for low concentrations (<20 %) and high concentrations (>75 %) and a plateau like region in-between.

The curve shapes for the *trans* and the *cis* state membranes are consistent with trends described in literature.[166] For mixtures composed of two components, the function of the bending rigidity in terms of the lipid compositions follows different curvatures depending on the homogeneity of the membrane. For ideal mixing, a positive curvature is expected while systems exhibiting domains show negative curvature, consistent with the behavior observed for the *azo*-**PC**/DPhPC mixture. The combination of micropipette aspiration and optical absorption measurements thus provides evidence for the formation of nanoscale domains, which can not be determined by simple diffraction limited optical observation.

## Summary

In summary, this chapter highlights the unique properties, that arise due to the azobenzene unit in one tail of the *azo*-**PC** lipid. The dipole-dipole coupling between the individual units gives rise to spectral changes and the resulting optical shifts are sensitive to the phase state of the membrane. This allows to observe ordering effects induced by the presence of cholesterol in the membrane and the existence of macroscopic do-

mains in ternary lipid mixtures containing *azo*-**PC** directly from absorbance spectra of vesicle suspensions.

On the other hand, the isomerization of the photolipid, and the resulting geometric reorganization of the lipid tails, allows to control membrane properties with light. This was used to control domain formation in GUVs. Several ternary mixtures were identified, that exhibit domain formation in combination with *azo*-**PC**. Further information about the different phase states of *azo*-**PC** membranes was obtained, since phase separation only occurred for one of the isomerization states. By precisely controlling the ratio of *cis* and *trans* state photolipids, domain formation in binary mixtures with cholesterol was observed.

Finally, the mechanical properties of the photolipid system were investigated. Results from micropipette aspiration measurements support the hypothesis for the bending rigidity obtained from previous optical observations, namely the increased softness in the *cis* state compared to the *trans* state. Further analysis of the measurement data suggests that *cis* state membranes are thinner compared to bilayers in the *trans* state. For binary lipid mixtures with DPhPC, the existence of nanoscopic domains, smaller than the diffraction limit, is postulated for the *trans* state and not for the *cis* state on the basis of the curve shape of the bending rigidity in dependence on the lipid ratio.

# Chapter 5

# Illumination dependent diffusion in photolipid bilayers

A central aspect of the Fluid-Mosaic Membrane Model is the fluidity of the bilayer, that is the ability of the phospholipids and the solutes to diffuse laterally in the membrane.[32,33] In addition, the dynamic rearrangement of membrane components between functional domains is critical in numerous cellular processes.[167,168]

Supported lipid bilayers (SLBs) have long been used as a model system to study lipid membranes in a controlled environment.[169] A SLB maintains high fluidity due to the thin water layer between the substrate and the bilayer.[6,170] The diffusion coefficients are comparable to the coefficients of lipids and membrane components in living cells.[170] Controlling the membrane diffusivity or creating distinct areas with defined properties has proven to be difficult. Several studies have been conducted employing metal lines, which are introduced on the substrate previous to the experiment and act as diffusion barriers.[171,172] Additionally, the metal lines can be used to apply an electric field tangential to the bilayer, thereby introducing a gradient of charged lipids.[171]

These strategies, however, are often laborious and do not allow to manipulate membrane properties on-demand and with geometries different than the predetermined structure on the substrate. In this chapter, the photolipid *azo*-**PC** is used to control lateral membrane diffusion with light. First, the diffusion coefficients of *trans* and *cis* state membranes are determined. Then, the ability to vary the diffusivity continuously by changing the ratio of the isomers is explored and compared to the temperature dependent behavior. Finally, using light with a predefined intensity pattern allows to

compartmentalize membrane properties locally, reversibly, and on demand. The main findings presented throughout this chapter are published in *Langmuir*.[173]

## 5.1 Lateral mobility in pure *azo*-PC membranes

Membrane parameters are very sensitive to small variations in the structure of the tail regions of the lipids.[174,175] In the previous chapter, it has been shown that membrane properties of *azo*-**PC** bilayers depend substantially on the isomeric state of the molecules. The origin for this is found in the intermolecular interaction, which changes upon isomerization, and can be seen directly through shifts of their absorption spectra.

It has already been speculated previously, that a pathway to control membrane self-diffusion with light is enabled by using photolipids.[94,139] The notion that the lateral diffusion of *azo*-**PC** membranes is different for the *trans* and the *cis* state has been implied indirectly from other observations, namely the change in mechanical properties upon isomerization.[94] Softer membranes are often an indication for a different phase state, e.g. the $l_d$ phase compared to the $l_o$ phase, which is also accompanied by an increased lipid diffusion.[49] To quantify the lipid mobility directly, the diffusion coefficient was measured with Fluorescence Recovery After Photobleaching (FRAP, see section 3.3 for experimental details).

SLBs were prepared by vesicle fusion on borosilicate glass (section 3.1). The bilayer consisted of 99 % *azo*-**PC** and 1 % TR-DHPE as a fluorescent label. The molecules were excited in epifluorescence configuration with either the green or the UV filter cube. The diffusion coefficients of the bilayer were determined by FRAP after 3 min illumination to guarantee that the measurement is performed at the respective PSS. Measurements were performed alternatingly in the *trans* state and in the *cis* state (Figure 5.1). The average diffusion coefficient for the *trans* state was found to be $0.47 \pm 0.04\,\mu m^2\,s^{-1}$ and for the *cis* state $0.81 \pm 0.06\,\mu m^2\,s^{-1}$.

A theoretical description of the lipid self diffusion is bilayer is given by the free area theory (see section 2.1). The free area theory essentially decouples the contribution from the area per lipid and from the interaction energies, summed up in the activation energy. Higher area per lipid implies increased free area available, and hence leads to an increased diffusion coefficient. A higher activation energy however leads to a decreased mobility, because a lipid needs more energy to move into the free area. The interaction term takes into account the intermolecular lipid interaction and the interaction with

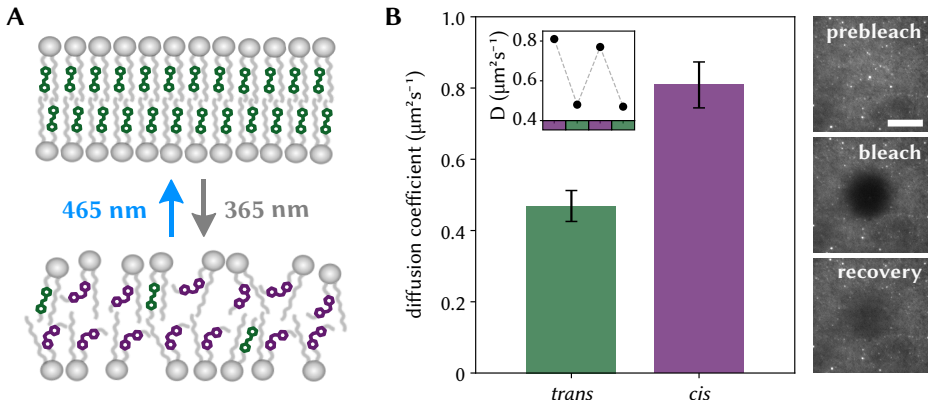


**Figure 5.1: Diffusion in *azo*-PC SLBs in the *trans* and the *cis* state. (A)** Isomerization of photolipids with light leads to a change in intermolecular interaction. One of the membrane parameters, that changes in this instance is the lateral lipid diffusion. **(B)** The diffusion coefficient in SLBs is measured after illumination with UV or visible light. The data is averaged over nine (UV) and eight (visible) measured values, respectively, recorded in alternating order (four values are depicted in the inset). Example pictures of the recovery of a *trans* state bilayer show the fluorescence of the unbleached SLB, directly after bleaching a circular area and after 30 s of recovery. Scale bar = 10 µm.

the bounding fluid.[45] The interaction with the fluid is usually relatively insensitive to conformational changes buried in the hydrocarbon region, since it is dominated by the type of headgroup. The headgroup does not change upon isomerization of *azo*-**PC**, and hence the interaction with the fluid exerts a negligible effect on the diffusion of photolipid membranes. The lipid-lipid interaction however changes dramatically for the *trans* and the *cis* state.

The contribution from the lipid area can be quantified trough monolayer measurements with a Langmuir-Blodgett trough.[176] A defined amount of lipid dissolved in organic solvent is spread on a water surface. Upon evaporation of the organic solvent, the lipid molecules form a monolayer. In a typical experiment, the surface area is continuously decreased while measuring the surface pressure. From the area-pressure isotherm, monolayer phase properties and lipid areas can be derived (see section 3.3 for measurement details).

Here, the experiment was performed for an *azo*-**PC** monolayer at room temperature once after illumination with 465 nm and once after illumination with 365 nm for 10 min (Figure 5.2). The compression rate was 22 mm $min^{-1}$. The isotherms exhibit no distinct phase transition, which would be observable as a plateau, over the entire measurement range. A monolayer with such a behavior is typically interpreted as being in a homo-

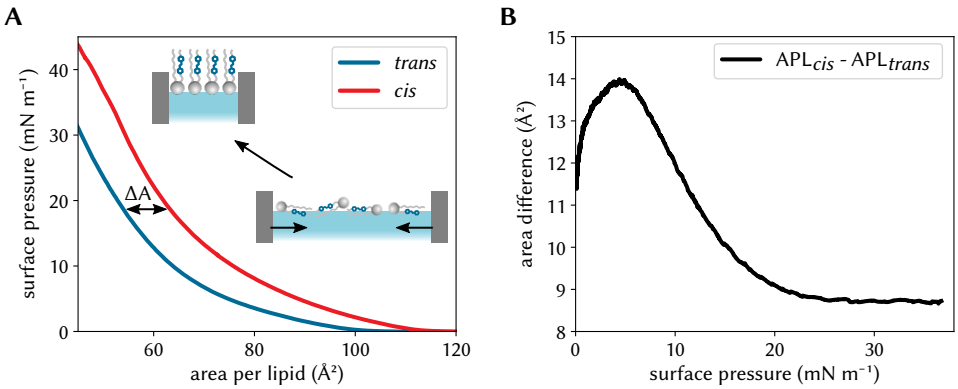


**Figure 5.2: Surface pressure-area isotherms of *azo*-PC in the *trans* and in the *cis* conformation. (A)** The isotherms were recorded on a Langmuir trough after LED illumination. The area per lipid is derived by dividing the total surface area by the number of lipids spread onto the surface. The area is larger for the *cis* than for the trans state at all surface pressure values. **(B)** The difference between the lipid areas depending on the surface pressure converges to a constant value.

geneous fluid phase, called *liquid expanded* or LE phase in Langmuir monolayers, for the examined pressure range.[169] This is in good agreement with measured diffusion coefficients, which also indicate a fluid phase. At any particular surface pressure, the area per lipid is higher for the *cis* state compared to the *trans* state. These results can be translated to bilayer measurements, since mono- and bilayers share many properties.[177] For bilayers, the decrease of the lipid area is implied indirectly from the membrane thickness (Figure 4.14). Assuming a constant lipid volume, a thinner bilayer implies that the area per lipid increases.

Upon examining the area difference between the *cis* and the *trans* state at any given pressure, one can see that the difference exhibits a maximum of 14 $Å^2$ at low pressure values and approaches a constant value of 9 $Å^2$ at high surface pressure. The surface pressure, for which the monolayer properties resemble the bilayer properties the most is usually put at 35–40 $mN\,m^{-1}$,[178,179] therefore the peak at low values is neglected. 9 $Å^2$ is thus a good estimate for the area difference in bilayers, which also leads to an increase of the diffusion coefficient when inserted in Equation 2.17.

Unsaturated double bonds in acyl chains of natural lipids can also be found in the *trans* or in the *cis* state (see section 2.1). The naturally occurring lipid 16:0-18:1 PC (POPC)[180] is a phospholipid with one C = C double bond in the *sn2* acyl chain and a

similar length as *azo*-**PC**. The double bond of POPC is in the *cis* conformation. The counterpart with a *trans* fatty acid is called PEPC.[181]

Comparing bilayer properties of these lipids, one finds a similar behavior as in *azo*-**PC**, namely a reduced area per lipid, lower diffusion coefficients and increased bilayer thickness for PEPC.[181,182] The magnitude of the difference of these properties is however smaller than for *azo*-**PC**. The average area per lipid, as calculated from molecular dynamics simulations, is only 3.4 $Å^2$ larger for POPC and the diffusion coefficient is increased by only 30 %.[181] The influence of the *cis* isomerization of azobenzene is thus larger than of the *cis* conformation of the C = C double bond, presumably due to the bulky aromatic ring of the benzene group, which disturbs the bilayer packing.

## 5.2 Tuning lateral diffusion with light

Unlike the natural phospholipids, *azo*-**PC** allows to tune the membrane composition with light and on fast timescales (e.g. seconds to milliseconds). To examine, how tuning the isomer ratio affects the membrane fluidity, the lateral diffusion coefficient was measured for different illumination conditions. It was previously shown (see section 4.1), that the isomer ratio depends on the length of illumination for a given light source with a constant intensity. For FRAP, the membrane composition has to be kept constant for a couple of minutes. The excitation light for the fluorescent dye will however potentially change the membrane composition questioning the validity of the calculated diffusion coefficient.

The procedure was therefore slightly adapted from the previous measurements. The SLB was imaged in TIRF configuration with a 562 nm laser as excitation light source. This had two advantages: First, the light source is at a higher wavelength compared to the epifluorescence excitation cube (530 nm to 550 nm). The redshift separates the excitation further from the $S_0 \longrightarrow S_1$ transition of *azo*-**PC** and therefore minimizes the impact on the isomer ratio. Secondly, the TIRF configuration leads to a better signal to noise ratio, allowing to reduce the illumination intensity.

The isomer composition was then tuned by varying the intensity of the UV LED. Here, the sample was illuminated from the unfocused fiber output, placed directly above the bilayer. The diffusion coefficient increases from the *trans* state value ($0.42 \pm 0.01\,\mu m^2\,s^{-1}$) without UV illumination up to $0.60 \pm 0.01\,\mu m^2\,s^{-1}$ for the maximum LED intensity (75 mW, Figure 5.3 A). The maximum diffusion coefficient is how-

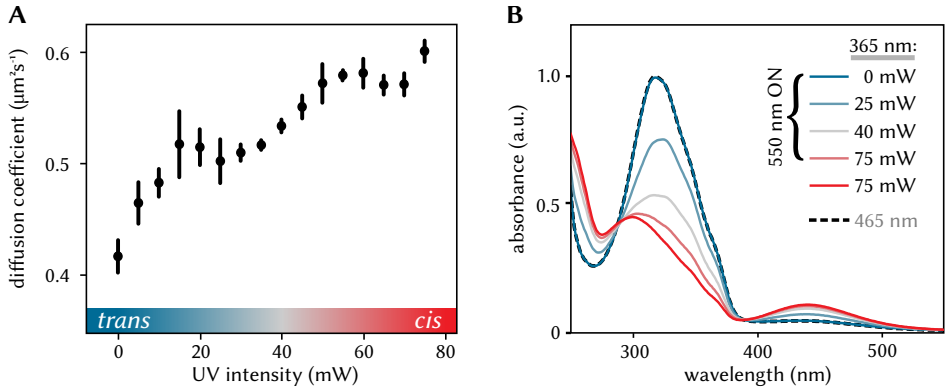


**Figure 5.3: Diffusion coefficient of *azo*-PC SLBs depending on the illumination condition. (A)** During the measurement series, the SLB is illuminated at a constant laser power in TIRF mode (562 nm). The diffusion coefficient can then be tuned by varying the intensity of the UV illumination. **(B)** The optical absorbance upon illumination with different ratios of green (550 nm) and UV (365 nm) illumination is shown. As in **(A)**, the illumination intensity of the 550 nm LED is kept constant, while the intensity of the UV LED is tuned. As reference, a spectra at the PSS after illumination with 465 nm light is included. All spectra are obtained at the PSS.

ever smaller than for the pure *cis* state membrane, due to the different illumination condition. The residual green light of the TIRF illumination is present for all measurements, producing a photostationary state with a substantial percentage of *trans* state molecules.

To verify, that the behavior of the diffusion coefficient is governed by the isomer composition, the absorbance of SUVs was measured with similar illumination conditions as for the FRAP measurements. SUVs consisting of 100 % *azo*-**PC** were prepared as previously discussed. The sample was illuminated with two LEDs, 365 nm and 550 nm, with varying intensity ratios for 2 min to ensure that the PSS is reached. Directly thereafter, the absorbance of the SUV suspension is measured (Figure 5.3 B). After illumination with green light, the PSS is very close to the pure *trans* state. For mixed illumination with both green and UV light, the PSS still contains a larger fraction of *trans* state molecules than the PSS after pure UV light illumination. The measurements of the diffusion coefficient and the absorbance measurements are thus consistent and demonstrate, that the lipid diffusion coefficient of photolipid membranes can be continuously tuned with light.

## 5.3 Temperature dependent diffusion in photolipid membranes

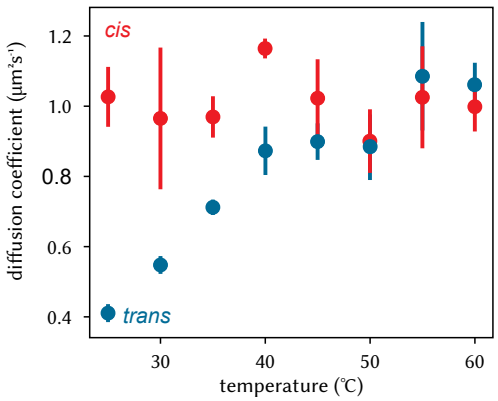


**Figure 5.4: Temperature dependent diffusion of the *trans* and the *cis* state of *azo*-PC membranes.** The lateral diffusion coefficient in *azo*-**PC** SLBs is measured at various temperatures, both after UV illumination (*cis*) and blue light illumination (*trans*).

Typically, the main parameter influencing the lateral diffusion of membranes is temperature. Similar to the previous measurements employing light (Figure 5.3), the diffusion coefficient also changes continuously with temperature.[45] To single out additional similarities, the photolipid system was further characterized by measuring its temperature dependent properties. As previously, SLBs were prepared from SUVs consisting of 99 % of *azo*-**PC** and 1 % of TR-DHPE. The diffusion was subsequently measured on a temperature controlled stage between 25 ˚C and 60 ˚C (Figure 5.4). Each data point represents the average of three measurements on different membrane areas.

The results show distinct behavior for the *trans* and the *cis* state. The diffusion coefficient for the *trans* state increases by more than 100 % for the investigated temperature range. For the *cis* state however, the diffusion coefficient stays roughly constant.

The diffusion of the *trans* state behaves as expected from a theoretical point of view. The diffusion coefficient increases with increasing temperature. The parameters of the free area model are the interaction energy, the temperature and the area per lipid (Equation 2.17).[49] The interaction energy is temperature independent, whereas the area per lipid is assumed to increase with temperature. Under these conditions, there is a clear trend towards higher diffusion coefficients at higher temperature. For SLBs of

several different phospholipids in the fluid phase, this has also been experimentally confirmed.[183]

Since the *cis* state membranes are fluid at the relevant temperatures as well, it is surprising that the appears to be independent of temperature. One possible explanation would be a shift in the isomer ratio at higher temperatures. However, increasing the temperature would shift the equilibrium toward the *cis* isomer[184] and thus to an overall higher diffusion coefficient.

Another reason might be found in the interaction with the substrate. At elevated temperatures, the activation energy $E_a$, which includes the effect of the substrate, would be required to be higher. The substrate contribution however depends mostly on the type of the lipid headgroup, which are the same for both the *cis* and the *trans* state. Yet, the diffusion of the *trans* state increases as expected. Also, it has been recently demonstrated, that the diffusion coefficient for SLBs consisting of DOPC, DLPC, DMPC and DPPC increases with temperature as well.[183] The interaction with the substrate is thus excluded as the reason for the behavior of the *cis* state.

The further reason for the temperature independence of the diffusion coefficient would be a decrease of the area per lipid at higher temperatures. Published data for standard lipids however suggests a clear increase in lipid area with temperature.[165,185] The origin for this increase is found in the increased probability of trans-gauche isomerization of the bonds in the fatty acids tail at elevated temperature.[165] The azobenzene unit in *azo*-**PC** is however quite bulky and probably disturbs the bilayer packing. Especially the *cis* conformation, which produces an artificial kink in the fatty acid tail, might lead to an unfavorable lipid conformation with poor packing properties. An increased probability in trans-gauche isomerization in the hydrocarbon segments both in the stearoyl chain and in the chain containing the azobenzene group helps to better accommodate the azobenzene unit, which decreases the area per lipid again.

The lipid area difference as determined from the monolayer experiments performed in the previous section support this view. At room temperature, the *cis* state lipid area is ≈9 Å$^2$ larger than the *trans* state area per lipid (Figure 5.2). The difference between area per lipid of POPC and PEPC membranes, which share many of the properties of the *azo*-**PC** system, is only 3.4 Å$^2$ and therefore substantially lower.[181] Hence, the packing in *cis* state *azo*-**PC** is worse compared to POPC. Future experiments to fully elucidate the origin of the constant diffusion coefficient of the *cis* state might entail temperature

dependent monolayer studies or experiments which are directly sensitive to the bilayer area per lipid, such as NMR[186] or X-ray and neutron scattering.[187]

Next, experiments were performed to find out how the temperature dependent bilayer properties affect the optical membrane properties. As previously explained, higher lateral mobility is an indication of a change in the intermolecular interaction and should therefore affect the ability of the molecules to form H-aggregates. Absorbance measurements in the *trans* state were performed for both *azo*-**PC** SUV suspensions and *azo*-**PC** dissolved in chloroform as reference for different temperatures (Figure 5.5).

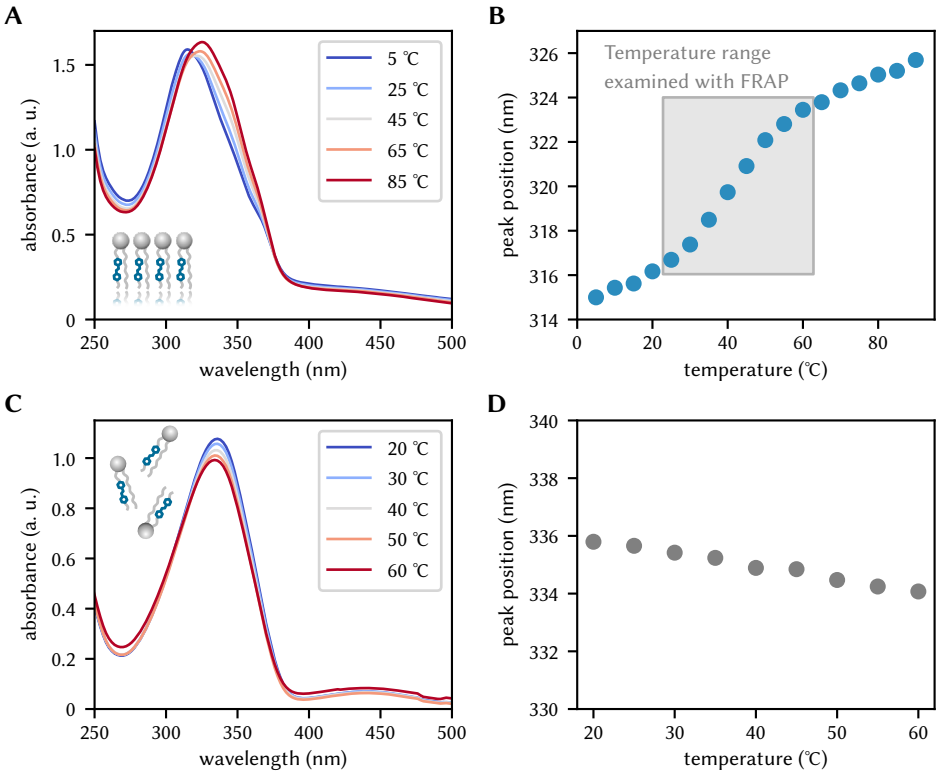


**Figure 5.5: Temperature dependence of the absorbance of *trans*-*azo*-PC in membranes and in solution.** **(A)** The absorbance spectra of *azo*-**PC** SUVs changes with temperature. **(B)** The peak position of the $S_0 \longrightarrow S_2$ transition shifts by ≈10 nm between 0 ˚C and 100 ˚C. **(C)** For comparison, the temperature dependent absorbance of *azo*-**PC** dissolved in chloroform is measured. **(D)** The peak position blueshifts by 1 nm between 20 ˚C and 60 ˚C.

The SUV spectra show a clear redshift of the $S_0 \longrightarrow S_2$ transition. Over the total temperature range examined, from 5 ˚C to 90 ˚C, the peak position shifts by 10 nm, with the steepest change happening between 20 ˚C and 60 ˚C. For *azo*-**PC** lipids dissolved in

chloroform, the spectra stay mostly constant, with only a small blueshift of the peak position by 1 nm between 20 °C and 60 °C.

Comparing to the diffusion measurements, one can see a similar trend. Both measurements increase nearly linearly with temperature from 25 °C on until the curves start to flatten above 40 °C, indicating a correlation between the two observations. Since the diffusion of *trans* state membranes shows a behavior that is consistent with observations for other phospholipid membranes, it is likely that the area per lipid increases with temperature in this instance. An increase in area per lipid however changes the mean distance between the azobenzene units and hence also the dipole-dipole interaction energy, which is responsible for the shift of the transition peak. Another aspect is the disorder of the lipid chains in the bilayer, which increases with higher temperature. A higher probability of trans-gauche isomerization between the headgroup and azobenzene unit will change the average orientation of the dipole moments and therefore directly influences the optical shifts as well.

The phase behavior of lipid membranes is usually characterized with differential scanning calorimetry (DSC). With calorimetric measurements, the phase transition temperature of lipid membranes can be determined.[188] In DSC, the sample and a reference is slowly heated with a constant rate and the temperature simultaneously measured. When the sample undergoes a phase transition, additional heat is needed to increase the temperature. The difference in heat flow between sample and reference can be used to calculate the amount of heat released or absorbed during the transition. Since no information is available about the thermal properties of *azo*-**PC**, DSC is performed for both the *trans* and the *cis* state between 5 °C and 80 °C (Figure 5.6).

An *azo*-**PC** SUV suspension was prepared at 20 mg ml$^{-1}$. For comparison, a solution of DPPC SUVs was measured. The measurements were performed in sealed aluminum crucibles containing 50 µl of the SUV suspension. As reference, a aluminum crucible with the same amount of dd$H_2O$ was used. For the *cis* state, the suspension was illuminated with an UV LED for 2 min immediately prior to the measurement. During the experiment, the sample chamber was flushed with nitrogen gas and the scan rate was 5 K min$^{-1}$.

While the main phase transition of DPPC at 41 °C[52] can be clearly resolved, no phase transition was observed for neither *trans* nor *cis* state *azo*-**PC**. This agrees with the diffusion measurements, which do not exhibit a discontinuity in the diffusion coefficient as would typical for the main phase transition. Since both *azo*-**PC** membranes appear to

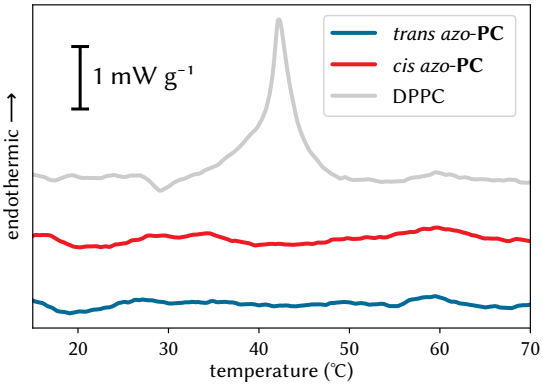


**Figure 5.6: Differential scanning calorimetry of *azo*-PC and DPPC.** DSC plot of the photolipids both in the *trans* and in the *cis* state. As reference, a scan of a DPPC sample is shown, obtained at the same concentration as the *azo*-**PC** samples. The plots are offset for clarity.

be fluid in this temperature range, phase transitions, if present, would be expected only at temperatures lower than 15 °C. This reveals another difference to POPC and PEPC. Here, the monounsaturated lipids in the *trans* state exhibit properties that are closer to the completely saturated lipid than to the *cis* isomer.[182] The phase transition temperature of PEPC is therefore expected to be close to 49 °C, the phase transition temperature of 16:0-18:0 PC. The phase transition temperature of the photolipid analogue, *azo*-**PC** in the *trans* state, is at least 20 K lower. A possible explanation for this behavior are the shorter hydrocarbon segments in the photoswitchable acyl chain. Shorter chain segments lead to a lower phase transition temperature (subsection 2.1.3), explaining the absence of the phase transition in the examined temperature range.

## 5.4 Toward optical membrane structuring

Since optical switching of the photolipid conformation allows to control membrane fluidity on fast timescales, employing *azo*-**PC** renders it possible to create patterns with differing diffusion coefficients on a SLB. It is relatively simple to create arbitrary light patterns on a surface, for example by inserting a transmission pattern in the light path,[189] by using interference patterns from multiple light beams[190] or by using spatial light modulators.[191] Here, a relatively crude pattern is used to conduct a proof of principle experiment. The pattern was generated by projecting the surface of a

light emitting diode onto the SLB. The contacts on top of the LED are non-transparent, blocking the UV light in certain areas.

Since the bleaching area of the FRAP experiment is larger than the structure of the UV pattern, the membrane diffusion was determined indirectly. The SLB was prepared as previously with TR-DHPE as the fluorescent label. Compounds based on azo groups are commonly used as fluorescence quenchers.[192–194] Furthermore, the quenching efficiency of azobenzene depends on its isomeric state.[195] The fluorescence intensity of TR-DHPE can hence be used to probe the local isomeric state, and thus the local fluidity, of the membrane.

PL measurements of *azo*-**PC**/TR-DHPE mixtures show that the fluorescent intensity depends on the isomer ratio of the photolipids, if the Texas Red dye is embedded in a membrane (Figure 5.7). When the lipids are dissolved in chloroform, the PL intensity of both the *trans* and the *cis* state is roughly the same. The intensity in the *cis* state is slightly lower than in the *trans* state, indicating that there is at least some quenching in this system as well. For PL measurements of SUVs however, there is a clear decrease of the fluorescence intensity in the *cis* state compared to the *trans* state. Since the lipids are assembled in a bilayer, the average distance between the Texas Red label, extending from a lipid headgroup, and the azobenzene units buried in the bilayer hydrophobic region, is dramatically reduced compared to the dilute solution in chloroform, where the lipids are presumed to be found as monomers. Due to this substantial difference in fluorescence intensity, the TR-DHPE emission can be used as a probe for the isomerization state and hence the phase state of the membrane. Additionally, the peak position of the emission is red shifted for the SUV suspension compared to the measurement in chloroform, due to the higher polarity of water compared to chloroform.[196]

The photolipid SLBs have been prepared as previously discussed, consisting of 99.5 % *azo*-**PC** and 0.5 % TR-DHPE. The fluorescence was excited in TIRF configuration with a green laser (562 nm), while the LED was projected from the top with a 100x water immersion objective. The direct projection of the pattern onto a glass substrate without any filter blocking the UV light is shown in Figure 5.8 A. Brighter areas correspond to higher UV intensity and hence a higher fraction of *cis* state molecules, leading to increased diffusion coefficients and thinner membranes.

When projected onto a SLB, the UV illumination excited additional fluorescence which overwhelms the signal from the bilayer itself. Therefore, fluorescent images of the bilayer directly after patterned illumination are shown. Directly after blocking the

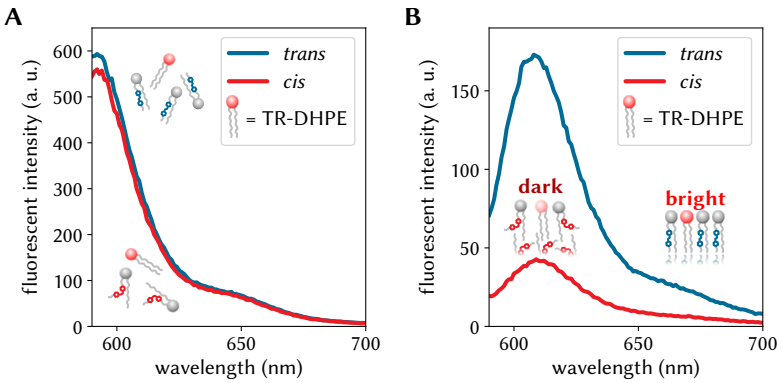


**Figure 5.7: Quenching of TR-DHPE in *azo*-PC membranes.** Fluorescence of TR-DHPE dissolved together with *azo*-**PC** in chloroform **(A)** and assembled in *azo*-**PC** SUVs **(B)**. The lipid concentration was the same for both measurements, with a ratio between *azo*-**PC** and TR-DHPE of 99:1. The signal was obtained both in *trans* and in *cis* state, with an excitation wavelength of 582 nm.

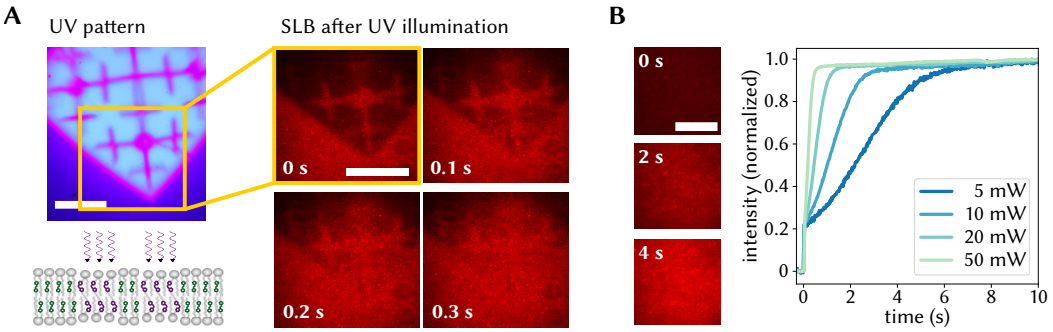


**Figure 5.8: Patterning of membrane properties with UV illumination. (A)** An UV pattern is used to create a pattern with different membrane properties. The bright areas correspond to higher UV intensity. After switching off the UV illumination, the pattern is clearly visible in the fluorescence of the SLB. The pattern disappears within tenths of seconds. (Scale bar = 30 µm) **(B)** Evolution of the fluorescent signal of *azo*-**PC** SLBs, stained with TR-DHPE (0.5 mol%). Previous to starting the measurement, the sample is switched into the PSS after UV illumination. At $t$ = 0 s, the excitation light (562 nm, TIRF) is switched on. Depending on the excitation intensity, the isomerization back to the *trans* state occurs with difference rates, as can be seen from the fluorescent signal. The fluorescence intensity is normalized to its maximum value. The images shows a SLB illuminated with a laser power of 5 mW. (Scale bar = 15 µm)

UV illumination, the pattern of the LED was clearly visible on the membrane. Darker regions on the membrane correspond to to areas exposed to high UV intensity. For this configuration, feature sizes down to ≈2 µm were achieved. The pattern disappears, depending on the laser intensity, within less than a second. For the depicted measurement, the time constant of recovery is ≈150 ms. This also shows, that the recovery is not due to diffusion of unbleached molecules into the dark areas, since this time constant would lead to unreasonably high diffusion coefficient.

To further demonstrate, that this experiment is not, the experiment was repeated without the pattern (Figure 5.8 B). The bilayer was prepared in a PSS containing a high fraction of *cis* state molecules with homogeneous UV illumination for ≈30 s, while the fluorescence excitation light was blocked. After turning on the excitation light, the fluorescence intensity recovered within seconds. Here, the recovery was homogeneous over the whole field of view. If the recovery had been due to diffusion of unbleached molecules from outside the field of view, the intensity would recover faster at the edges of the image. Additionally, the time needed for full recovery depended on the laser intensity. Higher excitation intensities lead to faster recovery, consistent with the isomerization rates, which also depend on the excitation intensities.

## Summary

This chapter demonstrates that the photosensitive nature of the *azo*-**PC** system allows to control membrane fluidity with light. Between the *trans* and the *cis* state, the diffusion coefficient differs by almost a factor of two. As the main driving factor for the difference, the different footprints of the two isomers in the membrane, as evident from the change in area per lipid is identified. Furthermore, by tuning the illumination, the diffusion coefficient can be precisely controlled in-between its two extremal values. This behavior emulates the temperature dependence of standard phospholipids, which also rely on conformational changes in the hydrocarbon chains, namely trans-gauche isomerization of the C – C bonds. In the *cis* state, the increased probability of gauche rotamers counteracts the unfavorable geometry of the azobenzene, leading to a constant diffusion coefficient over a large temperature range. The diffusion coefficient of a membrane consisting of *trans* or *cis* state molecules converges after ≈40 °C, which is a drawback for measurements at physiological temperatures. However, this can be easily overcome by synthesizing different photolipids with longer chains or

with the azobenzene unit at a different position within the acyl chain, which would raise the convergence temperature. The light sensitive nature of *azo*-**PC** membranes allows to locally "write and erase" regions with different properties onto a supported lipid bilayer with suitable light sources. The proof of principal experiment paves the way for future experiments requiring an on-demand change in membrane properties at locally defined positions, e.g. to study receptor clustering.

# Chapter 6

# Light-induced permeability of *azo*-PC membranes

The cell membrane is the protective barrier shielding the sensible cell interior from the environment. The lipid bilayer, the scaffold of the cell membrane, is considered to be almost impermeable to water soluble substances such as charged molecules or ions.[197] Active transport across the bilayer by specialized proteins however drives many vital cellular processes such as cell-cell communication or cell signaling,[198,199] either directly by delivering specific substances into the cell or passively by regulating electrochemical gradients[200] and intracellular pH levels.[201]

Manipulating the permeability is thus often attempted by addressing specific membrane channels, which is powerful but requires the genetic manipulation of cells[202] or the tailored synthesis of molecules binding specifically to the protein of interest.[82] A much simpler approach is achieved by manipulating the permeability of the lipid bilayer directly, which is possible by heat[20,21] or strong electric fields.[203,204]

Pure lipid membranes become especially permeable when undergoing a phase transition.[205] A similar situation can be created by switching between the two isomers of *azo*-**PC**. The ability of this system to control the permeability of photolipid membranes with light is investigated within this chapter. First, the macroscopic permeability of *azo*-**PC** GUVs for fluorescent dyes is examined. Then, the ion permeability is probed by measuring the current across a small membrane patch, yielding information about the transient nature of the pore formation.

## 6.1 Leaking of fluorescent dyes from GUVs upon isomerization

Leaking of dyes through the membrane of GUVs can be measured with standard fluorescence setups by tracking the fluorescence intensity within the vesicles. Due to its simplicity, the dye leaking assays have been used in many experiments which investigate membrane permeability, for instance to report on membrane permeability near the main phase transition temperature.[206,207] By observing and analyzing (self)quenching effects, information on membrane permeability can also be derived from bulk absorbance measurements.[208]

In this work, the fluorescence of dyes encapsulated in GUVs made of *azo*-**PC** was measured upon isomerization from *trans* to *cis* and vice versa, thereby tracking the permeability of the membrane. The GUVs were prepared in a sucrose solution (300 mM) containing water soluble ATTO 532 dye (ATTO-TEC). To reduce the dye concentration of the surrounding solution, the vesicle suspension was diluted by a factor of 1000 in glucose (300 mM).

At first, GUVs were observed in dark field configuration (Figure 6.1 A). The scattering of the lipid membrane allows to detect vesicles even if the fluorophore concentration in- and outside of the vesicle is the same. The vesicles were imaged with a 100x water immersion objective. Due to the dark field configuration, the vesicles were additionally subject to white light illumination . The PSS was thus determined by the ratio between the white light and the UV LED. The fluorescence was determined with ImageJ[209,210] by calculating the intensity counts for all pixels which are enclosed by the vesicle circumference, normalized by the number of pixel.

For the depicted GUV, the fluorescence decreased upon switching on the UV illumination, but recovered after a few seconds. After switching off the UV light, and thus increasing the *trans* state population due to the white light, the intensity increased slowly over ≈5 s. Both these events were accompanied by a change of the vesicle morphology. Then, the fluorescence started to decrease before the UV illumination is switched on for the second time. The fluorescence decreased until only the vesicle circumference is still visible, indicating that the membrane becomes permeable to the dye. The membrane is thus able to compensate the effects of the isomerization until a certain threshold is reached and the membrane starts to open pores.

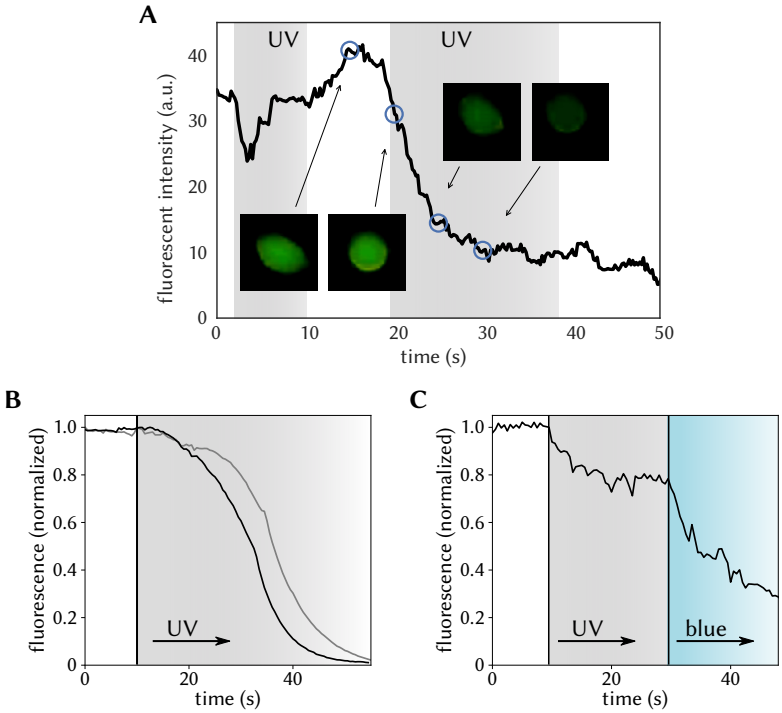


**Figure 6.1: Leaking of fluorescent dyes from GUVs. (A)** The average fluorescent intensity was measured in dark field configuration with a 100x objective, which allows to identify the membrane circumference. Upon UV illumination (365 nm), the vesicle deforms and eventually, the fluorescence decreases. **(B)**, **(C)** Example fluorescence traces measured in epifluorescence configuration with a 20x objective. The fluorescence was excited with either the UV or the blue filter cube, thereby guaranteeing a PSS with maximum isomer concentration.

The reason for this behavior is found in the response of the vesicles to the change of the total membrane area due to the different area per lipid of the isomers of *azo*-**PC**. The shape of a vesicle is largely defined by its spontaneous curvature and its reduced volume.[211] The reduced volume is a measure for the excess membrane area and is defined as the ratio between the vesicle volume $V$ and the volume of a sphere with equal surface area $A$:

$$v = \frac{6\sqrt{\pi}V}{A^{3/2}}. \tag{6.1}$$

At isotonic conditions, vesicles are slightly flaccid and its membrane exhibits thermal undulations, which ensures that the membrane is free of tension.[74] GUVs react to changes of the reduced volume by membrane deformations and, for large changes, either by forming daughter vesicles or by opening pores (Figure 6.2).[212,213] The fluorescence traces, together with the observed morphology changes of the depicted vesicle, suggests that a combination of both processes is induced for this illumination condition (white-light and UV-LED). The increase in fluorescence can also be attributed to the deformation of the vesicles. When a deflated vesicle reorganizes and becomes spherical again, the height of the vesicle increases. Due to the depth of field of the objective, the measured fluorescence intensity in the vesicle circumference increases as well.

Repeating the measurement in epifluorescence configuration yields a higher fraction of *cis* state molecules, since the isomerization light also excites the ATTO 532 dye. Furthermore, both the switching rate between the PSSs and the reproducibility are due to the fixed illumination through the 20x objective (Figure 6.1 B&C). However, the vesicle circumference is not visible since the membrane is not stained.

Upon switching from *trans* to *cis*, the fluorescence intensity of the GUVs stayed almost constant or only slightly decreased for a few seconds (Figure 6.1 B). Then, leaking accelerated until it reached a lower intensity level. Often, the fluorescence of the GUVs was thereafter indistinguishable from the background, suggesting a complete solution exchange. In a few cases however, the intensity stabilized at a lower, but finite level (Figure 6.1 C). For all GUVs exhibiting this behavior, the fluorescence started to decrease immediately after switching back with blue light, until the vesicle disappeared completely. The concentration of the dyes inside of the vesicles was thus the same as in its surrounding solution, within the detection limit of the CCD.

Upon isomerization from *trans* to *cis*, the lipid area increases, as discussed in chapter 5. Increasing the membrane area while keeping the volume constant decreases the

reduces volume *v*. Here, the vesicles relax predominantly due to pore formation and solution exchange as evident from the fluorescence traces. For pure *azo*-**PC** vesicles, we have already demonstrated that it is possible to induce a range of different shape deformations depending on the illumination conditions and the initial shape and size of the vesicles.[94] The difference between these experiments is the rate of isomerization, since unfocused LED illumination was used for isomerization in the dark-field configuration compared to the focused UV illumination in epifluorescence configuration. Whether the vesicle reacts to changes of the reduced volume by deformation or pore formation depends thus depends on the rate and the magnitude of the membrane area change. For a different azobenzene derivative, *ortho*-tetrafluoroazobenzene, administered at lower concentrations, budding without solution exchange has been observed.[211] Since only a fraction of the molecules contributed to the area change for this system, the reduced volume was only slightly changed and thus only shape deformation could be observed.

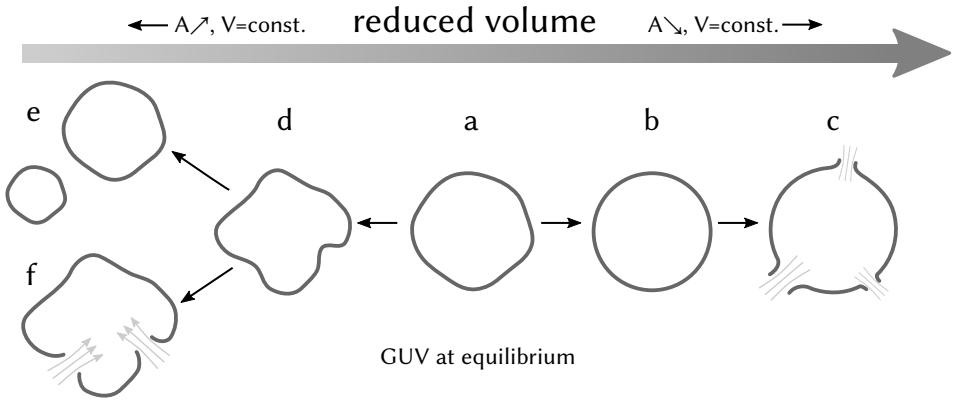


**Figure 6.2: Pore formation and deformation of GUVs.** At equilibrium, a GUV exhibit thermal undulations **(a)**. When the reduced volume is increased, the undulations are stretched out **(b)**, until the tension is too high and pores open, which allows for a rapid exchange of solution. On the other hand, when the reduced volume is decreased from its equilibrium, the vesicle adapts by deformation **(d)**. The strain on the membrane can be relaxed by either vesicle splitting **(e)**, or again by pore formation **(f)**.

The reverse process, switching from *cis* to *trans*, was achieved by blue light illumination of the vesicles that could still be seen after UV illumination. The measurement was started after the fluorescence intensity approaches a new, constant value, indicating that the vesicle assumed a new equilibrium shape representing the *trans*/*cis* ratio at the PSS. The lipid membrane is thus free of tension before illuminating with blue light.

Upon isomerization, the reduced area per lipid therefore leads to a built up of membrane tension, which is eventually relaxed by pore formation (Figure 6.2 a-c).[214,215]

GUVs can withstand a small increase of the reduced volume, since they are slightly flaccid at equilibrium. Above a certain value however, the membrane stress exceeds a threshold and responds by opening a membrane pore, which is only transient and closes again after some time driven by line tension.[216] The radius of the pores can be as large as several µm, thus it is possible that a large percentage of the solution enclosed by the vesicles is exchanged during the pore opening time. Here, the pore opening time is long enough, that the dye concentration in the vesicle cannot be discerned from the surrounding fluid for every observed vesicle. The pore itself was not observed for any of the vesicles measured in dark field, presumably due to the strong fluctuations induced upon switching.

## 6.2 Light-induced current steps in photolipid membranes

To gain further insight in the pore opening process, the ion permeability of *azo*-**PC** membranes was measured with the planar patch-clamp technique (see section 3.3 for measurement details). Permeation of ions through a lipid bilayer is either enabled by passive permeation of ions directly through the hydrophobic core of the membrane. The energy barrier for this process is however very high.[217] Passive permeation is therefore assumed to be facilitated by an ion induced defect mechanism.[218]

A second permeability process is enabled by transient pores.[219] The signature of permeability through pores is quite distinct in patch-clamp measurements. Bilayer pores are usually transient, showing rapid opening and closing kinetics.[220] Additionally, the physical reorganization of the photolipid membrane due to isomerization leads to a transient current spike upon switching. This *displacement current* is generated by reorientation of dipoles or spatial redistribution of ions at the interface to the aqueous solution.[221] The timescale of this event is however usually on the timescale of µs, faster than the chosen resolution of the current measurement (ms) and thus neglected for the following discussion.

Patch-clamp measurements of pure *azo*-**PC** membranes were performed in HCl solution (100 mM) at a holding potential of 50 mV (Figure 6.3 A). The bilayer was

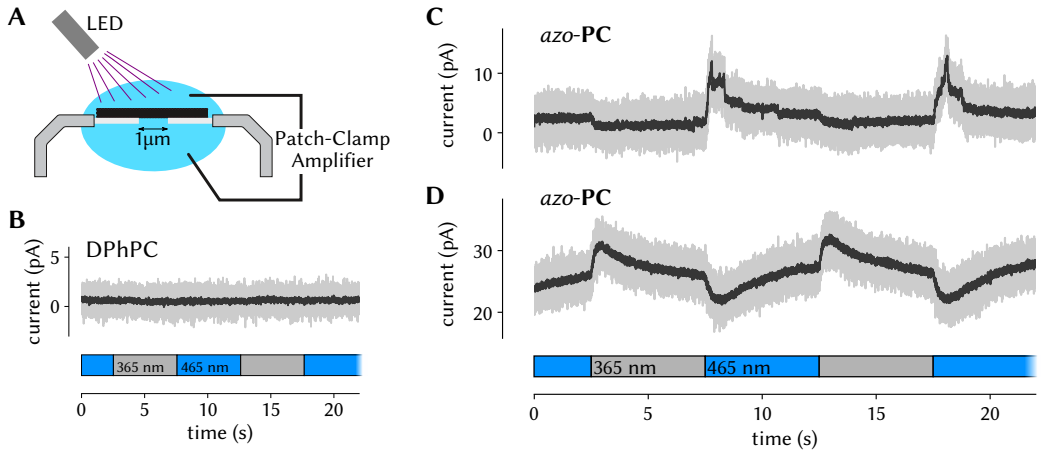


**Figure 6.3: Membrane permeability measured with planar patch-clamp. (A)** A lipid bilayer is spanned across a hole in a glass slide. The ion current across the bilayer is measured with a patch-clamp amplifier, while the bilayer is illuminated with either blue (465 nm) or UV (365 nm) light. **(B)** The current measured across a DPhPC bilayer is not influenced by the light.. For *azo*-**PC**, the current decreases upon UV illumination for a tight seal **(C)**, but increases for a looser seal **(D)**. Additionally, transient pores can be observed for a tight seal **(C)**.

illuminated by blue (465 nm) and UV (365 nm) light for 5 s alternatingly for several cycles. Control measurements of DPhPC bilayers exhibit no sensitivity to light exposure (Figure 6.3 B).

Upon switching between blue and UV light illumination, the measured current across *azo*-**PC** bilayers changed significantly (Figure 6.3 C,D). The direction however is different for the two traces. This indicates, that the results do not exclusively reflect the membrane permeability. The total permeability measured in this setup depends also on the area contributing to the Gigaseal. Since the membrane area changes upon isomerization, the current signal also changes. Additionally, in patch-clamp experiments employing GUVs, the membrane is sucked continuously into the glass aperture because of the adhesion between the membrane and the glass.[134] Due to the conical shape of the aperture,[135] the cross-section is larger for a bilayer that is sucked further in. The current for a bilayer that is already longer in Gigaseal configuration is consequently larger than for a fresh Gigaseals (trace **D** compared to trace **C** of Figure 6.3).

For bilayers exhibiting high baseline resistance, additional current events were observed in some instances (Figure 6.3 A). Upon switching from *cis* to *trans*, the current increased momentarily to a higher value, but returned back to the baseline value after a

few seconds. The transition back to the baseline occurred via discrete steps, similar to the current signature of pores in bilayer systems.[220] The magnitude of the steps (1 pA to 10 pA) was also consistent with typical values for ion channel pores.[220]

The process is thus similar to the observations for the fluorescence dyes. Switching to the *cis* state increases the membrane area which can be compensated to a certain extent by deformation of the bilayer and adhesion to the glass surface. Switching back after the new equilibrium has been reached induces tension since the bilayer has to overcome the adhesion forces between the glass and the membrane. The release of tension via the formation of pores can then be observed by conduction events, as has been observed already for micropipette aspirated vesicles.[222] The conduction states are with a few seconds rather long-lived, as typical pore life-times are in the range of tens of ms.[220] The adhesion forces thus stabilizes the membrane pore, prolonging the life-time in the process, until enough lipids are pulled off the glass surface to close the pore.

In summary, this chapter demonstrates how light can be used to control the permeability of photolipid membranes. The permeability is indirectly driven by the change of the lipid area. In conjunction with the low baseline permeability of lipid bilayers, the abrupt change in membrane area upon isomerization leads to built-up of forces, which is released under exchange of solution. Especially the isomerization from *cis* to *trans*, respectively the decrease of lipid area, leads to lateral tension, which induces transient pores. These pores can be observed, since fluorescent dyes leak out of GUVs and typical signatures are observed in patch-clamp measurements. Given the similarities to results for vesicles in hyper- and hypotonic solutions, these results help in understanding the effects of osmotic pressure on vesicles and cells. Repeating these experiments on a micropipette setup with proper fluorescence illumination and detection would allow to gain further quantitative information on pore formation and lifetime.

# Chapter 7

# Conclusion: Controlling lipid interaction with light

Membranes are unique biological structures due to their extreme thinness compared to their lateral extension. Many, if not all physical bilayer parameters are fundamentally governed by intermolecular interaction. Photolipids thus provide an excellent avenue to control and monitor membrane parameters. Isomerizing the azobenzene moiety in one of the acyl chains of *azo*-**PC** allows to control the interaction between the lipids *in situ* and on demand with light. Additionally, the interaction between the individual azobenzene groups gives rise to optical absorbance profiles that are sensitive to the local concentration of *azo*-**PC** and the phase state of the membrane.

Within this work, photosensitive membrane systems were prepared and characterized. To this end, supported bilayers and bilayer vesicles containing the photolipid *azo*-**PC** have been prepared. Since most characterization techniques rely on light interaction in one way or another, new protocols for the investigation of membrane properties have been devised. The experimental work depicted throughout this thesis demonstrates the precise control that can be attained by thoroughly understanding and manipulating the lipid interaction.

In chapter 4, the absorbance of *azo*-**PC** in bilayer assemblies has been characterized. Notably, the $S_0 \longrightarrow S_2$ transition of the *trans* isomer exhibits a blue shift by 20 nm in pure *azo*-**PC** membranes compared to monomer spectra in chloroform. The underlying mechanism is attributed to dipole coupling due to the quasi crystalline orientation of the azobenzene units. The magnitude of the shift is dependent on the concentration

of *azo*-**PC** in combination with standard phospholipids and cholesterol. The addition of cholesterol at moderate levels induces additional blue-shift, implying that the absorbance is sensitive to the phase state of the membrane. Some properties of membrane samples can thus be characterize with simple absorbance measurements. This is especially useful to determine, if the photolipid are homogeneously distributed or clustered in domains, as can be observed in ternary domain forming lipid mixtures.

Furthermore, the photolipid isomers have distinct intermolecular interaction. Membranes composed of *trans* or *cis* state lipids thus have different physical properties and exhibit phase separation in different lipid mixtures. Isomerizing with light allows to reversibly induce macroscopic domains in ternary mixtures and, by precisely controlling the illumination conditions, in binary mixtures containing *azo*-**PC** and cholesterol.

Isomerization also affects the mechanical properties of photolipid membranes. Due to the kink in *cis* state lipids, the membrane is softer and thinner compared to the *trans* state. The presence of domains changes the membrane bending rigidity due to contribution from the domains boundaries. The different curve shapes of the *trans* and the *cis* state hint toward the presence of nanodomains.

The self-diffusion of lipids in a bilayer is mainly dependent on the average area a lipid takes up in the two dimensional bilayer sheet. The free area theory sums up all the energetic contributions in an effective area, that is available for a lipid to diffuse into. The footprint of the *cis* state is larger than of the *trans* state. Photolipids thus enables the control of the lipid diffusion with light, resembling the temperature dependence of bilayer properties, as outlined in chapter 5. By carefully tuning the illumination condition, the diffusion coefficient can be tuned between the two extremal values. The thermal dependency of the diffusion coefficient of the *trans* state correlates well with the temperature dependent absorbance spectra, highlighting the importance of the interaction between the lipids. With increasing temperature, the diffusion coefficients of the *trans* and the *cis* state converge to the same value, due to the increasing importance of the trans-gauche isomerization of the acyl chains. Finally, membrane areas with distinct diffusion coefficients were created by illuminating with a patterned light source.

For applications, vesicles are often proposed as vehicles for targeted release of drugs.[223] In chapter 6, the permeability of the photolipid membranes is examined. GUVs start to leak fluorescent dyes upon isomerization. The mechanism for the *trans* to *cis* isomerization is however different than for the reverse process. Due to the semi-permeable nature of the lipid bilayer in combination with its mechanical properties, the

response of the bilayer to a decrease or an increase of the membrane area with a fixed volume leads to different relaxation mechanisms. The effect is similar to the behavior of GUVs when put into a hyper- or a hypotonic solution. A decrease in membrane area leads to the formation of pores, while the release of membrane stress after area increase can additionally occur via budding. Current measurements through a small membrane patch compliment the results obtained for dye permeability. Area increase is solely compensated for by membrane deformation, while the reverse process leads to the formation of transient pores, as indicated by current steps.

In summary, the unique properties of photolipid membranes facilitates the manipulation and measurement of many membrane properties with high spatial and temporal resolution. While the application of the purely synthetic *azo*-**PC** lipid *in vivo* is questionable, the immediate response to light stimuli enables new measurements of the underlying physical characteristics. The coupling of the optical dipoles highlights the importance of intermolecular interaction in lipid membranes. Light-sensitivity also enables fast and reversible formation of domains with distinct properties, which helps overcoming challenges in studies of receptor dynamics using lipid bilayers as scaffolds.

# Appendix A

## A.1 Determination of the *trans*/*cis* ratio

The isomerization of azobenzene-derived molecules with light yields a photostationary state that contains both isomers. The relative concentration of each isomer depends on the illumination spectrum and the absorbance of each isomer at the respective wavelength. The concentration of *trans* state *azo*-**PC** molecules after illumination with 365 nm light is determined by the TEM method.[224,225] This method has been shown to reliably determine the pure *cis* state absorbance spectrum.[142] The absorbance spectra are obtained with a quartz cuvette (2 mm or 10 mm) by a UV-Vis Spectrophotometer (Cary 60, Agilent). The lipid concentration is for both the measurements in chloroform and in SUVs was 212 µM. To keep the lipid concentration constant, the photolipid concentration is 10.6 µM for the sample containing 5 % *azo*-**PC** and 95 % DPhPC.

The method uses the vibronic structure, which is visible in the absorbance spectrum of *trans azo*-**PC**, but not in the *cis* state spectrum. The vibronic features are especially visible when plotting the second derivatives of the spectra. By subtracting the *trans* state component, weighted for its concentration, the *cis* state spectrum can be obtained.

$$\frac{\mathrm{d}^2 A_{PSS}}{\mathrm{d}\lambda^2} - c \cdot \frac{\mathrm{d}^2 \varepsilon_{trans}}{\mathrm{d}\lambda^2} \tag{A.1}$$

where $A_{PSS}$ is the respective absorbance at the PSS and $\varepsilon_{trans}$ is the *trans* state absorbance spectrum. The coefficient $c$ is chosen so that the vibronic features in the range of 340 – 380 nm are minimized (Figure A.1 A). The optimal value for $c$ determines the *trans* fraction at the PSS.

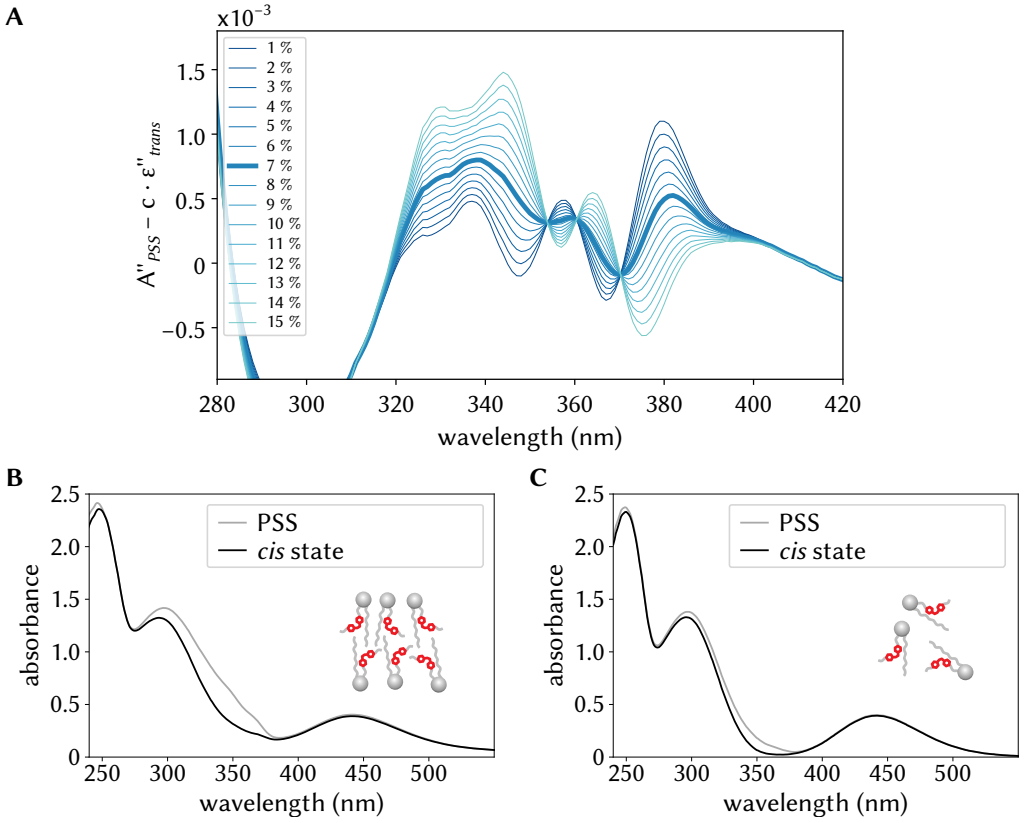


**Figure A.1: Determination of the *trans* fraction at the photostationary state. (A)** The second derivative of the absorbance spectra are calculated after smoothing with a Savitzky-Golay filter. The resulting *trans* state curve is subtracted from the PSS, weighted with different factors. The concentration that reduces the vibronic features between 340 nm and 380 nm best is chosen as the *trans* state fraction. The pure *cis* state spectra are shown for 100 % *azo*-**PC** SUVs **(B)** and for *azo*-**PC** in chloroform **(C)**.

The *trans* state absorbance spectrum $\varepsilon_{trans}$ is taken as the spectrum at thermal equilibrium. For *azo*-**PC** SUVs, the calculation is complicated by the optical shifts induced due to H-aggregation. The low concentration of *trans* state photolipids after UV illumination is shifted compared to the pure *trans* state spectrum in thermal equilibrium. In this case, a spectrum of a suspension of SUVs consisting of DPhPC (95 %) and *azo*-**PC** (5 %) is used as the *trans* state spectrum. Previous to the calculation, the spectrum is scaled to match the same photolipid concentration as in the case of 100 % *azo*-**PC** SUVs.

Subtracting $\varepsilon_{trans}$ scaled by the concentration $c$ from the spectrum at the PSS yields the pure *cis* state spectrum (Figure A.1 B,C). For the SUVs, the PSS after illumination with 365 nm contains still 7 % of *trans* state molecules, while for *azo*-**PC** dissolved in

chloroform, the fraction is only 3 %. After subtraction, the SUV spectrum does not show increased absorbance in the region between 320 and 370 nm any more.

## A.2 Synthesis of *azo*-PC

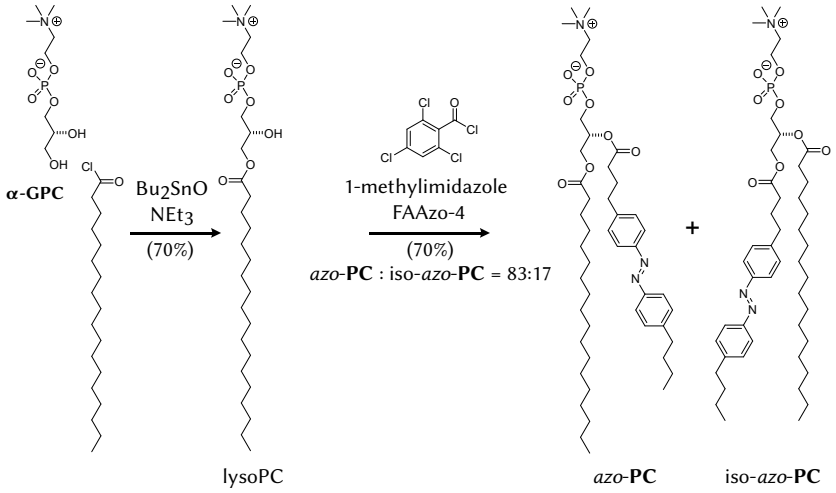


**Figure A.2: Reaction Scheme.** *Azo*-**PC** and its regioisomer iso-*azo*-**PC** were synthesized with a new synthesis employing an optimized Yamaguchi esterification protocol. For the experiments reported here, only *azo*-**PC** was used. Please refer to Urban *et al.*[139] for further details.

## A.3 Chemical structure of lipids

DPhPC

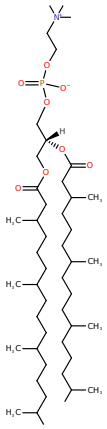

DOPC

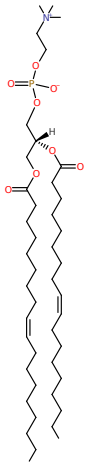

DMPC

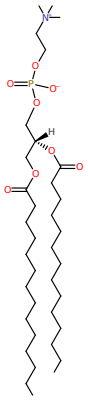

DPPC

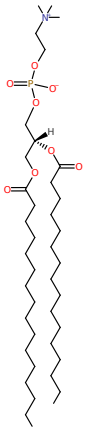

DSPC

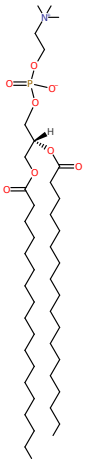

Texas Red DHPE

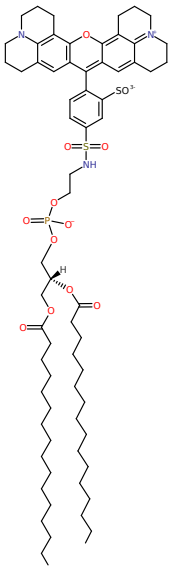

Marina Blue DHPE

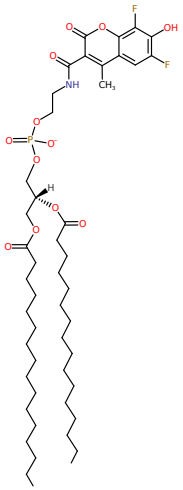

Cholesterol

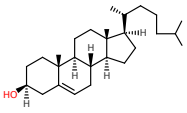

# Bibliography


[1] J. C. Skou. "The influence of some cations on an adenosine triphosphatase from peripheral nerves". In: *Biochimica et Biophysica Acta* 23 (1957), pp. 394–401. DOI: 10.1016/0006-3002(57)90343-8.

[2] W. Kühlbrandt. "Biology, structure and mechanism of P-type ATPases". In: *Nature Reviews Molecular Cell Biology* 5.4 (2004), pp. 282–95. DOI: 10.1038/nrm1354.

[3] H. T. McMahon and J. L. Gallop. "Membrane curvature and mechanisms of dynamic cell membrane remodelling". In: *Nature* 438.7068 (2005), pp. 590–596. DOI: 10.1038/nature04396.

[4] N. B. Cole et al. "Diffusional Mobility of Golgi Proteins in Membranes of Living Cells". In: *Science* 273.5276 (1996), pp. 797–801. DOI: 10.1126/science.273.5276.797.

[5] C. L. Wey, R. A. Cone, and M. A. Edidin. "Lateral diffusion of rhodopsin in photoreceptor cells measured by fluorescence photobleaching and recovery". In: *Biophysical Journal* 33.2 (1981), pp. 225–232. DOI: 10.1016/s0006-3495(81)84883-7.

[6] R. Macháň and M. Hof. "Lipid diffusion in planar membranes investigated by fluorescence correlation spectroscopy". In: *Biochimica et Biophysica Acta (BBA) - Biomembranes* 1798.7 (2010), pp. 1377–91. DOI: 10.1016/j.bbamem.2010.02.014.

[7] L. Guo et al. "Molecular diffusion measurement in lipid bilayers over wide concentration ranges: a comparative study". In: *ChemPhysChem* 9.5 (2008), pp. 721–8. DOI: 10.1002/cphc.200700611.

[8] Y. Sakuma and M. Imai. "From vesicles to protocells: the roles of amphiphilic molecules". In: *Life (Basel)* 5.1 (2015), pp. 651–75. DOI: 10.3390/life5010651.

[9] E. Sezgin et al. "The mystery of membrane organization: composition, regulation and roles of lipid rafts". In: *Nature Reviews Molecular Cell Biology* 18.6 (2017), pp. 361–374. DOI: 10.1038/nrm.2017.16.

[10] S. L. Veatch and S. L. Keller. "A Closer Look at the Canonical 'Raft Mixture' in Model Membrane Studies". In: *Biophysical Journal* 84.1 (2003), pp. 725–726. DOI: 10.1016/s0006-3495(03)74891-7.

[11] L. J. Pike. "Rafts defined: a report on the Keystone symposium on lipid rafts and cell function". In: *Journal of Lipid Research* 47.7 (2006), pp. 1597–1598. DOI: 10.1194/jlr.E600002-JLR200.

[12] C. Dietrich et al. "Lipid Rafts Reconstituted in Model Membranes". In: *Biophysical Journal* 80.3 (2001), pp. 1417–1428. DOI: 10.1016/s0006-3495(01)76114-0.

[13] T. Baumgart, S. T. Hess, and W. W. Webb. "Imaging coexisting fluid domains in biomembrane models coupling curvature and line tension". In: *Nature* 425.6960 (2003), pp. 821–4. DOI: 10.1038/nature02013.

[14] S. L. Veatch and S. L. Keller. "Separation of liquid phases in giant vesicles of ternary mixtures of phospholipids and cholesterol". In: *Biophysical Journal* 85.5 (2003), pp. 3074–83. DOI: 10.1016/S0006-3495(03)74726-2.

[15] S. L. Veatch and S. L. Keller. "Seeing spots: complex phase behavior in simple membranes". In: *Biochimica et Biophysica Acta (BBA) - Molecular Cell Research* 1746.3 (2005), pp. 172–85. DOI: 10.1016/j.bbamcr.2005.06.010.

[16] D. Marsh. "Cholesterol-induced fluid membrane domains: a compendium of lipid-raft ternary phase diagrams". In: *Biochimica et Biophysica Acta (BBA) - Biomembranes* 1788.10 (2009), pp. 2114–23. DOI: 10.1016/j.bbamem.2009.08.004.

[17] T. M. Konyakhina et al. "Control of a Nanoscopic-to-Macroscopic Transition: Modulated Phases in Four-Component DSPC/DOPC/POPC/Chol Giant Unilamellar Vesicles". In: *Biophysical Journal* 101.2 (2011), pp. L8–L10. DOI: 10.1016/j.bpj.2011.06.019.

[18] S. L. Goh, J. J. Amazon, and G. W. Feigenson. "Toward a better raft model: modulated phases in the four-component bilayer, DSPC/DOPC/POPC/CHOL". In: *Biophysical Journal* 104.4 (2013), pp. 853–62. DOI: 10.1016/j.bpj.2013.01.003.

[19] R. Palankar et al. "Nanoplasmonically-induced defects in lipid membrane monitored by ion current: transient nanopores versus membrane rupture". In: *Nano Letters* 14.8 (2014), pp. 4273–9. DOI: 10.1021/nl500907k.

[20] P. Urban et al. "Reversible control of current across lipid membranes by local heating". In: *Scientific Reports* 6 (2016), p. 22686. DOI: 10.1038/srep22686.

[21] Q. Liu et al. "Exciting cell membranes with a blustering heat shock". In: *Biophysical Journal* 106.8 (2014), pp. 1570–7. DOI: 10.1016/j.bpj.2014.03.008.

[22] A. Rettenmaier, T. Lenarz, and G. Reuter. "Nanosecond laser pulse stimulation of spiral ganglion neurons and model cells". In: *Biomedical Optics Express* 5.4 (2014), pp. 1014–25. DOI: 10.1364/BOE.5.001014.

[23] T. Weber et al. "SNAREpins: Minimal Machinery for Membrane Fusion". In: *Cell* 92.6 (1998), pp. 759–772. DOI: 10.1016/s0092-8674(00)81404-x.

[24] Y. H. M. Chan, B. van Lengerich, and S. G. Boxer. "Effects of linker sequences on vesicle fusion mediated by lipid-anchored DNA oligonucleotides". In: *Proceedings of the National Academy of Sciences* 106.4 (2009), pp. 979–984. DOI: 10.1073/pnas.0812356106.

[25] C. G. Morgan et al. "Incorporation of a novel photochromic phospholipid molecule into vesicles of dipalmitoylphosphatidylcholine". In: *Biochimica et Biophysica Acta (BBA) - Biomembranes* 820.1 (1985), pp. 107–114. DOI: 10.1016/0005-2736(85)90221-4.

[26] C. G. Morgan et al. "The phase behaviour of dispersions of Bis-Azo PC: photoregulation of bilayer dynamics via lipid photochromism". In: *Biochimica et Biophysica Acta (BBA) - Biomembranes* 903.3 (1987), pp. 495–503. DOI: 10.1016/0005-2736(87)90056-3.

[27] C. G. Morgan et al. "Light-induced fusion of liposomes with release of trapped marker dye is sensitised by photochromic phospholipid". In: *Biochimica et Biophysica Acta (BBA) - Biomembranes* 903.3 (1987), pp. 504–509. DOI: 10.1016/0005-2736(87)90057-5.

[28] T. Hamada et al. "Photochemical control of membrane raft organization". In: *Soft Matter* 7.1 (2011), pp. 220–224. DOI: 10.1039/c0sm00797h.

[29] J. A. Frank et al. "Optical Control of Lipid Rafts with Photoswitchable Ceramides". In: *Journal of the American Chemical Society* 138.39 (2016), pp. 12981–12986. DOI: 10.1021/jacs.6b07278.

[30] G. Guidotti. "Membrane proteins". In: *Annual Review of Biochemistry* 41 (1972), pp. 731–52. DOI: 10.1146/annurev.bi.41.070172.003503.

[31] H. Lodish et al. *Molecular cell biology*. Vol. 3. New York: WH Freeman, 1995.

[32] S. J. Singer and G. L. Nicolson. "The fluid mosaic model of the structure of cell membranes". In: *Science* 175.4023 (1972), pp. 720–31. DOI: 10.1126/science.175.4023.720.

[33] G. L. Nicolson. "The Fluid-Mosaic Model of Membrane Structure: still relevant to understanding the structure, function and dynamics of biological membranes after more than 40 years". In: *Biochimica et Biophysica Acta (BBA) - Biomembranes* 1838.6 (2014), pp. 1451–66. DOI: 10.1016/j.bbamem.2013.10.019.

[34] K. Simons and E. Ikonen. "Functional rafts in cell membranes". In: *Nature* 387.6633 (1997), pp. 569–72. DOI: 10.1038/42408.

[35] K. Simons and M. J. Gerl. "Revitalizing membrane rafts: new tools and insights". In: *Nature Reviews. Molecular Cell Biology* 11.10 (2010), pp. 688–99. DOI: 10.1038/nrm2977.

[36] R. Alemany et al. "G protein-coupled receptor systems and their lipid environment in health disorders during aging". In: *Biochimica et Biophysica Acta (BBA) - Biomembranes* 1768.4 (2007), pp. 964–975. DOI: 10.1016/j.bbamem.2006.09.024.

[37] Q.-X. Jiang and T. Gonen. "The influence of lipids on voltage-gated ion channels". In: *Current Opinion in Structural Biology* 22.4 (2012), pp. 529–536. DOI: 10.1016/j.sbi.2012.03.009.

[38] C. Tanford. *Hydrophobic Effect: Formation of Micelles and Biological Membranes*. John Wiley & Sons Inc, 1973.

[39] J. N. Israelachvili, D. J. Mitchell, and B. W. Ninham. "Theory of self-assembly of lipid bilayers and vesicles". In: *Biochimica et Biophysica Acta (BBA) - Biomembranes* 470.2 (1977), pp. 185–201. DOI: 10.1016/0005-2736(77)90099-2.

[40] J. N. Israelachvili, D. J. Mitchell, and B. W. Ninham. "Theory of self-assembly of hydrocarbon amphiphiles into micelles and bilayers". In: *Journal of the Chemical Society, Faraday Transactions 2* 72 (1976). DOI: 10.1039/f29767201525.

[41] J. N. Israelachvili. "Soft and Biological Structures". In: *Intermolecular and Surface Forces*. Elsevier, 2011, pp. 535–576. DOI: 10.1016/b978-0-12-391927-4.10020-9.

[42] D. Axelrod. "Lateral motion of membrane proteins and biological function". In: *The Journal of Membrane Biology* 75.1 (1983), pp. 1–10. DOI: 10.1007/bf01870794.

[43] A. Einstein. "Über die von der molekularkinetischen Theorie der Wärme geforderte Bewegung von in ruhenden Flüssigkeiten suspendierten Teilchen". In: *Annalen der Physik* 322.8 (1905), pp. 549–560. DOI: 10.1002/andp.19053220806.

[44] G. Vereb et al. "Dynamic, yet structured: The cell membrane three decades after the Singer-Nicolson model". In: *Proceedings of the National Academy of Sciences of the United States of America* 100.14 (2003), pp. 8053–8. DOI: 10.1073/pnas.1332550100.

[45] P. F. F. Almeida and W. L. C. Vaz. "Lateral Diffusion in Membranes". In: *Structure and Dynamics of Membranes - From Cells to Vesicles*. Ed. by R. Lipowsky Sackmann and E. 1st ed. Vol. 1. Handbook of Biological Physics. Elsevier Science B.V, 1995. Chap. 6, pp. 305–357. DOI: 10.1016/s1383-8121(06)80023-0.

[46] M. H. Cohen and D. Turnbull. "Molecular Transport in Liquids and Glasses". In: *The Journal of Chemical Physics* 31.5 (1959), pp. 1164–1169. DOI: 10.1063/1.1730566.

[47] P. B. Macedo and T. A. Litovitz. "On the Relative Roles of Free Volume and Activation Energy in the Viscosity of Liquids". In: *The Journal of Chemical Physics* 42.1 (1965), pp. 245–256. DOI: 10.1063/1.1695683.

[48] W. L. C. Vaz, R. M. Clegg, and D. Hallmann. "Translational diffusion of lipids in liquid crystalline phase phosphatidylcholine multibilayers. A comparison of experiment with theory". In: *Biochemistry* 24.3 (1985), pp. 781–786. DOI: 10.1021/bi00324a037.

[49] P. F. F. Almeida, W. L. C. Vaz, and T. E. Thompson. "Lateral diffusion in the liquid phases of dimyristoylphosphatidylcholine/cholesterol lipid bilayers: a free volume analysis". In: *Biochemistry* 31.29 (1992), pp. 6739–6747. DOI: 10.1021/bi00144a013.

[50] J. E. MacCarthy and J. J. Kozak. "Lateral diffusion in fluid systems". In: *The Journal of Chemical Physics* 77.4 (1982), pp. 2214–2216. DOI: 10.1063/1.444032.

[51] Thomas Heimburg. *Thermal Biophysics of Membranes*. Weinheim: Wiley VCH Verlag GmbH, 2007. DOI: 10.1002/9783527611591.

[52] Avanti Polar Lipids. *Phase Transition Temperatures for Glycerophospholipids*. URL: https://avantilipids.com/tech-support/physical-properties/phase-transition-temps (visited on 08/06/2018).

[53] D. Marsh. "Structural and thermodynamic determinants of chain-melting transition temperatures for phospholipid and glycolipids membranes". In: *Biochimica et Biophysica Acta (BBA) - Biomembranes* 1798.1 (2010), pp. 40–51. DOI: 10.1016/j.bbamem.2009.10.010.

[54] J. F. Nagle. "Theory of lipid monolayer and bilayer phase transitions: Effect of headgroup interactions". In: *The Journal of Membrane Biology* 27.1 (1976), pp. 233–250. DOI: 10.1007/bf01869138.

[55] Philip L. Yeagle, ed. *The Structure of Biological Membranes, Second Edition*. CRC Press, 2004.

[56] I. K. Jarsch et al. "Plasma Membranes Are Subcompartmentalized into a Plethora of Coexisting and Diverse Microdomains in Arabidopsis and Nicotiana benthamiana". In: *The Plant Cell* 26.4 (2014), pp. 1698–1711. DOI: 10.1105/tpc.114.124446.

[57] J. Coburn et al. "Proving Lipid Rafts Exist: Membrane Domains in the Prokaryote Borrelia burgdorferi Have the Same Properties as Eukaryotic Lipid Rafts". In: *PLoS Pathogens* 9.5 (2013). DOI: 10.1371/journal.ppat.1003353.

[58] J. Korlach et al. "Characterization of lipid bilayer phases by confocal microscopy and fluorescence correlation spectroscopy". In: *Proceedings of the National Academy of Sciences* 96.15 (1999), pp. 8461–8466. DOI: 10.1073/pnas.96.15.8461.

[59] S. L. Veatch and S. L. Keller. "Organization in lipid membranes containing cholesterol". In: *Physical Review Letters* 89.26 (2002), p. 268101. DOI: 10.1103/PhysRevLett.89.268101.

[60] J. Zhao et al. "Phase studies of model biomembranes: complex behavior of DSPC/DOPC/cholesterol". In: *Biochimica et Biophysica Acta (BBA) - Biomembranes* 1768.11 (2007), pp. 2764–76. DOI: 10.1016/j.bbamem.2007.07.008.

[61] G. W. Feigenson. "Phase boundaries and biological membranes". In: *Annual Review of Biophysics and Biomolecular Structure* 36 (2007), pp. 63–77. DOI: 10.1146/annurev.biophys.36.040306.132721.

[62] P. F. F. Almeida, A. Pokorny, and A. Hinderliter. "Thermodynamics of membrane domains". In: *Biochimica et Biophysica Acta (BBA) - Biomembranes* 1720.1-2 (2005), pp. 1–13. DOI: 10.1016/j.bbamem.2005.12.004.

[63] P. F. F. Almeida. "A Simple Thermodynamic Model of the Liquid-Ordered State and the Interactions between Phospholipids and Cholesterol". In: *Biophysical Journal* 100.2 (2011), pp. 420–429. DOI: 10.1016/j.bpj.2010.12.3694.

[64] M. Sugahara, M. Uragami, and S. L. Regen. "Selective Sterol-Phospholipid Associations in Fluid Bilayers". In: *Journal of the American Chemical Society* 124.16 (2002), pp. 4253–4256. DOI: 10.1021/ja017269i.

[65] E. Beltrán-Heredia et al. "Modeling the Mechanics of Cell Division: Influence of Spontaneous Membrane Curvature, Surface Tension, and Osmotic Pressure". In: *Frontiers in Physiology* 8 (2017). DOI: 10.3389/fphys.2017.00312.

[66] A. Sakashita et al. "Three-dimensional analysis of lipid vesicle transformations". In: *Soft Matter* 8.33 (2012). DOI: 10.1039/c2sm25759a.

[67] H. G. Döbereiner et al. "Mapping vesicle shapes into the phase diagram: A comparison of experiment and theory". In: *Physical Review E* 55.4 (1997), pp. 4458–4474. DOI: 10.1103/PhysRevE.55.4458.

[68] M. Deserno. "Fluid lipid membranes: from differential geometry to curvature stresses". In: *Chemistry and Physics of Lipids* 185 (2015), pp. 11–45. DOI: 10.1016/j.chemphyslip.2014.05.001.

[69] W. Rawicz et al. "Effect of Chain Length and Unsaturation on Elasticity of Lipid Bilayers". In: *Biophysical Journal* 79.1 (2000), pp. 328–339. DOI: 10.1016/s0006-3495(00)76295-3.

[70] E. Evans et al. "Dynamic Tension Spectroscopy and Strength of Biomembranes". In: *Biophysical Journal* 85.4 (2003), pp. 2342–2350. DOI: 10.1016/s0006-3495(03)74658-x.

[71] W. Helfrich. "Elastic properties of lipid bilayers: theory and possible experiments". In: *Zeitschrift für Naturforschung C: A Journal of Biosciences* 28.11 (1973), pp. 693–703.

[72] M. Hu, J. J. Briguglio, and M. Deserno. "Determining the Gaussian Curvature Modulus of Lipid Membranes in Simulations". In: *Biophysical Journal* 102.6 (2012), pp. 1403–1410. DOI: 10.1016/j.bpj.2012.02.013.

[73] R. Dimova. "Recent developments in the field of bending rigidity measurements on membranes". In: *Advances in Colloid and Interface Science* 208 (2014), pp. 225–34. DOI: 10.1016/j.cis.2014.03.003.

[74] U. Seifert. "Configurations of fluid membranes and vesicles". In: *Advances in Physics* 46.1 (1997), pp. 13–137. DOI: 10.1080/00018739700101488.

[75] R. Lipowsky. "Budding of membranes induced by intramembrane domains". In: *Journal de Physique II* 2.10 (1992), pp. 1825–1840. DOI: 10.1051/jp2:1992238.

[76] U. Seifert. "Curvature-induced lateral phase segregation in two-component vesicles". In: *Physical Review Letters* 70.9 (1993), pp. 1335–1338. DOI: 10.1103/PhysRevLett.70.1335.

[77] G. D. Scholes et al. "Lessons from nature about solar light harvesting". In: *Nature Chemistry* 3.10 (2011), pp. 763–774. DOI: 10.1038/nchem.1145.

[78] G. McDermott et al. "Crystal structure of an integral membrane light-harvesting complex from photosynthetic bacteria". In: *Nature* 374.6522 (1995), pp. 517–521. DOI: 10.1038/374517a0.

[79] R. Schoenlein et al. "The first step in vision: femtosecond isomerization of rhodopsin". In: *Science* 254.5030 (1991), pp. 412–415. DOI: 10.1126/science.1925597.

[80] B. Stiller et al. "Optical patterning in azobenzene polymer films". In: *Journal of Microscopy* 219.3 (2005), pp. 109–114. DOI: 10.1111/j.1365-2818.2005.01500.x.

[81] H. Wen et al. “Photomechanical bending of linear azobenzene polymer”. In: *RSC Adv.* 4.23 (2014), pp. 11776–11781. DOI: 10.1039/c3ra48035f.

[82] J. Broichhagen, J. A. Frank, and D. Trauner. “A Roadmap to Success in Photopharmacology”. In: *Acc Chem Res* 48.7 (2015), pp. 1947–60. DOI: 10.1021/acs.accounts.5b00129.

[83] T. Kumpulainen et al. “Ultrafast Elementary Photochemical Processes of Organic Molecules in Liquid Solution”. In: *Chemical Reviews* 117.16 (2017), pp. 10826–10939. DOI: 10.1021/acs.chemrev.6b00491.

[84] H. Rau. “Azo Compounds”. In: *Photochromism*. Ed. by Heinz Dürr and Henri Bouas-Laurent. Amsterdam: Elsevier Science, 2003, pp. 165–192. DOI: https://doi.org/10.1016/B978-044451322-9/50008-7.

[85] A. D. McNaught and A. Wilkinson. “Kasha–Vavilov rule”. In: *IUPAC. Compendium of Chemical Terminology, 2nd ed. (the “Gold Book”)*. Blackwell Scientific Publications, 2006. DOI: 10.1351/goldbook.K03371.

[86] H. M. Bandara and S. C. Burdette. “Photoisomerization in different classes of azobenzene”. In: *Chemical Society Reviews* 41.5 (2012), pp. 1809–25. DOI: 10.1039/c1cs15179g.

[87] M. Quick et al. “Photoisomerization dynamics and pathways of trans- and cis-azobenzene in solution from broadband femtosecond spectroscopies and calculations”. In: *Journal of Physical Chemistry B* 118.29 (2014), pp. 8756–71. DOI: 10.1021/jp504999f.

[88] A. Nenov et al. “UV-Light-Induced Vibrational Coherences: The Key to Understand Kasha Rule Violation in trans-Azobenzene”. In: *The Journal of Physical Chemistry Letters* (2018), pp. 1534–1541. DOI: 10.1021/acs.jpclett.8b00152.

[89] S. S. Sandhu et al. “The formation and Langmuir-Blodgett deposition of monolayers of novel photochromic azobenzene-containing phospholipid molecules”. In: *Biochimica et Biophysica Acta (BBA) - Biomembranes* 860.2 (1986), pp. 253–262. DOI: 10.1016/0005-2736(86)90521-3.

[90] X. Song, J. Perlstein, and D. G. Whitten. “Supramolecular Aggregates of Azobenzene Phospholipids and Related Compounds in Bilayer Assemblies and Other Microheterogeneous Media: Structure, Properties, and Photoreactivity1”. In: *Journal of the American Chemical Society* 119.39 (1997), pp. 9144–9159. DOI: 10.1021/ja971291n.

[91] K. Ishii et al. “Reversible Control of Exo- and Endo-Budding Transitions in a Photosensitive Lipid Membrane”. In: *ChemBioChem* 10.2 (2009), pp. 251–256. DOI: 10.1002/cbic.200800482.

[92] All work related to the synthesis of *azo*-**PC** was done in the group of Prof. Dirk Trauner (Chemistry Department, LMU Munich) by Dr. James A. Frank and Dr. David B. Konrad. The synthetic routes are published in detail elsewhere.[94,139].

[93] E. Titov et al. “Dynamics of Azobenzene Dimer Photoisomerization: Electronic and Steric Effects”. In: *The Journal of Physical Chemistry Letters* 7.18 (2016), pp. 3591–3596. DOI: 10.1021/acs.jpclett.6b01401.

[94] C. Pernpeintner et al. “Light-Controlled Membrane Mechanics and Shape Transitions of Photoswitchable Lipid Vesicles”. In: *Langmuir* 33.16 (2017), pp. 4083–4089. DOI: 10.1021/acs.langmuir.7b01020.

[95] T. A. Nieminen et al. “Optical tweezers: Theory and modelling”. In: *Journal of Quantitative Spectroscopy and Radiative Transfer* 146 (2014), pp. 59–80. DOI: 10.1016/j.jqsrt.2014.04.003.

[96] E. E. Jelley. “Spectral Absorption and Fluorescence of Dyes in the Molecular State”. In: *Nature* 138.3502 (1936), pp. 1009–1010. DOI: 10.1038/1381009a0.

[97] G. Scheibe, L. Kandler, and H. Ecker. "Polymerisation und polymere Adsorption als Ursache neuartiger Absorptionsbanden von organischen Farbstoffen". In: *Die Naturwissenschaften* 25.5 (1937), pp. 75–75. DOI: 10.1007/bf01493278.

[98] F. Würthner, T. E. Kaiser, and C. R. Saha-Möller. "J-aggregates: from serendipitous discovery to supramolecular engineering of functional dye materials". In: *Angewandte Chemie International Edition* 50.15 (2011), pp. 3376–410. DOI: 10.1002/anie.201002307.

[99] M. Kasha, H. R. Rawls, and M. Ashraf El-Bayoumi. "The exciton model in molecular spectroscopy". In: *Pure and Applied Chemistry* 11.3-4 (1965). DOI: 10.1351/pac196511030371.

[100] A. Eisfeld and J. S. Briggs. "The J-band of organic dyes: lineshape and coherence length". In: *Chemical Physics* 281.1 (2002), pp. 61–70. DOI: 10.1016/s0301-0104(02)00594-3.

[101] O. S. Andersen and R. E. 2nd Koeppe. "Bilayer thickness and membrane protein function: an energetic perspective". In: *Annual Review of Biophysics and Biomolecular Structure* 36 (2007), pp. 107–30. DOI: 10.1146/annurev.biophys.36.040306.132643.

[102] P. Walde et al. "Giant vesicles: preparations and applications". In: *ChemBioChem* 11.7 (2010), pp. 848–65. DOI: 10.1002/cbic.201000010.

[103] M. I. Angelova and D. S. Dimitrov. "Liposome Electroformation". In: *Faraday Discussions* 81 (1986), pp. 303–311. DOI: 10.1039/Dc9868100303.

[104] M. I. Angelova and D. S. Dimitrov. "A mechanism of liposome electroformation". In: *Trends in Colloid and Interface Science II*. Ed. by V. Degiorgio. Darmstadt: Steinkopff, 1988, pp. 59–67. DOI: 10.1007/BFb0114171.

[105] Sigma Aldrich. *Solvent Stabilizer Systems*. URL: https://www.sigmaaldrich.com/chemistry/solvents/learning-center/stabilizer-systems.html (visited on 03/19/2018).

[106] R. L. Brown and S. E. Stein. "Boiling Point Data". In: *NIST Chemistry WebBook, NIST Standard Reference Database Number 69*. Ed. by P.J. Linstrom and W.G. Mallard. Gaithersburg MD, 20899: National Institute of Standards and Technology. DOI: 10.18434/T4D303.

[107] M. J. Hope et al. "Production of large unilamellar vesicles by a rapid extrusion procedure. Characterization of size distribution, trapped volume and ability to maintain a membrane potential". In: *Biochimica et Biophysica Acta (BBA) - Biomembranes* 812.1 (1985), pp. 55–65. DOI: 10.1016/0005-2736(85)90521-8.

[108] C. Huang. "Phosphatidylcholine vesicles. Formation and physical characteristics". In: *Biochemistry* 8.1 (1969), pp. 344–352. DOI: 10.1021/bi00829a048.

[109] R. C. MacDonald, F. D. Jones, and R. Qui. "Fragmentation into small vesicles of dioleoylphosphatidylcholine bilayers during freezing and thawing". In: *Biochimica et Biophysica Acta (BBA) - Biomembranes* 1191.2 (1994), pp. 362–370. DOI: 10.1016/0005-2736(94)90187-2.

[110] W. C. Lin et al. "Supported Membrane Formation, Characterization, Functionalization, and Patterning for Application in Biological Science and Technology". In: *Current Protocols in Chemical Biology* 2.4 (2010), pp. 235–69. DOI: 10.1002/9780470559277.ch100131.

[111] C. A. Keller and B. Kasemo. "Surface Specific Kinetics of Lipid Vesicle Adsorption Measured with a Quartz Crystal Microbalance". In: *Biophysical Journal* 75.3 (1998), pp. 1397–1402. DOI: 10.1016/s0006-3495(98)74057-3.

[112] I. Reviakine and A. Brisson. "Formation of Supported Phospholipid Bilayers from Unilamellar Vesicles Investigated by Atomic Force Microscopy". In: *Langmuir* 16.4 (2000), pp. 1806–1815. DOI: 10.1021/la9903043.

[113] K. Tawa and K. Morigaki. “Substrate-supported phospholipid membranes studied by surface plasmon resonance and surface plasmon fluorescence spectroscopy”. In: *Biophysical Journal* 89.4 (2005), pp. 2750–8. DOI: 10.1529/biophysj.105.065482.

[114] R. Tero, H. Watanabe, and T. Urisu. “Supported phospholipid bilayer formation on hydrophilicity-controlled silicon dioxide surfaces”. In: *Physical Chemistry Chemical Physics* 8.33 (2006). DOI: 10.1039/b606052h.

[115] P. Y. Liu et al. “Cell refractive index for cell biology and disease diagnosis: past, present and future”. In: *Lab on a Chip* 16.4 (2016), pp. 634–44. DOI: 10.1039/c5lc01445j.

[116] F. Zernike. “How I Discovered Phase Contrast”. In: *Science* 121.3141 (1955), pp. 345–349. DOI: 10.1126/science.121.3141.345.

[117] G. Nomarski. “Interferential Polarizing Device For Study Of Phase Objects”. US 2924142 A (US). Feb. 1960.

[118] B. N. Giepmans et al. “The fluorescent toolbox for assessing protein location and function”. In: *Science* 312.5771 (2006), pp. 217–24. DOI: 10.1126/science.1124618.

[119] A. Small and S. Stahlheber. “Fluorophore localization algorithms for super-resolution microscopy”. In: *Nature Methods* 11.3 (2014), pp. 267–79. DOI: 10.1038/nmeth.2844.

[120] W. Margolin. “The price of tags in protein localization studies”. In: *Journal of Bacteriology* 194.23 (2012), pp. 6369–71. DOI: 10.1128/JB.01640-12.

[121] T. Baumgart et al. “Fluorescence probe partitioning between Lo/Ld phases in lipid membranes”. In: *Biochimica et Biophysica Acta (BBA) - Biomembranes* 1768.9 (2007), pp. 2182–94. DOI: 10.1016/j.bbamem.2007.05.012.

[122] W. I. Goldburg. “Dynamic light scattering”. In: *American Journal of Physics* 67.12 (1999), pp. 1152–1160. DOI: 10.1119/1.19101.

[123] E. Evans and W. Rawicz. “Entropy-driven tension and bending elasticity in condensed-fluid membranes”. In: *Physical Review Letters* 64.17 (1990), pp. 2094–2097. DOI: 10.1103/PhysRevLett.64.2094.

[124] R. Kwok and E. Evans. “Thermoelasticity of large lecithin bilayer vesicles”. In: *Biophysical Journal* 35.3 (1981), pp. 637–652. DOI: 10.1016/s0006-3495(81)84817-5.

[125] W. Helfrich and R. M. Servuss. “Undulations, steric interaction and cohesion of fluid membranes”. In: *Il Nuovo Cimento D* 3.1 (1984), pp. 137–151. DOI: 10.1007/bf02452208.

[126] D. Axelrod et al. “Mobility measurement by analysis of fluorescence photobleaching recovery kinetics”. In: *Biophysical Journal* 16.9 (1976), pp. 1055–1069. DOI: 10.1016/s0006-3495(76)85755-4.

[127] N. Lorén et al. “Fluorescence recovery after photobleaching in material and life sciences: putting theory into practice”. In: *Quarterly Reviews of Biophysics* 48.3 (2015), pp. 323–87. DOI: 10.1017/S0033583515000013.

[128] D. M. Soumpasis. “Theoretical analysis of fluorescence photobleaching recovery experiments”. In: *Biophysical Journal* 41.1 (1983), pp. 95–97. DOI: 10.1016/s0006-3495(83)84410-5.

[129] P. Jonsson et al. “A method improving the accuracy of fluorescence recovery after photobleaching analysis”. In: *Biophys J* 95.11 (2008), pp. 5334–48. DOI: 10.1529/biophysj.108.134874.

[130] MATLAB. *frap_analysis*. URL: https://www.mathworks.com/matlabcentral/fileexchange/29388-frap_analysis (visited on 01/03/2019).

[131] E. Neher and B. Sakmann. "Single-channel currents recorded from membrane of denervated frog muscle fibres". In: *Nature* 260.5554 (1976), pp. 799–802. DOI: 10.1038/260799a0.

[132] B. Sakmann and E. Neher. "Patch clamp techniques for studying ionic channels in excitable membranes". In: *Annual Review of Physiology* 46 (1984), pp. 455–72. DOI: 10.1146/annurev.ph.46.030184.002323.

[133] S. Aimon et al. "Functional reconstitution of a voltage-gated potassium channel in giant unilamellar vesicles". In: *PLoS One* 6.10 (2011), e25529. DOI: 10.1371/journal.pone.0025529.

[134] M. Garten et al. "Whole-GUV patch-clamping". In: *Proceedings of the National Academy of Sciences* 114.2 (2017), pp. 328–333. DOI: 10.1073/pnas.1609142114.

[135] N. Fertig, R. H. Blick, and J. C. Behrends. "Whole cell patch clamp recording performed on a planar glass chip". In: *Biophysical Journal* 82.6 (2002), pp. 3056–62. DOI: 10.1016/S0006-3495(02)75646-4.

[136] R. Maget-Dana. "The monolayer technique: a potent tool for studying the interfacial properties of antimicrobial and membrane-lytic peptides and their interactions with lipid membranes". In: *Biochimica et Biophysica Acta (BBA) - Biomembranes* 1462.1-2 (1999), pp. 109–140. DOI: 10.1016/s0005-2736(99)00203-5.

[137] H. Brockman. "Lipid monolayers: why use half a membrane to characterize protein-membrane interactions?" In: *Current Opinion in Structural Biology* 9.4 (1999), pp. 438–443. DOI: 10.1016/s0959-440x(99)80061-x.

[138] R. Pichot, R. L. Watson, and I. T. Norton. "Phospholipids at the interface: current trends and challenges". In: *International journal of molecular sciences* 14.6 (2013), pp. 11767–94. DOI: 10.3390/ijms140611767.

[139] P. Urban et al. "Light-Controlled Lipid Interaction and Membrane Organization in Photolipid Bilayer Vesicles". In: *Langmuir* 34.44 (2018), pp. 13368–13374. DOI: 10.1021/acs.langmuir.8b03241.

[140] J. M. Kuiper and Jan B. F. N. Engberts. "H-Aggregation of Azobenzene-Substituted Amphiphiles in Vesicular Membranes". In: *Langmuir* 20.4 (2004), pp. 1152–1160. DOI: 10.1021/la0358724.

[141] V. Cantatore, G. Granucci, and M. Persico. "The photo-orientation of azobenzene in viscous solutions, simulated by a stochastic model". In: *Physical Chemistry Chemical Physics* 16.45 (2014), pp. 25081–92. DOI: 10.1039/c4cp03472d.

[142] Ľ. Vetráková et al. "The Absorption Spectrum of cis-Azobenzene". In: *Photochemical & Photobiological Sciences* 16.12 (2017), pp. 1749–1756. DOI: 10.1039/c7pp00314e.

[143] J. F. Nagle. "Theory of the Main Lipid Bilayer Phase-Transition". In: *Annual Review of Physical Chemistry* 31.1 (1980), pp. 157–195. DOI: 10.1146/annurev.pc.31.100180.001105.

[144] T. Róg et al. "Ordering effects of cholesterol and its analogues". In: *Biochimica et Biophysica Acta (BBA) - Biomembranes* 1788.1 (2009), pp. 97–121. DOI: 10.1016/j.bbamem.2008.08.022.

[145] T. M. Ferreira et al. "Cholesterol and POPC segmental order parameters in lipid membranes: solid state 1H-13C NMR and MD simulation studies". In: *Physical Chemistry Chemical Physics* 15.6 (2013), pp. 1976–89. DOI: 10.1039/c2cp42738a.

[146] S. Wagner et al. "Reversible photoisomerization of an azobenzene-functionalized self-assembled monolayer probed by sum-frequency generation vibrational spectroscopy". In: *Physical Chemistry Chemical Physics* 11.29 (2009). DOI: 10.1039/b823330f.

[147] D. T. Valley et al. "Steric Hindrance of Photoswitching in Self-Assembled Monolayers of Azobenzene and Alkane Thiols". In: *Langmuir* 29.37 (2013), pp. 11623–11631. DOI: 10.1021/la402144g.

[148] K. Tamada, H. Akiyama, and T. X. Wei. "Photoisomerization Reaction of Unsymmetrical Azobenzene Disulfide Self-Assembled Monolayers Studied by Surface Plasmon Spectroscopy: Influences of Side Chain Length and Contacting Medium". In: *Langmuir* 18.13 (2002), pp. 5239–5246. DOI: 10.1021/la0157667.

[149] R. Wang et al. "Structural investigation of azobenzene-containing self-assembled monolayer films". In: *Journal of Electroanalytical Chemistry* 438.1-2 (1997), pp. 213–219. DOI: 10.1016/s0022-0728(96)05031-0.

[150] Z. F. Liu, K. Hashimoto, and A. Fujishima. "Photoelectrochemical information storage using an azobenzene derivative". In: *Nature* 347.6294 (1990), pp. 658–660. DOI: 10.1038/347658a0.

[151] C. Zhang et al. "Coherent Electron Transport through an Azobenzene Molecule: A Light-Driven Molecular Switch". In: *Physical Review Letters* 92.15 (2004). DOI: 10.1103/PhysRevLett.92.158301.

[152] J. M. Mativetsky et al. "Azobenzenes as Light-Controlled Molecular Electronic Switches in Nanoscale Metal–Molecule–Metal Junctions". In: *Journal of the American Chemical Society* 130.29 (2008), pp. 9192–9193. DOI: 10.1021/ja8018093.

[153] E. Jeoung and V. M. Rotello. "Photochemical control of molecular recognition on self-assembled monolayer-protected gold clusters". In: *Journal of Supramolecular Chemistry* 2.1-3 (2002), pp. 53–55. DOI: 10.1016/s1472-7862(02)00078-3.

[154] T. Baumgart et al. "Fluorescence probe partitioning between Lo/Ld phases in lipid membranes". In: *Biochimica et Biophysica Acta (BBA) - Biomembranes* 1768.9 (2007), pp. 2182–94. DOI: 10.1016/j.bbamem.2007.05.012.

[155] O. Bakht, P. Pathak, and E. London. "Effect of the structure of lipids favoring disordered domain formation on the stability of cholesterol-containing ordered domains (lipid rafts): identification of multiple raft-stabilization mechanisms". In: *Biophysical Journal* 93.12 (2007), pp. 4307–18. DOI: 10.1529/biophysj.107.114967.

[156] S. L. Veatch, K. Gawrisch, and S. L. Keller. "Closed-loop miscibility gap and quantitative tie-lines in ternary membranes containing diphytanoyl PC". In: *Biophysical Journal* 90.12 (2006), pp. 4428–36. DOI: 10.1529/biophysj.105.080283.

[157] W. Kulig, M. Pasenkiewicz-Gierula, and T. Róg. "Cis and trans unsaturated phosphatidylcholine bilayers: A molecular dynamics simulation study". In: *Chemistry and Physics of Lipids* 195 (2016), pp. 12–20. DOI: 10.1016/j.chemphyslip.2015.07.002.

[158] A. J. García-Sáez, S. Chiantia, and P. Schwille. "Effect of line tension on the lateral organization of lipid membranes". In: *Journal of Biological Chemistry* 282.46 (2007), pp. 33537–44. DOI: 10.1074/jbc.M706162200.

[159] R. D. Usery et al. "Line Tension Controls Liquid-Disordered + Liquid-Ordered Domain Size Transition in Lipid Bilayers". In: *Biophysical Journal* 112.7 (2017), pp. 1431–1443. DOI: 10.1016/j.bpj.2017.02.033.

[160] P. I. Kuzmin et al. "Line tension and interaction energies of membrane rafts calculated from lipid splay and tilt". In: *Biophysical Journal* 88.2 (2005), pp. 1120–33. DOI: 10.1529/biophysj.104.048223.

[161] C. M. Rosetti, G. G. Montich, and C. Pastorino. "Molecular Insight into the Line Tension of Bilayer Membranes Containing Hybrid Polyunsaturated Lipids". In: *The Journal of Physical Chemistry B* 121.7 (2017), pp. 1587–1600. DOI: 10.1021/acs.jpcb.6b10836.

[162] A. K. Chaurasia et al. "Evaluation of bending modulus of lipid bilayers using undulation and orientation analysis". In: *Physical Review E* 97.3-1 (2018), p. 032421. DOI: 10.1103/PhysRevE.97.032421.

[163] W. Shinoda et al. “Molecular dynamics study of bipolar tetraether lipid membranes”. In: *Biophysical Journal* 89.5 (2005), pp. 3195–202. DOI: 10.1529/biophysj.105.060962.

[164] N. Kučerka, S. Tristram-Nagle, and J. F. Nagle. “Structure of fully hydrated fluid phase lipid bilayers with monounsaturated chains”. In: *Journal of Membrane Biology* 208.3 (2005), pp. 193–202. DOI: 10.1007/s00232-005-7006-8.

[165] N. Kučerka, M. P. Nieh, and J. Katsaras. “Fluid phase lipid areas and bilayer thicknesses of commonly used phosphatidylcholines as a function of temperature”. In: *Biochimica et Biophysica Acta (BBA) - Biomembranes* 1808.11 (2011), pp. 2761–71. DOI: 10.1016/j.bbamem.2011.07.022.

[166] G. Illya, R. Lipowsky, and J. C. Shillcock. “Two-component membrane material properties and domain formation from dissipative particle dynamics”. In: *Journal of Chemical Physics* 125.11 (2006), p. 114710. DOI: 10.1063/1.2353114.

[167] F. G. Giancotti. “Integrin Signaling”. In: *Science* 285.5430 (1999), pp. 1028–1033. DOI: 10.1126/science.285.5430.1028.

[168] A. Grakoui. “The Immunological Synapse: A Molecular Machine Controlling T Cell Activation”. In: *Science* 285.5425 (1999), pp. 221–227. DOI: 10.1126/science.285.5425.221.

[169] L. K. Tamm and H. M. McConnell. “Supported phospholipid bilayers”. In: *Biophysical Journal* 47.1 (1985), pp. 105–13. DOI: 10.1016/S0006-3495(85)83882-0.

[170] E. Sackmann. “Supported Membranes: Scientific and Practical Applications”. In: *Science* 271.5245 (1996), pp. 43–48.

[171] J. T. Groves and S. G. Boxer. “Micropattern Formation in Supported Lipid Membranes”. In: *Accounts of Chemical Research* 35.3 (2002), pp. 149–157. DOI: 10.1021/ar950039m.

[172] L. Iversen et al. “Ras activation by SOS: Allosteric regulation by altered fluctuation dynamics”. In: *Science* 345.6192 (2014), pp. 50–54. DOI: 10.1126/science.1250373.

[173] P. Urban et al. “Light-Controlled Lipid Interaction and Membrane Organization in Photolipid Bilayer Vesicles”. In: *Langmuir* (2020). DOI: 10.1021/acs.langmuir.9b02942.

[174] N. Yellin and I. W. Levin. “Hydrocarbon chain trans-gauche isomerization in phospholipid bilayer gel assemblies”. In: *Biochemistry* 16.4 (2002), pp. 642–647. DOI: 10.1021/bi00623a014.

[175] R. W. Taylor et al. “Watching individual molecules flex within lipid membranes using SERS”. In: *Scientific Reports* 4 (2014), p. 5940. DOI: 10.1038/srep05940.

[176] A. P. Girard-Egrot and L. J. Blum. “Langmuir-Blodgett Technique for Synthesis of Biomimetic Lipid Membranes”. In: *Nanobiotechnology of Biomimetic Membranes*. Ed. by Donald K. Martin. Boston, MA: Springer US, 2007, pp. 23–74. DOI: 10.1007/0-387-37740-9_2.

[177] J. F. Nagle. “Theory of lipid monolayer and bilayer chain-melting phase transitions”. In: *Faraday Discussions of the Chemical Society* 81 (1986). DOI: 10.1039/dc9868100151.

[178] D. Marsh. “Lateral pressure in membranes”. In: *Biochimica et Biophysica Acta (BBA) - Reviews on Biomembranes* 1286.3 (1996), pp. 183–223. DOI: 10.1016/s0304-4157(96)00009-3.

[179] M. Dahim et al. “Physical and Photophysical Characterization of a BODIPY Phosphatidylcholine as a Membrane Probe”. In: *Biophysical Journal* 83.3 (2002), pp. 1511–1524. DOI: 10.1016/s0006-3495(02)73921-0.

[180] Avanti Polar Lipids. *16:0-18:1 PC (POPC)*. URL: https://avantilipids.com/product/850457 (visited on 05/09/2019).

[181] H. H. Tsai et al. “Geometrical effects of phospholipid olefinic bonds on the structure and dynamics of membranes: A molecular dynamics study”. In: *Biochim Biophys Acta* 1848.5 (2015), pp. 1234–47. DOI: 10.1016/j.bbamem.2015.02.016.

[182] C. Roach et al. “Comparison of cis and trans fatty acid containing phosphatidylcholines on membrane properties”. In: *Biochemistry* 43.20 (2004), pp. 6344–51. DOI: 10.1021/bi049917r.

[183] N. Bag, D. H. X. Yap, and T. Wohland. “Temperature dependence of diffusion in model and live cell membranes characterized by imaging fluorescence correlation spectroscopy”. In: *Biochimica et Biophysica Acta (BBA) - Biomembranes* 1838.3 (2014), pp. 802–813. DOI: 10.1016/j.bbamem.2013.10.009.

[184] E. Fischer. “Temperature Dependence of Photoisomerization Equilibria. Part I. Azobenzene and the Azonaphthalenes”. In: *Journal of the American Chemical Society* 82.13 (1960), pp. 3249–3252. DOI: 10.1021/ja01498a005.

[185] V. Chaban. “Computationally efficient prediction of area per lipid”. In: *Chemical Physics Letters* 616-617 (Nov. 2014), pp. 25–29. DOI: 10.1016/j.cplett.2014.10.015.

[186] H. I. Petrache, S. W. Dodd, and M. F. Brown. “Area per Lipid and Acyl Length Distributions in Fluid Phosphatidylcholines Determined by 2H NMR Spectroscopy”. In: *Biophysical Journal* 79.6 (2000), pp. 3172–3192. DOI: 10.1016/s0006-3495(00)76551-9.

[187] P. Heftberger et al. “Global small-angle X-ray scattering data analysis for multilamellar vesicles: the evolution of the scattering density profile model”. In: *Journal of Applied Crystallography* 47.Pt 1 (2014), pp. 173–180. DOI: 10.1107/S1600576713029798.

[188] S. Mabrey and J. M. Sturtevant. “Investigation of phase transitions of lipids and lipid mixtures by sensitivity differential scanning calorimetry”. In: *Proceedings of the National Academy of Sciences* 73.11 (1976), pp. 3862–3866. DOI: 10.1073/pnas.73.11.3862.

[189] B. A. Smith and H. M. McConnell. “Determination of molecular motion in membranes using periodic pattern photobleaching”. In: *Proceedings of the National Academy of Sciences* 75.6 (1978), pp. 2759–2763. DOI: 10.1073/pnas.75.6.2759.

[190] M. G. L. Gustafsson. “Surpassing the lateral resolution limit by a factor of two using structured illumination microscopy”. In: *Journal of Microscopy* 198.2 (2000), pp. 82–87. DOI: DOI10.1046/j.1365-2818.2000.00710.x.

[191] S. D. Coomber et al. *Optically addressed spatial light modulators for replaying computer-generated holograms*. Vol. 4457. International Symposium on Optical Science and Technology. SPIE, 2001, p. 11.

[192] A. Chevalier et al. “Universal dark quencher based on ’clicked’ spectrally distinct azo dyes”. In: *Organic Letters* 15.23 (2013), pp. 6082–5. DOI: 10.1021/ol402972y.

[193] O. Kempf et al. “Hydrodabcyl: A Superior Hydrophilic Alternative to the Dark Fluorescence Quencher Dabcyl”. In: *Analytical Chemistry* 89.22 (2017), pp. 11893–11897. DOI: 10.1021/acs.analchem.7b03488.

[194] P. Crisalli and E. T. Kool. “Multi-path quenchers: efficient quenching of common fluorophores”. In: *Bioconjugate Chemistry* 22.11 (2011), pp. 2345–54. DOI: 10.1021/bc200424r.

[195] S. Monti et al. “The triplet state of azobenzene”. In: *Chemical Physics Letters* 77.1 (1981), pp. 115–119. DOI: 10.1016/0009-2614(81)85611-4.

[196] J. R. Lakowicz. “Effects of Solvents on Fluorescence Emission Spectra”. In: *Principles of Fluorescence Spectroscopy*. Boston, MA: Springer US, 1983, pp. 187–215. DOI: 10.1007/978-1-4615-7658-7_7.

[197] M. Edidin. "Lipids on the frontier: a century of cell-membrane bilayers". In: *Nature Reviews Molecular Cell Biology* 4.5 (2003), pp. 414–8. DOI: 10.1038/nrm1102.

[198] A. Ghosh and M. Greenberg. "Calcium signaling in neurons: molecular mechanisms and cellular consequences". In: *Science* 268.5208 (1995), pp. 239–247. DOI: 10.1126/science.7716515.

[199] N. M. Kumar and N. B. Gilula. "The Gap Junction Communication Channel". In: *Cell* 84.3 (1996), pp. 381–388. DOI: 10.1016/s0092-8674(00)81282-9.

[200] E. Gouaux and R. Mackinnon. "Principles of selective ion transport in channels and pumps". In: *Science* 310.5753 (2005), pp. 1461–5. DOI: 10.1126/science.1113666.

[201] G. Eisenman and J. A. Dani. "An introduction to molecular architecture and permeability of ion channels". In: *Annual Review of Biophysics and Biophysical Chemistry* 16 (1987), pp. 205–26. DOI: 10.1146/annurev.bb.16.060187.001225.

[202] C. Cosentino et al. "Optogenetics. Engineering of a light-gated potassium channel". In: *Science* 348.6235 (2015), pp. 707–10. DOI: 10.1126/science.aaa2787.

[203] T. Y. Tsong. "Electroporation of cell membranes". In: *Biophysical Journal* 60.2 (1991), pp. 297–306. DOI: 10.1016/s0006-3495(91)82054-9.

[204] J. C. Weaver and Y. A. Chizmadzhev. "Theory of electroporation: A review". In: *Bioelectrochemistry and Bioenergetics* 41.2 (1996), pp. 135–160. DOI: Doi10.1016/S0302-4598(96)05062-3.

[205] A. Blicher et al. "The temperature dependence of lipid membrane permeability, its quantized nature, and the influence of anesthetics". In: *Biophysical Journal* 96.11 (2009), pp. 4581–91. DOI: 10.1016/j.bpj.2009.01.062.

[206] P. Y. Bolinger, D. Stamou, and H. Vogel. "Integrated nanoreactor systems: triggering the release and mixing of compounds inside single vesicles". In: *Journal of the American Chemical Society* 126.28 (2004), pp. 8594–5. DOI: 10.1021/ja049023u.

[207] A. Kyrsting et al. "Heat profiling of three-dimensionally optically trapped gold nanoparticles using vesicle cargo release". In: *Nano Letters* 11.2 (2010), pp. 888–892. DOI: 10.1021/nl104280c.

[208] A. S. Ladokhin, W. C. Wimley, and S. H. White. "Leakage of membrane vesicle contents: determination of mechanism using fluorescence requenching". In: *Biophysical Journal* 69.5 (1995), pp. 1964–1971. DOI: 10.1016/s0006-3495(95)80066-4.

[209] J. Schindelin et al. "Fiji: an open-source platform for biological-image analysis". In: *Nature Methods* 9.7 (2012), pp. 676–82. DOI: 10.1038/nmeth.2019.

[210] J. Schindelin et al. "The ImageJ ecosystem: An open platform for biomedical image analysis". In: *Molecular Reproduction & Development* 82.7-8 (2015), pp. 518–29. DOI: 10.1002/mrd.22489.

[211] V. N. Georgiev et al. "Area Increase and Budding in Giant Vesicles Triggered by Light: Behind the Scene". In: *Advanced Science (Weinheim, Germany)* (2018). DOI: 10.1002/advs.201800432.

[212] M. Ohno et al. "Dynamic behavior of giant liposomes at desired osmotic pressures". In: *Langmuir* 25.19 (2009), pp. 11680–5. DOI: 10.1021/la900777g.

[213] W. Zong et al. "Deformation of giant unilamellar vesicles under osmotic stress". In: *Colloids and Surfaces B: Biointerfaces* 172 (2018), pp. 459–463. DOI: 10.1016/j.colsurfb.2018.08.053.

[214] F. Brochard-Wyart, P. G. de Gennes, and O. Sandre. "Transient pores in stretched vesicles: role of leak-out". In: *Physica A: Statistical Mechanics and its Applications* 278.1-2 (2000), pp. 32–51. DOI: 10.1016/s0378-4371(99)00559-2.

[215] E. Karatekin et al. “Cascades of Transient Pores in Giant Vesicles: Line Tension and Transport”. In: *Biophysical Journal* 84.3 (2003), pp. 1734–1749. DOI: 10.1016/s0006-3495(03)74981-9.

[216] E. Karatekin, O. Sandre, and F. Brochard-Wyart. “Transient pores in vesicles”. In: *Polymer International* 52.4 (2003), pp. 486–493. DOI: 10.1002/pi.1007.

[217] A. Parsegian. “Energy of an Ion crossing a Low Dielectric Membrane: Solutions to Four Relevant Electrostatic Problems”. In: *Nature* 221.5183 (1969), pp. 844–846. DOI: 10.1038/221844a0.

[218] M. A. Wilson and A. Pohorille. “Mechanism of Unassisted Ion Transport across Membrane Bilayers”. In: *Journal of the American Chemical Society* 118.28 (1996), pp. 6580–6587. DOI: 10.1021/ja9540381.

[219] K. C. Melikov et al. “Voltage-Induced Nonconductive Pre-Pores and Metastable Single Pores in Unmodified Planar Lipid Bilayer”. In: *Biophysical Journal* 80.4 (2001), pp. 1829–1836. DOI: 10.1016/s0006-3495(01)76153-x.

[220] T. Heimburg. “Lipid ion channels”. In: *Biophysical Chemistry* 150.1-3 (2010), pp. 2–22. DOI: 10.1016/j.bpc.2010.02.018.

[221] Rangarajan. S. K. and R. de Levie. “On the ionic displacement current in lipid bilayer membranes”. In: *Biophysical Journal* 25.2 (1979), pp. 235–252. DOI: 10.1016/s0006-3495(79)85288-1.

[222] K. Kaufmann, W. Hanke, and A. Corcia. “BOOK 3: Ion channel fluctuations in pure lipid bilayer membranes: Control by voltage.” In: (1989). DOI: http://membranes.nbi.dk/Kaufmann/pdf/1989_Kaufmann_book3_ed.pdf.

[223] T. M. Allen and P. R. Cullis. “Drug delivery systems: entering the mainstream”. In: *Science* 303.5665 (2004), pp. 1818–22. DOI: 10.1126/science.1095833.

[224] J. Michl, E. W. Thulstrup, and J. H. Eggers. “Polarization spectra in stretched polymer sheets. Physical significance of the orientation factors and determination of .pi.-.pi.*transition moment directions in molecules of low symmetry”. In: *The Journal of Physical Chemistry* 74.22 (1970), pp. 3878–3884. DOI: 10.1021/j100716a006.

[225] J. Michl and E. W. Thulstrup. “Ultraviolet and infrared linear dichroism: polarized light as a probe of molecular and electronic structure”. In: *Accounts of Chemical Research* 20.5 (1987), pp. 192–199. DOI: 10.1021/ar00137a006.

# Acknowledgments

The last six years at the Chair for Photonics and Optoelectronics helped me grow, both professionally and personally. At this point, I would like to thank the people would supported me during this time.

First of all, I am especially grateful to **PD Dr. Theo Lohmüller**, who supervised my PhD thesis. His enthusiasm for scientific topics was very inspiring and guided me through the challenging process of finding and mastering a new topic. I thoroughly enjoyed the lively discussion we had, and I profited a lot from his knowledge on interdisciplinary research, which he willingly passed on.

I want to thank **Prof. Dr. Jochen Feldmann** for giving me the opportunity to perform research in his lab. I am grateful for the freedom I had for pursuing independent research, while still gaining insight from his experience as a scientist.

I would like to thank the many people I could cooperate with. In particular, I would like to thank **Dr. David Konrad**, **Dr. James Frank** and **Prof. Dr. Dirk Trauner** for their endless supply of photoswitchable molecules and the support regarding their properties. Without your invaluable synthetic work, this thesis wouldn't have been possible. Further, I want to thank **Martina Ober** and **PD Dr. Bert Nickel**. Being so close both spatially and topic-wise helped immensely in identifying and tackling the scientific challenges of photoswitchable systems. Finally, many thanks to **Dr. Eva-Maria Roller** and **Prof. Tim Liedl** for a fruitful collaboration and to **James Schuck** for hosting me for two wonderful months at the LBNL.

During my time in the group I got to know many wonderful people. Special thanks go to **Dr. Carla Pernpeintner**, **Stefanie Pritzl** and **Christoph Maier** for innumerous exciting hours in and out of the lab and to my long time office mates, **Dr. Verena Hintermayr** and **Aurora Manzi**, for making my day brighter. **Florian Ehrat**, I thoroughly enjoyed the time we spent together at the group, during our studies and playing in various bands and orchestras.

I would like to thank **Gerlinde Adam** for the endearing administrative support, and to **Stefan Niedermaier** and **Christian Holopirek** for helping me solve all the technical questions.

Last but not least, I want to thank my parents, **Cornelia Urban** and **Peter Urban** for their never-ending support, and for nurturing my early curiosity for technical and physical topics. Finally, my biggest *thank you* goes to my wife, **Christina Urban**, for always being there for me, no matter what and giving me the strength to finish this thesis.